MICRO-NANOSTRUCTURED OPTOELECTRONIC DEVICES

EDITED BY: Yue-Feng Liu, Yun-Fei Li and Pengcheng Sun
PUBLISHED IN: Frontiers in Chemistry

frontiers Research Topics

frontiers

ISSN 1664-8714
ISBN 978-2-88976-442-6
DOI 10.3389/978-2-88976-442-6

About Frontiers

Frontiers is more than just an open-access publisher of scholarly articles: it is a pioneering approach to the world of academia, radically improving the way scholarly research is managed. The grand vision of Frontiers is a world where all people have an equal opportunity to seek, share and generate knowledge. Frontiers provides immediate and permanent online open access to all its publications, but this alone is not enough to realize our grand goals.

Frontiers Journal Series

The Frontiers Journal Series is a multi-tier and interdisciplinary set of open-access, online journals, promising a paradigm shift from the current review, selection and dissemination processes in academic publishing. All Frontiers journals are driven by researchers for researchers; therefore, they constitute a service to the scholarly community. At the same time, the Frontiers Journal Series operates on a revolutionary invention, the tiered publishing system, initially addressing specific communities of scholars, and gradually climbing up to broader public understanding, thus serving the interests of the lay society, too.

Dedication to Quality

Each Frontiers article is a landmark of the highest quality, thanks to genuinely collaborative interactions between authors and review editors, who include some of the world's best academicians. Research must be certified by peers before entering a stream of knowledge that may eventually reach the public - and shape society; therefore, Frontiers only applies the most rigorous and unbiased reviews.
Frontiers revolutionizes research publishing by freely delivering the most outstanding research, evaluated with no bias from both the academic and social point of view. By applying the most advanced information technologies, Frontiers is catapulting scholarly publishing into a new generation.

What are Frontiers Research Topics?

Frontiers Research Topics are very popular trademarks of the Frontiers Journals Series: they are collections of at least ten articles, all centered on a particular subject. With their unique mix of varied contributions from Original Research to Review Articles, Frontiers Research Topics unify the most influential researchers, the latest key findings and historical advances in a hot research area! Find out more on how to host your own Frontiers Research Topic or contribute to one as an author by contacting the Frontiers Editorial Office: frontiersin.org/about/contact

MICRO-NANOSTRUCTURED OPTOELECTRONIC DEVICES

Topic Editors:
Yue-Feng Liu, Jilin University, China
Yun-Fei Li, Hebei University of Technology, China
Pengcheng Sun, University of Illinois at Urbana-Champaign, United States

Citation: Liu, Y.-F., Li, Y.-F., Sun, P., eds. (2022). Micro-nanostructured Optoelectronic Devices. Lausanne: Frontiers Media SA. doi: 10.3389/978-2-88976-442-6

Table of Contents

frontiers | Frontiers in Chemistry

EDITORIAL
published: 02 June 2022
doi: 10.3389/fchem.2022.920807

Editorial: Recent Advances in Micro-Nanostructured Optoelectronic Devices

Yue-Feng Liu[1]*, *Xiu-Min Gao*[1] and *Yun-Fei Li*[2,3]

[1]State Key Laboratory of Integrated Optoelectronics, College of Electronic Science and Engineering, Jilin University, Changchun, China, [2]Center for Advanced Laser Technology, Hebei University of Technology, Tianjin, China, [3]Hebei Key Laboratory of Advanced Laser Technology and Equipment, Tianjin, China

Keywords: optoelectronic (OE) devices, micro-nano structure, light emitting device (LED), laser, sensor, perovskite

Editorial on the Research Topic

Recent Advances in Micro-Nanostructured Optoelectronic Devices

Optoelectronic devices, including lasers, light-emitting diodes (LED), optical detectors and solar cells, have gained substantial attention in scientific research and been widely used in military and national economy fields such as laser detection and measurement, display and solid-state lighting, optical communications and environmental monitoring, and renewable energy sources (Bonaccorso et al., 2010; Lopez-Sanchez et al., 2013; Cao and Yan, 2021; Ye et al., 2021; Mao et al., 2021). The performance of optoelectronic devices needs to be continuously optimized towards high efficiency, small size, and low power consumption to meet the increasing demand of consumers. However, further improvement in performance remains a daunting challenge due to limited light extraction or absorption in conventional device architectures. Inspired by the organisms in nature, a growing number of researchers have demonstrated that micro-nanostructures could attribute unique optical, electrical, and mechanical properties to optoelectronic devices thus serving as one of the most promising solutions to this problem (Bi et al., 2013; Feng et al., 2017; Fusella et al., 2020; Linic et al., 2021). By designing and optimizing the construction in optoelectronic devices, the various micro-nanostructures can be acquired to realize corresponding efficient light manipulation effect such as enhancing light scattering and reducing light reflection, utilizing resonant plasmonic structures to improve light extraction or light absorption, adopting specific resonator geometries to achieve optical feedback, using photonic crystal to guide light propagation path and designing optical metasurfaces to control radiation properties directly at the source level (Choi et al., 2019; Joo et al., 2020; Liu et al., 2020; Zhou et al., 2020; Fu et al., 2021).

To present these inspiring developments, we launched a Research Topic in Frontiers in Chemistry entitled "*Recent Advances in Micro-Nanostructured Optoelectronic Devices*." This Research Topic covers fabrication, light management mechanisms of micro-nanostructures in optoelectronic devices, and their emerging applications in display and lighting, solar energy harvesting, telecommunication, light sensing and detection, and other fields, including seven minireviews and three original research articles contributed from 51 researchers.

The controllable fabrication of micro-nanostructures is a crucial condition to construct efficient micro-nanostructured optoelectronic devices. With the emergence of various kinds of micro-nanostructures manufacturing technologies, laser fabrication technologies can be used to fabricate micro-nanostructures by the interaction between lasers and materials, which show high efficiency, high precision, and low thermal effect, proving to be a competitive manufacturing method.

OPEN ACCESS

Edited and reviewed by:
Baiquan Liu,
Sun Yat-sen University, China

***Correspondence:**
Yue-Feng Liu
yfliu23@jlu.edu.cn

Specialty section:
This article was submitted to Nanoscience, a section of the journal Frontiers in Chemistry

Received: *15 April 2022*
Accepted: *21 April 2022*
Published: *02 June 2022*

Citation:
Liu Y-F, Gao X-M and Li Y-F (2022) Editorial: Recent Advances in Micro-Nanostructured Optoelectronic Devices. Front. Chem. 10:920807. doi: 10.3389/fchem.2022.920807

To this end, a minireview article was delivered to address recent advances in micro-nanostructures fabricated by laser technologies for optoelectronic devices (Yi et al.), which covers both typical light trapping mechanism and surface plasmon-polariton of micro-nanostructures and outlines the typical applications such as photodetectors, photovoltaic cells, organic light-emitting devices. Among kinds of structures, grating structures have demonstrated the superior light trapping properties, coupled with simple fabrication process and easy adjusting of size and morph, which make it widely used optical management structures. Bai et al. introduced 1D and 2D grating structures into the hole injection layer of organic light emitting diode (OLED) to couple the power loss trapped in devices. As a result, both 1D and 2D grating OLEDs gained significant improvement both in luminance and efficiency compared with planar devices. Besides, 2D grating OLED could bring greater enhancement than 1D grating OLED because 2D grating has higher coupling and excitation efficiency for surface plasma and WG mode. This method provides an effective strategy to improve the performance of OLEDs. Wang et al. summarized recent developments of grating structures in optoelectronic devices regarding their typical mechanisms in photon-related devices and their application in many optoelectronic devices. They also have presented how to improve the controllability of fabrication for grating structure and balance the relationship between optical and electrical performance are the bottlenecks that still need to be solved.

Regarding the application examples, several minireviews summarized the recent research activities in developing micro-nanostructures for different optoelectronic devices fields. In the direction of lasers, Chen et al. reviewed the recent advances and existing problems toward microlasers based on organic-conjugated polymers, and the configurations and working mechanism of several typical optical feedback, relevant micro/nano-fabrication strategies and their applications in biological/chemical sensing and organic laser display were also discussed in detail. Periodically arranged photonic crystals fibers could overcome the problems in fiber lasers such as small mode field, low degree of nonlinearity, and non-adjustable dispersion because of their unique nonlinear effects and have been the most important gain medium for high-power ultrashort pulse lasers. Hou et al. discussed recent developments in photonic crystal fiber lasers doped with different ions. They pointed out the major challenge at present is the pulling of photonic crystal fibers and 3D printing microstructured optical fiber process might be an effective approach to solve this problem. In the area of monitoring and sensing, micro-nanostructures are also crucial for optimizing the performance of optoelectronic devices. Yu et al. reviewed latest achievements, the challenges and future prospects of photodetectors with different micro-nanostructures in environmental monitoring, optical communication and electronic information. Meanwhile, Ma et al. gave a minireview of gas sensors based on different micro-nanostructure materials under UV light and visible light activation. They discussed the light activation mechanism and introduced the applications of light-assisted gas sensors with improved properties under light activation.

In addition to the above, in the framework of this special topic, there are also two highly innovative manuscripts on light emitting diodes and carrier dynamics of strong coupling system. Chuai et al. reported the epitaxial growth of Bi_2Se_3 thin film by means of molecular beam deposition (MBE) method. The Bi_2Se_3 thin film was incorporated into N-Bi_2Se_3/P-$CuScO_2$ infrared transparent heterojunction diodes because of its remarkable optical transparency in the wide-band infrared region and great *n*-type electrical conductivity. The diodes had an abrupt interface and exhibited rectifying I-V characteristics with the threshold voltage of ~3.3 V. It provides a promising window electrodes alternatives in infrared detectors, as well as other scenarios in the wide infrared wavelength range. Another research article from Luo et al. investigated a strong coupled system composed of MAPbIxCl3-x perovskite film and Al conical nanopits array by steady-state measurements, which experimentally demonstrated that strong coupling could be achieved with SPs and free charge carriers generated in $CH_3NH_3PbCl_XI_{3-X}$ film. Benefiting from intriguing phenomena originated in strong coupling regime, this work is conducive to develop low-cost nanoplasmonic optoelectronic devices working in a strong coupling regime.

The investigation on transparent conductive electrode is an important complementary part to development of flexible optoelectronic devices in next-generation wearable display and lighting fields (Fan et al., 2019; Kayser and Lipomi, 2019; Wang et al., 2019; Chen et al., 2020). A minireview from Hou et al. firstly systematically analysed advantages and shortcomings of several notable alternative transparent electrodes, and focused on the recent advances in silver nanowire electrodes for flexible organic/perovskite light-emitting diodes regarding the relationship between electrode optimization and device performance. They have presented a perspective on the current challenges and future directions for development of physical mechanisms and encapsulation approach in flexible OLEDs and PeLEDs.

In brief, this Research Topic presents some excellent minireviews and leading-edge researches on the recent advances in micro-nanostructured optoelectronic devices, which shows great potential in military and numerous national economy fields. At this point, we would like to thank all those who have devoted valuable time and effort to this special issue. At the same time, we would also thank the readers for their interests on this special issue. Lastly, we sincerely hope that this Research Topic will inspire the enthusiasm of researchers about micro-nanostructures in optoelectronic devices.

AUTHOR CONTRIBUTIONS

Y-FLiu—Participated in the writing and revision of the research topic editorial. In addition participated as topic editor and promoted the research topic. X-MG—Participated in the writing and revision of the research topic editorial. Y-FLi—Participated in the writing and revision of the research topic editorial. In addition participated as topic editor and promoted the research topic.

REFERENCES

Bi, Y.-G., Feng, J., Li, Y.-F., Zhang, X.-L., Liu, Y.-F., Jin, Y., et al. (2013). Broadband Light Extraction from White Organic Light-Emitting Devices by Employing Corrugated Metallic Electrodes with Dual Periodicity. *Adv. Mater.* 25, 6969–6974. doi:10.1002/adma.201302367

Bonaccorso, F., Sun, Z., Hasan, T., and Ferrari, A. C. (2010). Graphene Photonics and Optoelectronics. *Nat. Phot.* 4, 611–622. doi:10.1038/nphoton.2010.186

Cao, J., and Yan, F. (2021). Recent Progress in Tin-Based Perovskite Solar Cells. *Energy Environ. Sci.* 14, 1286–1325. doi:10.1039/d0ee04007j

Chen, X., Xu, G., Zeng, G., Gu, H., Chen, H., Xu, H., et al. (2020). Realizing Ultrahigh Mechanical Flexibility and >15% Efficiency of Flexible Organic Solar Cells via a "Welding" Flexible Transparent Electrode. *Adv. Mater.* 32, e1908478. doi:10.1002/adma.201908478

Choi, D. H., Nam, S. K., Jung, K., and Moon, J. H. (2019). 2D Photonic Crystal Nanodisk Array as Electron Transport Layer for Highly Efficient Perovskite Solar Cells. *Nano Energy* 56, 365–372. doi:10.1016/j.nanoen.2018.11.050

Fan, X., Nie, W., Tsai, H., Wang, N., Huang, H., Cheng, Y., et al. (2019). PEDOT:PSS for Flexible and Stretchable Electronics: Modifications, Strategies, and Applications. *Adv. Sci.* 6, 1900813. doi:10.1002/advs.201900813

Feng, J., Liu, Y.-F., Bi, Y.-G., and Sun, H.-B. (2017). Light Manipulation in Organic Light-Emitting Devices by Integrating Micro/Nano Patterns. *Laser Photon. Rev.* 11, 1600145. doi:10.1002/lpor.201600145

Fu, X., Mehta, Y., Chen, Y. A., Lei, L., Zhu, L., Barange, N., et al. (2021). Directional Polarized Light Emission from Thin-Film Light-Emitting Diodes. *Adv. Mater.* 33, 2006801. doi:10.1002/adma.202006801

Fusella, M. A., Saramak, R., Bushati, R., Menon, V. M., Weaver, M. S., Thompson, N. J., et al. (2020). Plasmonic Enhancement of Stability and Brightness in Organic Light-Emitting Devices. *Nature* 585, 379–382. doi:10.1038/s41586-020-2684-z

Joo, W.-J., Kyoung, J., Esfandyarpour, M., Lee, S.-H., Koo, H., Song, S., et al. (2020). Metasurface-Driven OLED Displays Beyond 10,000 Pixels Per Inch. *Science* 370, 459–463. doi:10.1126/science.abc8530

Kayser, L. V., and Lipomi, D. J. (2019). Stretchable Conductive Polymers and Composites Based on PEDOT and PEDOT:PSS. *Adv. Mater.* 31, 1806133. doi:10.1002/adma.201806133

Linic, S., Chavez, S., and Elias, R. (2021). Flow and Extraction of Energy and Charge Carriers in Hybrid Plasmonic Nanostructures. *Nat. Mater.* 20, 916–924. doi:10.1038/s41563-020-00858-4

Liu, W., Liu, M., Liu, X., Wang, X., Deng, H. X., Lei, M., et al. (2020). Recent Advances of 2D Materials in Nonlinear Photonics and Fiber Lasers. *Adv. Opt. Mater.* 8, 1901631. doi:10.1002/adom.201901631

Lopez-Sanchez, O., Lembke, D., Kayci, M., Radenovic, A., and Kis, A. (2013). Ultrasensitive Photodetectors Based on Monolayer MoS2. *Nat. Nanotech* 8, 497–501. doi:10.1038/nnano.2013.100

Mao, P., Liu, C., Li, X., Liu, M., Chen, Q., Han, M., et al. (2021). Single-Step-Fabricated Disordered Metasurfaces for Enhanced Light Extraction from LEDs. *Light Sci. Appl.* 10, 180. doi:10.1038/s41377-021-00621-7

Wang, C., Xia, K., Wang, H., Liang, X., Yin, Z., and Zhang, Y. (2019). Advanced Carbon for Flexible and Wearable Electronics. *Adv. Mater.* 31, 1801072. doi:10.1002/adma.201801072

Ye, J., Byranvand, M. M., Martínez, C. O., Hoye, R. L. Z., Saliba, M., and Polavarapu, L. (2021). Defect Passivation in Lead-Halide Perovskite Nanocrystals and Thin Films: Toward Efficient LEDs and Solar Cells. *Angew. Chem. Int. Ed.* 60, 21636–21660. doi:10.1002/anie.202102360

Zhou, L., Zhou, Y., Fan, B. L., Nan, F., Zhou, G. H., Fan, Y. Y., et al. (2020). Tailored Polarization Conversion and Light-Energy Recycling for Highly Linearly Polarized White Organic Light-Emitting Diodes. *Laser Photon. Rev.* 14, 1900341. doi:10.1002/lpor.201900341

Conflict of Interest: The authors declare that the research was conducted in the absence of any commercial or financial relationships that could be construed as a potential conflict of interest.

Publisher's Note: All claims expressed in this article are solely those of the authors and do not necessarily represent those of their affiliated organizations, or those of the publisher, the editors and the reviewers. Any product that may be evaluated in this article, or claim that may be made by its manufacturer, is not guaranteed or endorsed by the publisher.

frontiers in Chemistry

MINI REVIEW
published: 28 July 2021
doi: 10.3389/fchem.2021.737679

Light Management With Grating Structures in Optoelectronic Devices

Wei Wang[1,2,3], *Gong Wang*[1,2]*, *Yang Zhang*[4], *Xiang-Chao Sun*[3], *Yu Yu*[1,2] *and Yudong Lian*[1,2]

[1]*Center for Advanced Laser Technology, Hebei University of Technology, Tianjin, China,* [2]*Hebei Key Laboratory of Advanced Laser Technology and Equipment, Tianjin, China,* [3]*State Key Laboratory of Integrated Optoelectronics, College of Electronic Science and Engineering, Jilin University, Changchun, China,* [4]*Department of Experimental Pharmacology and Toxicology, School of Pharmacy, Jilin University, Changchun, China*

Ordered and patterned micro/nanostructure arrays have emerged as powerful platforms for optoelectronic devices due to their unique ordered-dependent optical properties. Among various structures, grating structure is widely applied because of its simple fabrication process, easy adjusting of size and morph, and efficient light trapping. Herein, we summarized recent developments of light management with grating structures in optoelectronic devices. Typical mechanisms about the grating structures in optoelectronic devices have been reviewed. Moreover, the applications of grating structures in various optoelectronic devices have been presented. Meanwhile, the remaining bottlenecks and perspectives for future development have been discussed.

Keywords: grating structures, optoelectronic devices, micro/nanostructure, nanoimprint lithography, light management

OPEN ACCESS

Edited by:
Yun-Fei Li,
Hebei University of Technology, China

Reviewed by:
Yangang Bi,
The University of Hong Kong, SAR China
Zhuo-Chen Ma,
Shanghai Jiao Tong University, China
Rongqing Xu,
Nanjing University of Posts and Telecommunications, China

***Correspondence:**
Gong Wang
wanggong@hebut.edu.cn

Specialty section:
This article was submitted to Nanoscience, a section of the journal Frontiers in Chemistry

Received: *07 July 2021*
Accepted: *19 July 2021*
Published: *28 July 2021*

Citation:
Wang W, Wang G, Zhang Y, Sun X-C, Yu Y and Lian Y (2021) Light Management With Grating Structures in Optoelectronic Devices. Front. Chem. 9:737679. doi: 10.3389/fchem.2021.737679

INTRODUCTION

There are many interesting and ordered micro/nanostructures in nature, organisms and plants, which play essential roles. The micro/nanostructures in lotus leaves can make water droplets roll freely (Zhang et al., 2012b); while rose petals can keep water droplets stay on it with the help of micro/nanostructures (Zhang et al., 2012a). The micro/nanostructures of reed leaves can guide the movement direction of water droplets (Wang et al., 2015). At the same time, more and more researches focus on applying micro/nanostructures in science. Ordered or patterned micro/nanostructure arrays have emerged as powerful platforms for cutting-edge applications due to their unique ordered-dependent properties, especially in optoelectronic devices, such as photodetectors, light emitting diodes, lasers, solar cells, bioelectronic, etc. The reasons why the micro/nanostructure arrays can be widely applied in many fields are they can enhance light scattering and reduce light reflection, improve the light extraction of organic light-emitting devices (OLEDs) and surface-to-volume ratio (Gao et al., 2021), produce photonic metasurfaces (Li et al., 2021). Various functions can be realized by adjusting the size, arrangement, and shape of each micro/nanostructure. Such as the light scattering effect can be improved by concave nanonets structure. Meanwhile, the antireflection effect can be realized by nanocone structure.

At present, the fabrication of excellent micro/nanostructure always depends on the development of nanofabrication technology, including templated method, lithographic technology, *in situ* preparation, direct laser writing, and self-assembly approaches. Many novel architectures have been fabricated through the above technologies to improve the performance of devices, such as microlens arrays, gratings, pyramid arrays, micro/nanorods, nanowire arrays, microsphere arrays, and so on (Zhmakin, 2011; Geng et al., 2014; Zhao and Ma, 2017). Microlens are arranged in 2D arrays to form an ordered array, micrometer or millimeter size usually are applied in light collimating

(Song et al., 2013; Yu et al., 2013; Yuan et al., 2018). In addition, the microlens array can also enhance light trapping to improve the performance of optoelectronic devices (Choy et al., 2014; Kang et al., 2015). More importantly, they can be used in 3D imaging systems with large view angles, high temporal resolution, and so on (Yuan et al., 2018). Except for the microlens array, Chueh et al. reported the pyramid-patterned sapphire substrate could enhance the strong light interaction between MoS_2 bilayers and the substrate to improve photodetector performance (Wang et al., 2017). Moreover, it has been speculated that a perovskite whispering gallery mode (WGM) microsphere array would have higher optical absorption for solar cells (Grandidier et al., 2011; Mihi et al., 2013). And with the help of 3D structures of nanowire and nanorod arrays, which make incident light undergo multiple scattering inside the structure. They are usually used in various solar conversion devices to enhance light-harvesting ability (Cho et al., 2011). Nanorod array also can be applied in the field of light-emitting diodes (LED), Chang et al. reported a kind of LED that could adjust the polarization of the emitted light with the help of nanorod arrays (Chou et al., 2018). Every structure has unique properties, while the gratings architectures are more popular due to the simple fabrication process, easy adjusting of size and morph, and excellent performance of light trapping. The grating structure has been applied in most optoelectronic devices and other cutting-edge applications. It's necessary to summarize the researches about grating structure in optoelectronic devices.

In this minireview, we focus on the recent advancements in the application of grating structure in optoelectronic devices. Firstly, the typical light trapping mechanisms of grating structures in devices are discussed. And typical examples, such as the applications in photodetectors, solar cells, organic light-emitting devices, and lasers are summarized. Finally, the challenges and future perspectives for optoelectronic devices with grating structures are also discussed.

MECHANISM

Micro/nanostructures largely determined the performance of optoelectronic devices due to they can influence the optical properties of devices. However, it is important to balance the relationship between optical properties and electrical properties. The light management mechanisms of grating structure in optoelectronic devices are usually summarized as the resonant effect, plasmonic effect and scattering enhancements. Among various resonant strategies, the Mie theory is generally applied to spherical structures and whispering gallery mode (WGM) usually used to the sphere, toroid, and ring structures. These structures can limit light circulate at the periphery of the resonator. As for the grating structure, guided mode resonance (GMR) is applied. The normally incident plane wave can be coupled into a waveguide mode with the help of diffraction gratings (Yamada et al., 2017). The grating layer and supporting layer are necessary for GMR. They can induce sharp reflection and transmission anomalies. There will be a strong interaction between light and matter as long as it matches the outgoing emission or incoming excitation with the guided mode wavelengths (Collin, 2014). As shown in **Figure 1A**, Cunningham et al. fabricate Si_3N_4 periodic grating structures on a kind of soda-lime glass to form a GMR filter. While the GMR can be excited when the incident light satisfies Bragg diffraction by adjusting the period, depth of grating, and thickness of waveguide (Liu et al., 2011; Ko and Magnusson, 2018). Rational grating structures can induce plasmonic effects because these structures can redistribute optical fields and scatter light (Meinzer et al., 2014). Surface plasmon polariton (SPP) loss usually appeared in OLED devices, and the loss happened at the interface between dielectric and metal, which metal always serves as electrodes for OLED. And the metallic film can couple light to induce SPP modes, which transfer incident light into photo carriers (Atwater and Polman, 2010). Actually, SPP is a guided electromagnetic surface mode with transverse magnetic polarization. In general, the SPP modes coupled with excitons can't support the energy couple out from the OLED devices for the traditional planar OLED with non-grating structures. As shown in **Figure 1B**, Barnes et al. have illustrated that the SPP loss was up to ~40% for traditional planar OLEDs, resulting in the obvious limitation on the OLED development (Hobson et al., 2002). It is noticed that the grating structures within OLED devices can realize light extraction effectively. Such as the tunable grating array was fabricated on the metallic electrode to match the SPP mode with the energy and momentum of light along with the interface, leading to the occurrence of SPP resonance and increase of light extraction (Zayats et al., 2005). Besides the resonant effect and plasmonic effect, grating structures also can improve light scattering efficiently due to the structure prolong the optical path and increase the reflections and refractions (Han and Chen, 2010; Chi et al., 2017). The absorption ability always is limited by the Lambertian limit for films. However, light scattering will be increased among the micro/nanostructures when the size of each structure is larger than the wavelength. For example, the grating structures can produce multiple reflections and refractions of the incident light, leading to the prolongation of optical path length and the increase of absorption to reach or exceed the Lambertian limit. There are two typical ways to fabricate the increased scattering surface, including integrating a textured layer and preparing ordered structures. Such as the grating structure with an appropriate periodicity that meets the condition of Bragg scattering can make the light appear Bragg-scattered to enhance the light extraction (Bruetting et al., 2013; Cai and Qi, 2015).

THE APPLICATIONS IN OPTOELECTRONIC DEVICES

Photodetectors

The photodetector is a kind of typical optoelectronic device, which can be adopted in many fields like clinical medical, aerospace industry, military project, communication, and sensors since photodetector can convert the light signal into electrical signals for followed processes. However, photodetector development still faces low conversion

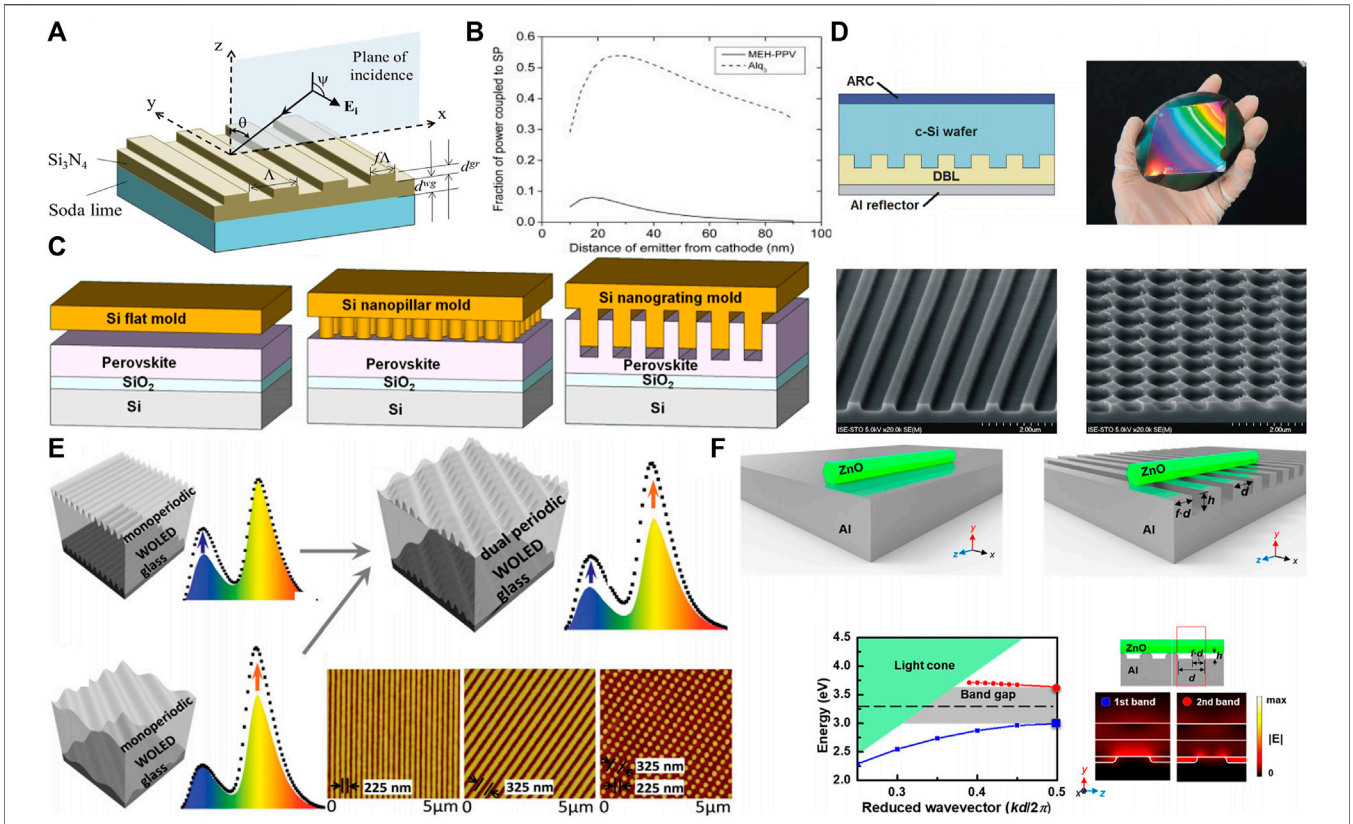

FIGURE 1 | The grating structures in optoelectronic devices, **(A)** GMR filter with grating structure. **(B)** The calculated fraction of power lost from radiative excitons to surface plasmon modes is shown as a function of position of the exciton within the organic layer. **(C)**. Schematic of nanoimprint lithography process with different Si molds. **(D)** The schematic diagram, photograph and SEM of the grating structures in solar cell. **(E)** Schematic of the broadband light extraction using OLED with dual-periodic grating structures and the morphologies of a serious of grating structures. **(F)** Schematic representation and characteristics of surface plasmon waveguide and periodic grating structures. Reproduced from Cunningham et al. (2011) with permission of Optical Society of America. Reproduced from Barnes et al. (2002) with permission of WILEY. Reproduced from Hu et al. (2016) with permission of American Chemical Society. Reproduced from Mellor et al. (2013) with permission of Optical Society of America. Reproduced from Sun et al. (2013) with permission of WILEY. Reproduced from Lin et al. (2018) with permission of American Chemical Society.

efficiency, while the micro/nanostructures can improve the light absorption by various strategies (Wang and Kim, 2017; Zhou and Huang, 2018). Among many structures, gratings play an essential role. For example, Hu et al. reported an excellent perovskite photodetector with nanograting through nanoimprint lithography (**Figure 1C**). The performance of photodetector was improved after grating imprinted. The width of fabricated nanograting was 270 nm, and the pitch was 600 nm, which could reduce reflectance during the entire spectrum. Meanwhile, the transmission also appeared to decrease in the range of 550–800 nm. In addition, perovskite film showed higher crystallinity under the appearance of nanograting. The combined effects lead to the improvement of ~35 times in responsivity and ~7 times in on/off current ratio (Wang et al., 2016). Besides the above traditional grating structure, more complex grating structures are applied in many devices gradually. Li et al. prepared a kind of moiré perovskite photodetector using a stacked dual shallow grating structure (Song et al., 2021). The dual grating structure induced feedback reflection, diffraction, and appearance of waveguide modes, resulting in the enhanced light-harvesting of the photodetector. Compared with flat perovskite photodetector, the detectivity and responsivity were improved by 7.8 and 6.7 times, respectively. In practical applications, the polarization states of light usually have more potential value. Hence, the detection of polarized light also is important. For example, Xia et al. reported a photodetector comprised of a stable 2D layered Ruddlesden–Popper perovskite arranged in grating structures. And the photodetector performed high responsivity of 3.5 AW^{-1}, detectivity exceeding 1×10^{15} Jones, and a fast response with a rise time of 4.1 ms and a decay time of 3.3 ms. It is noticed that the photodetector could realize polarization detection, in which the photocurrent varies with polarization angle due to the different dielectric constants of the perovskite grating structures in different directions (Li et al., 2019).

Solar Cells

The conversion of environmental energy into effective energy is more critical for modern society. The solar cell is an effective strategy in this field. Solar cells usually absorb photons to induce the generation and transport of charge carriers, and the electric energy was collected finally (Lewis, 2016; Polman et al., 2016). Although solar cells have been developed for many years, there

are still many problems, including the path length of light absorption mismatched the diffusion length of photo-generated carriers. While the increase of path length of the light absorption layer means the thickness of the absorbing layer increased, limiting the portability and the cost. The ordered grating structures can solve the above problems by unique optical properties without changing the thickness of light absorbing layer. Mellor et al. reported an excellent crystalline silicon solar cell with diffraction gratings fabricated through nanoimprinted technology. As shown in **Figure 1D**, the grating structure enhanced the incident light absorption obviously, especially the crossed grating structure with the depth of 200 nm appeared the stronger ability in light absorption than linear grating with the depth of 300 nm. Firstly, weakly absorbed photons were trapped and deflected into oblique orders through the diffraction gratings on the rear-side. Secondly, the path of light absorption was extended efficiently because the incident light was trapped within the absorber layer by the total internal reflection of the front side (Mellor et al., 2013). As mentioned above, the perovskite with grating structures can improve the ability of light absorption and scattering. At the same time, the crystallinity of perovskite also was enhanced. Therefore, the patterned perovskite not only was applied in photodetector but also was applied in solar cells. Song et al. reported a new imprinting method to fabricate the solar cells using the perovskite with grating structures as the active layer. And the larger area grating structures were fabricated by commercial optical discs, which the size of grating depended on the area of the CD or DVD (The diameter of CD and DVD is 12 cm). The improved scattering and absorption abilities of solar cells can trap more incident light and suppress carrier recombination simultaneously. Utilizing CD or DVD as a mold would have different grating structures, for example, when CD as a mold leading to the grating period and line width was ~1.5 and ~1.0 μm, respectively. When DVD was a mold, the grating period and line width was ~0.75 and ~0.5 μm, respectively. And the heights of gratings were all ~0.1 μm. Actually, the height of structures will influence the performance of devices, such as the continuity of perovskite film can be broken when the height was exceeded the threshold value. On the opposite, the light trapping effect will be limited by the low height. Therefore, it is essential to consider the range of height. Under the synergistic effect of the above results, the power conversion efficiency and photocurrent density of perovskite solar cells with grating structures compared with non-structures have been improved from 16.71 to 19.71% and 21.67 mA cm^{-2} to 23.11 mA cm^{-2}. The authors have proved the grating structure has perfect homogeneity through the atomic force microscope images. Additionally, the stability of perovskite solar cells was also enhanced that the efficiency still keeps above 90% after one month exposure on air (Wang et al., 2018).

ORGANIC LIGHT-EMITTING DEVICE

Organic light-emitting devices (OLEDs) are a kind of essential and representative optoelectronic devices, which have been applied in display and light panels with the advantages of color tunability, low cost, self-emitting property, and so on. However, there is an obvious problem in organic light-emitting devices, which is ~80% generated photons are trapped in devices leading to low light extraction efficiency. It is noticed that the ordered micro/nanostructures within the OLEDs can induce the outcoupling effect of trapped photons and regulate the emitting properties to improve light extraction efficiency (Feng et al., 2017). During the internal light extraction processes, about 40% SPPs mode loss happened around the interface between organic layer and electrode. And the grating structure can relieve SPP loss. Therefore, the fabrication of micro/nanostructures on a metal electrode is important because the electrode has better stability. Ma et al. prepared grating structures on the ultrathin gold electrode through polymer-assisted thermal nanoimprint technology, and the fabricated gratings were 320 nm in period and 60 nm in depth. Taking the advantages of nanograting structures, the momenta of SPPs and photons could realize momentum compensation to improve light extraction and performance of OLEDs (Ma et al., 2020). For the white organic light-emitting devices (WOLEDs), broadband light extraction is deserved to devote the effort. As shown in **Figure 1E**, Sun et al. reported a kind of WOLEDs involved dual-periodic gratings, in which the maximum current efficiency was enhanced by 37% (from 16.27 cd/A up to 22.33 cd/A). In addition, compared to single periodic gratings, the dual-periodic gratings could broaden the SPP resonance (Bi et al., 2013). Besides the unpolarized light, the polarized light has become more and more important as an important and appealing functional expansion in practical applications. And the grating structures also was applied in OLEDs to emit linear polarized light. Zhou et al. prepared a series of aluminum and polyurethane acrylate nanograting structures on the green OLED substrate using developed soft nanoimprinting technology to emit linear polarized light. The devices produced an angle-invariant average extinction ratio as high as 20dB when the viewing angle within ± 60° due to both surface plasmons and cavity modes contributed to the TM-polarized light selection (Zhou et al., 2020). At the same time, the development of nanofabrication technology influences the light extraction efficiency of OLEDs to a considerable degree. At present, there are two typical methods to fabricate grating structures, including laser ablating method and nanoimprinting method. The laser ablation method takes advantages of simple processes and the adjustable period according to the applied laser wavelength to reach the smaller grating period. However, the substrate may be damaged by the high power of the laser during the ablation process. In contrast, the nanoimprint method can avoid the above damages because nanoimprint is a secondary transfer process. Therefore, compared to laser ablation, the nanoimprint method usually involves complex fabrication processes and the limitation of long periods. For example, Sun et al. utilized a simple one-step laser ablating method to prepare the OLEDs with periodic grating structures. The method of two interference beams was taken to avoid destroying the polymers because of the low ablation threshold. The grating structures play an important role in recovering power lost whatever in SPPs or waveguide mode,

and the efficiency was proved enhanced three times finally (Bai et al., 2011).

Lasers

For the rapid development of integrated photonic circuits or chips, a miniature laser source is necessary. Laser with perfect intensity and directionality can be emitted from lasers through stimulated emission of radiation and amplification. Organic-inorganic-perovskites can be applied in miniature lasers due to their excellent and unique properties, including tunable bandgaps. For example, Gu et al. firstly reported perovskite distributed feedback resonator with grating structures using thermal nanoimprint lithography, which proposed a new method for the design and fabrication of perovskite lasers. The resonator performed the ability of narrow amplified spontaneous emission (The full width half-maximum was 2.4 nm) even the pump power was only 0.1 W/cm^2 and a 16-fold reduction than pristine thin film (Gharajeh et al., 2018). Actually, both light and electric sources can excite the lasers, such as Takenobu et al., who reported electroluminescence from a single-crystal light-emitting transistor (LET) with a grating resonator using the soft ultraviolet-nanoimprint lithography. And the electroluminescence could be controlled by the sub-micrometer grating structure. Moreover, the final realization of single-mode lasing depended on the Bragg diffraction and mode coupling distributed feedback (DFB) system. The above research overcame the combination problem between LET and DFB resonators (Maruyama et al., 2015). Except for frontier research, the lasers with grating structures have been applied in practical applications. Lin et al. reported a kind of hybrid plasmonic nanolaser for sensing applications, and the role of Al grating structures were plasmonic Bragg reflectors to decrease the mirror loss. As shown in **Figure 1F**, the nanolaser could serve as a refractive index sensor to detect glucose solutions. The sensitivity of the nanolaser was 249 nm/RIU under the resonant wavelength of 373 nm (Cheng et al., 2018). Strong light trapping ability will bring new paths for next-generation lasers.

CONCLUSION AND OUTLOOK

In this minireview, we have summarized the mechanisms of grating structures in photon-related devices, including resonant effect, scattering enhancements, and plasmonic effect. Taking advantages of light management strategies of grating structures, the structures have been applied in many optoelectronic devices, such as photodetectors, solar cells, organic light-emitting devices, and lasers. Although the various devices have proved the important role of grating structures successfully. However, there are still many bottlenecks that need to be solved, including 1. how to improve the controllability of fabrication for grating structure; 2. how to balance the relationship between optical and electrical performance; 3. although the grating structure is more simple than others, but decrease the cost and simplify the preparing processes are still crucial for applications in business. Nevertheless, with the rapid developments of nanofabrication technologies, rational structure design, and advanced fundamental theories, more grating structures will be applied in excellent optoelectronic devices, which will bring our better daily life.

AUTHOR CONTRIBUTIONS

All authors listed have made a substantial, direct and intellectual contribution to the work, and approved it for publication.

FUNDING

This work was supported by the National Natural Science Foundation of China (Grant No. 62004059, 62005074, and 61905062) and Natural Science Foundation of Hebei Province (No. F2021202047).

REFERENCES

Atwater, H. A., and Polman, A. (2010). Plasmonics for Improved Photovoltaic Devices. *Nat. Mater* 9 (3), 205–213. doi:10.1038/nmat2629

Bai, Y., Feng, J., Liu, Y.-F., Song, J.-F., Simonen, J., Jin, Y., et al. (2011). Outcoupling of Trapped Optical Modes in Organic Light-Emitting Devices with One-step Fabricated Periodic Corrugation by Laser Ablation. *Org. Electron.* 12 (11), 1927–1935. doi:10.1016/j.orgel.2011.08.004

Bi, Y.-G., Feng, J., Li, Y.-F., Zhang, X.-L., Liu, Y.-F., Jin, Y., et al. (2013). Broadband Light Extraction from White Organic Light-Emitting Devices by Employing Corrugated Metallic Electrodes with Dual Periodicity. *Adv. Mater.* 25 (48), 6969–6974. doi:10.1002/adma.201302367

Bruetting, W., Frischeisen, J., Schmidt, T. D., Scholz, B. J., and Mayr, C. (2013). Device Efficiency of Organic Light-Emitting Diodes: Progress by Improved Light Outcoupling. *Phys. Status Solidi A App. Mater. Sci.* 210 (1), 44–65. doi:10.1002/pssa.201228320

Cai, J., and Qi, L. (2015). Recent Advances in Antireflective Surfaces Based on Nanostructure Arrays. *Mater. Horiz.* 2 (1), 37–53. doi:10.1039/C4MH00140K

Cheng, P.-J., Huang, Z.-T., Li, J.-H., Chou, B.-T., Chou, Y.-H., Lo, W.-C., et al. (2018). High-Performance Plasmonic Nanolasers with a Nanotrench Defect Cavity for Sensing Applications. *Acs Photon.* 5 (7), 2638–2644. doi:10.1021/acsphotonics.8b00337

Chi, K., Yang, L., Liu, Z., Gao, P., Ye, J., and He, S. (2017). Large-scale Nanostructured Low-Temperature Solar Selective Absorber. *Opt. Lett.* 42 (10), 1891–1894. doi:10.1364/OL.42.001891

Cho, I. S., Chen, Z., Forman, A. J., Kim, D. R., Rao, P. M., Jaramillo, T. F., et al. (2011). Branched TiO2Nanorods for Photoelectrochemical Hydrogen Production. *Nano Lett.* 11 (11), 4978–4984. doi:10.1021/nl2029392

Chou, M.-C., Lin, C.-Y., Lin, B.-L., Wang, C.-H., Chang, S.-H., Lai, W.-C., et al. (2018). Polarization-Selecting III-Nitride Elliptical Nanorod Light-Emitting Diodes Fabricated with Nanospherical-Lens Lithography. *ACS Nano* 12 (8), 8748–8757. doi:10.1021/acsnano.8b04933

Choy, W. C. H., Chan, W. K., and Yuan, Y. (2014). Recent Advances in Transition Metal Complexes and Light-Management Engineering in Organic Optoelectronic Devices. *Adv. Mater.* 26 (31), 5368–5399. doi:10.1002/adma.201306133

Collin, S. (2014). Nanostructure Arrays in Free-Space: Optical Properties and Applications. *Rep. Prog. Phys.* 77 (12), 126402. doi:10.1088/0034-4885/77/12/126402

Feng, J., Liu, Y.-F., Bi, Y.-G., and Sun, H.-B. (2017). Light Manipulation in Organic Light-Emitting Devices by Integrating Micro/nano Patterns. *Laser Photon. Rev.* 11 (2), 1600145. doi:10.1002/lpor.201600145

Gao, X.-m., Liu, Y. F., Liu, Y.-f., Zhang, H.-j., Zhang, T.-r., Bi, Y.-g., et al. (2021). Nanoimprinted Structures for Organic Light-Emitting Devices and Lasers. *Chin. J. Liq. Cryst. Disp.* 36 (1), 8–20. doi:10.37188/cjlcd.2020-0277

Geng, C., Wei, T., Wang, X., Shen, D., Hao, Z., and Yan, Q. (2014). Enhancement of Light Output Power from LEDs Based on Monolayer Colloidal Crystal. *Small* 10 (9), 1668–1686. doi:10.1002/smll.201303599

Gharajeh, A., Haroldson, R., Li, Z., Moon, J., Balachandran, B., Hu, W., et al. (2018). Continuous-wave Operation in Directly Patterned Perovskite Distributed Feedback Light Source at Room Temperature. *Opt. Lett.* 43 (3), 611–614. doi:10.1364/ol.43.000611

Grandidier, J., Callahan, D. M., Munday, J. N., and Atwater, H. A. (2011). Light Absorption Enhancement in Thin-Film Solar Cells Using Whispering Gallery Modes in Dielectric Nanospheres. *Adv. Mater.* 23 (10), 1272–1276. doi:10.1002/adma.201004393

Han, S. E., and Chen, G. (2010). Toward the Lambertian Limit of Light Trapping in Thin Nanostructured Silicon Solar Cells. *Nano Lett.* 10 (11), 4692–4696. doi:10.1021/nl1029804

Hobson, P. A., Wedge, S., Wasey, J. A. E., Sage, I., and Barnes, W. L. (2002). Surface Plasmon Mediated Emission from Organic Light-Emitting Diodes. *Adv. Mater.* 14 (19), 1393–1396. doi:10.1002/1521-4095(20021002)14:19<1393::Aid-adma1393>3.0.Co;2-b

Kang, G., Yoo, J., Ahn, J., and Kim, K. (2015). Transparent Dielectric Nanostructures for Efficient Light Management in Optoelectronic Applications. *Nano Today* 10 (1), 22–47. doi:10.1016/j.nantod.2015.01.008

Ko, Y. H., and Magnusson, R. (2018). Wideband Dielectric Metamaterial Reflectors: Mie Scattering or Leaky Bloch Mode Resonance?. *Optica* 5 (3), 289–294. doi:10.1364/OPTICA.5.000289

Lewis, N. S. (2016). Research Opportunities to advance Solar Energy Utilization. *Science* 351 (6271), aad1920. doi:10.1126/science.aad1920

Li, H., Gu, S., Zhang, Q., Song, E., Kuang, T., Chen, F., et al. (2021). Recent Advances in Biofluid Detection with Micro/nanostructured Bioelectronic Devices. *Nanoscale* 13 (6), 3436–3453. doi:10.1039/d0nr07478k

Li, S.-X., Zhang, G.-P., Xia, H., Xu, Y.-S., Lv, C., and Sun, H.-B. (2019). Template-confined Growth of Ruddlesden-Popper Perovskite Micro-wire Arrays for Stable Polarized Photodetectors. *Nanoscale* 11 (39), 18272–18281. doi:10.1039/c9nr05396d

Liu, J.-N., Schulmerich, M. V., Bhargava, R., and Cunningham, B. T. (2011). Optimally Designed Narrowband Guided-Mode Resonance Reflectance Filters for Mid-infrared Spectroscopy. *Opt. Express* 19 (24), 24182–24197. doi:10.1364/OE.19.024182

Ma, C., Liu, Y.-F., Gao, X.-M., Bi, Y.-G., Zhang, X.-L., Yin, D., et al. (2020). Enhanced Efficiency of Organic Light-Emitting Devices by Using a Directly Imprinted Nanopillared Ultrathin Metallic Electrode. *Opt. Lett.* 45 (17), 4879–4882. doi:10.1364/ol.402754

Maruyama, K., Sawabe, K., Sakanoue, T., Li, J., Takahashi, W., Hotta, S., et al. (2015). Ambipolar Light-Emitting Organic Single-crystal Transistors with a Grating Resonator. *Sci. Rep.* 5. doi:10.1038/srep10221

Meinzer, N., Barnes, W. L., and Hooper, I. R. (2014). Plasmonic Meta-Atoms and Metasurfaces. *Nat. Photon* 8 (12), 889–898. doi:10.1038/nphoton.2014.247

Mellor, A., Hauser, H., Wellens, C., Benick, J., Eisenlohr, J., Peters, M., et al. (2013). Nanoimprinted Diffraction Gratings for Crystalline Silicon Solar Cells: Implementation, Characterization and Simulation. *Opt. Express* 21 (5), A295–A304. doi:10.1364/oe.21.00a295

Mihi, A., Bernechea, M., Kufer, D., and Konstantatos, G. (2013). Coupling Resonant Modes of Embedded Dielectric Microspheres in Solution-Processed Solar Cells. *Adv. Opt. Mater.* 1 (2), 139–143. doi:10.1002/adom.201200015

Polman, A., Knight, M., Garnett, E. C., Ehrler, B., and Sinke, W. C. (2016). Photovoltaic Materials: Present Efficiencies and Future Challenges. *Science* 352 (6283), aad4424. doi:10.1126/science.aad4424

Song, Q., Wang, Y., Vogelbacher, F., Zhan, Y., Zhu, D., Lan, Y., et al. (2021). Moiré Perovskite Photodetector toward High-Sensitive Digital Polarization Imaging. *Adv. Energ. Mater.*, 2100742. doi:10.1002/aenm.202100742

Song, Y. M., Xie, Y., Malyarchuk, V., Xiao, J., Jung, I., Choi, K.-J., et al. (2013). Digital Cameras with Designs Inspired by the Arthropod Eye. *Nature* 497 (7447), 95–99. doi:10.1038/nature12083

Wang, H., Haroldson, R., Balachandran, B., Zakhidov, A., Sohal, S., Chan, J. Y., et al. (2016). Nanoimprinted Perovskite Nanograting Photodetector with Improved Efficiency. *ACS Nano* 10 (12), 10921–10928. doi:10.1021/acsnano.6b05535

Wang, H., and Kim, D. H. (2017). Perovskite-based Photodetectors: Materials and Devices. *Chem. Soc. Rev.* 46 (17), 5204–5236. doi:10.1039/C6CS00896H

Wang, J.-N., Zhang, Y.-L., Liu, Y., Zheng, W., Lee, L. P., and Sun, H.-B. (2015). Recent Developments in Superhydrophobic Graphene and Graphene-Related Materials: from Preparation to Potential Applications. *Nanoscale* 7 (16), 7101–7114. doi:10.1039/C5NR00719D

Wang, S.-W., Medina, H., Hong, K.-B., Wu, C.-C., Qu, Y., Manikandan, A., et al. (2017). Thermally Strained Band Gap Engineering of Transition-Metal Dichalcogenide Bilayers with Enhanced Light-Matter Interaction toward Excellent Photodetectors. *ACS Nano* 11 (9), 8768–8776. doi:10.1021/acsnano.7b02444

Wang, Y., Wang, P., Zhou, X., Li, C., Li, H., Hu, X., et al. (2018). Diffraction-Grated Perovskite Induced Highly Efficient Solar Cells through Nanophotonic Light Trapping. *Adv. Energ. Mater.* 8 (12), 1702960. doi:10.1002/aenm.201702960

Yamada, K., Lee, K. J., Ko, Y. H., Inoue, J., Kintaka, K., Ura, S., et al. (2017). Flat-top Narrowband Filters Enabled by Guided-Mode Resonance in Two-Level Waveguides. *Opt. Lett.* 42 (20), 4127–4130. doi:10.1364/OL.42.004127

Yu, K., Fan, T., Lou, S., and Zhang, D. (2013). Biomimetic Optical Materials: Integration of Nature's Design for Manipulation of Light. *Prog. Mater. Sci.* 58 (6), 825–873. doi:10.1016/j.pmatsci.2013.03.003

Yuan, W., Li, L.-H., Lee, W.-B., and Chan, C.-Y. (2018). Fabrication of Microlens Array and its Application: A Review. *Chin. J. Mech. Eng.* 31 (1), 16. doi:10.1186/s10033-018-0204-y

Zayats, A. V., Smolyaninov, I. I., and Maradudin, A. A. (2005). Nano-optics of Surface Plasmon Polaritons. *Phys. Rep.* 408 (3), 131–314. doi:10.1016/j.physrep.2004.11.001

Zhang, Y.-L., Chen, Q.-D., Jin, Z., Kim, E., and Sun, H.-B. (2012a). Biomimetic Graphene Films and Their Properties. *Nanoscale* 4 (16), 4858–4869. doi:10.1039/C2NR30813D

Zhang, Y.-L., Xia, H., Kim, E., and Sun, H.-B. (2012b). Recent Developments in Superhydrophobic Surfaces with Unique Structural and Functional Properties. *Soft Matter* 8 (44), 11217–11231. doi:10.1039/C2SM26517F

Zhao, F., and Ma, D. (2017). Approaches to High Performance white Organic Light-Emitting Diodes for General Lighting. *Mater. Chem. Front.* 1 (10), 1933–1950. doi:10.1039/C6QM00365F

Zhmakin, A. I. (2011). Enhancement of Light Extraction from Light Emitting Diodes. *Phys. Rep.* 498 (4), 189–241. doi:10.1016/j.physrep.2010.11.001

Zhou, J., and Huang, J. (2018). Photodetectors Based on Organic-Inorganic Hybrid Lead Halide Perovskites. *Adv. Sci.* 5 (1), 1700256. doi:10.1002/advs.201700256

Zhou, L., Zhu, Y.-F., Zhang, Q.-Y., Zhou, Y., Wang, Y.-Z., Zhou, G.-H., et al. (2020). Highly Linearly Polarized Light Emission from Flexible Organic Light-Emitting Devices Capitalized on Integrated Ultrathin Metal-Dielectric Nanograting. *Opt. Express* 28 (9), 13826–13836. doi:10.1364/oe.391624

Conflict of Interest: The authors declare that the research was conducted in the absence of any commercial or financial relationships that could be construed as a potential conflict of interest.

Publisher's Note: All claims expressed in this article are solely those of the authors and do not necessarily represent those of their affiliated organizations, or those of the publisher, the editors and the reviewers. Any product that may be evaluated in this article, or claim that may be made by its manufacturer, is not guaranteed or endorsed by the publisher.

frontiers in Chemistry

MINI REVIEW
published: 13 December 2021
doi: 10.3389/fchem.2021.807605

Low Threshold Microlasers Based on Organic-Conjugated Polymers

Hong-xu Chen[1,2], *Meng-dan Qian*[1]*, *Kun Yu*[1]* and *Yu-fang Liu*[1]

[1]Henan Key Laboratory of Infrared Materials and Spectrum Measures and Applications, School of Physics, Henan Normal University, Xinxiang, China, [2]School of Artificial Intelligence, Jilin University, Changchun, China

Conjugated polymers have emerged as ideal organic laser materials for the excellent optoelectrical properties and facile processability. During a typical lasing process, resonator configurations with specific geometry are essential to provide optical feedback and then amplified light. Herein, we summarized the geometry and working mechanism of several typical resonator configurations formed with conjugated polymers. Meanwhile, recent advances in fabrication techniques and lasing performance are also discussed to provide new ideas for the design and optimization of microcavity geometries. Followed by the advances of practical applications in fields of laser sensing, bioimaging, and laser illumination/display, we make a summary of the existing bottlenecks and future perspectives of electrically driven organic lasers toward laser display and illumination.

Keywords: organic-conjugated polymers, microlasers, resonator configurations, micro/nanofabrication techniques, optical sensing

OPEN ACCESS

Edited by:
Yun-Fei Li,
Hebei University of Technology, China

Reviewed by:
Xiaofeng Fang,
Southern University of Science and Technology, China
Libo Zhou,
University of Connecticut, United States

***Correspondence:**
Meng-dan Qian
qianmengdan@htu.edu.cn
Kun Yu
yukun@htu.edu.cn

Specialty section:
This article was submitted to Nanoscience, a section of the journal Frontiers in Chemistry

Received: *02 November 2021*
Accepted: *10 November 2021*
Published: *13 December 2021*

Citation:
Chen H-x, Qian M-d, Yu K and Liu Y-f (2021) Low Threshold Microlasers Based on Organic-Conjugated Polymers. Front. Chem. 9:807605. doi: 10.3389/fchem.2021.807605

INTRODUCTION

In the past decades, lasers have led to great revolution in technology and industrial fields because of their unique and excellent properties, including high intensity, good monochromaticity, directionality, and strong coherence. The emergence of laser has greatly accelerated the development of technologies in industrial manufacturing, telecommunication, and biomedical science (Samuel and Turnbull, 2007). For instance, the scientific cognition is largely improved because of the ultra-high sensitivity and resolution in spectroscopy brought by lasers. Besides, lasers with low pumping thresholds hold promising applications in the display and lighting industry for their high brightness and monochromaticity that contribute to the highly vivid colors (Chellappan et al., 2010). The development of new lasers depends mainly on the advances of gain materials. According to early reports, both inorganic emitter materials and organic gain materials were well applied in the generation of lasers. The former materials, mostly inorganic semiconductors, generally have stable properties but inherent brittleness, requiring sophisticated processing techniques and costly configurations. By contrast, organic gain materials are easily available and mechanically flexible, allowing convenient fabrication of integratable photonic devices with low-cost processing equipment (Grivas and Pollnau, 2012). Moreover, organic molecules are of wide tunability in spectroscopy, and the chemical structures can be easily modified to satisfy the requirement of specific lasing wavelength and low pumping threshold (Xia et al., 2003). It has been found that various organic materials had high optical gain property and could be used as laser gain media, including some small organic dyes and conjugated polymers (Kuehne and Gather, 2016).

Organic-conjugated polymer is an attractive gain material because of the excellent optoelectronic property and structural processability for device fabrication (Amarasinghe et al., 2009). Conjugated polymers usually comprise long chain units with alternate single and double C–C bonds, which are responsible for their semiconducting property (**Figure 1A**). The remarkable photoelectronic

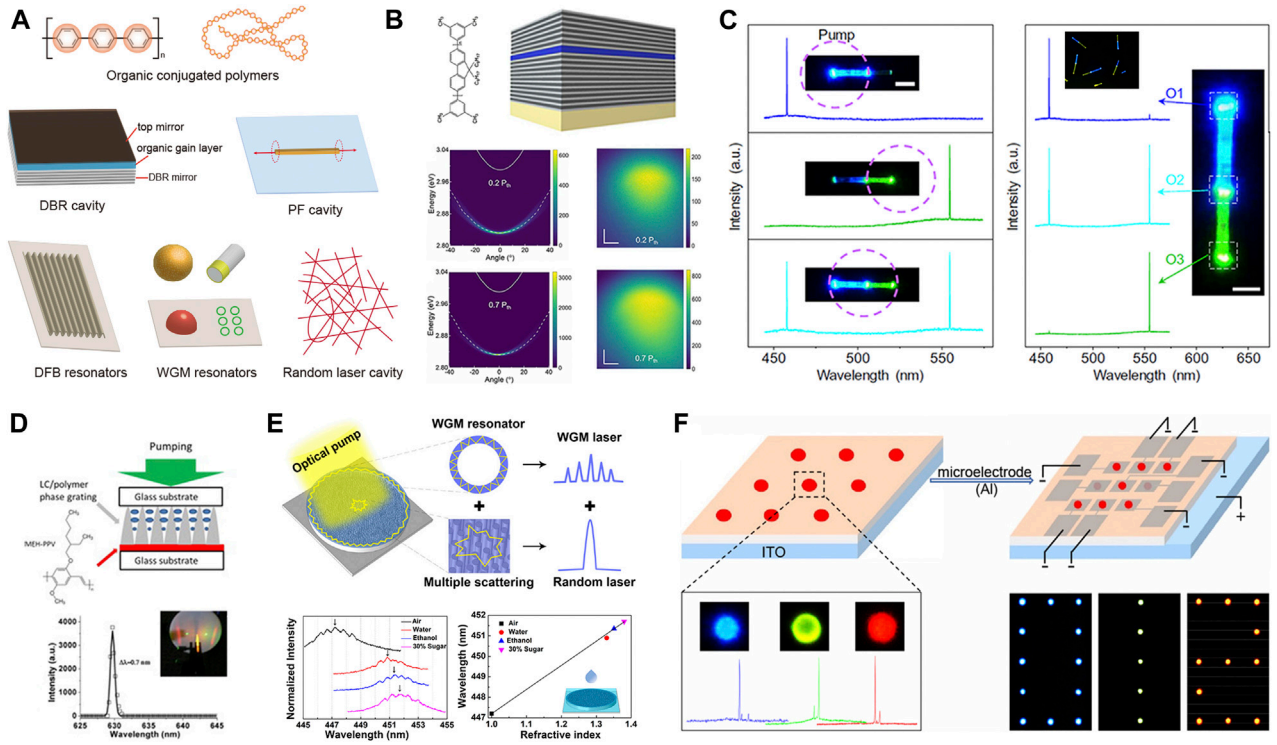

FIGURE 1 | (A) Schematic framework of π-conjugated polymers and resonator configurations for organic laser, **(B)** A typical planar microcavity composed of poly(9,9-diochylfluorene (PFO) film and distributed Bragg reflector (DBR) mirrors for the generation of low threshold polariton lasers; reproduced with permission from Wei et al. (2019). **(C)** Axially coupled nanowire resonators for the modulation of laser modes based on the mutual mode mechanism; reproduced with permission from Zhang et al. (2017). **(D)** Conjugated polymer-associated distributed feedback (DFB) lasers prepared by the holographic polymerization method. **(E)** The whispering gallery mode (WGM) random laser from PFO/Ag-nanoparticle compound cavity used for potential sensing applications of different liquids; reproduced with permission from Xu et al. (2020). **(F)** Microscale light-emitting electrochemical cell arrays based on conjugated polymers and electrolytes for optical pumping laser and the potential electrically driven laser panel display; reproduced with permission from Liang et al. (2020).

properties make conjugated polymers a good laser alternative for some inorganic materials (McGehee and Heeger, 2000). The first observation of organic laser from conjugated polymers was reported in 1992 with poly[2-methoxy, 5-(2′ethyl-hexoxy)-p-phenylenevinylene] (MEH-PPV) solutions as gain media (Moses, 1992). Then solid-state lasers based on semiconducting polymers attracted more attention and made remarkable advances for its practical prospects in integrated optoelectronic devices. Compared with some small organic laser molecules, conjugated polymers show unparalleled merits such as high absorption coefficients, broad spectra across the visible region, and most importantly, the resistance to light quenching at solid-state thanks to the long-chain barriers among each other, which make them an attractive low-threshold laser material for research (Xia et al., 2004). In addition to the optical source, some conjugated polymers can also be electrically pumped to emit bright fluorescence and laser (Rothe et al., 2006), which greatly broaden their practical foreground in optical sensing and electrically driven laser display.

In this mini review, we summarize the recent advances of conjugated polymers emitting low-threshold organic lasers with focus on the resonator configurations and patterning strategies involved, and then typical applications of organic microlasers in biological/chemical sensing and organic laser display are discussed. Finally, we provide the perspectives on the existing challenges and future outlooks of conjugated polymer-induced organic lasers.

OPTICAL FEEDBACK CONFIGURATIONS AND FABRICATION STRATEGIES

In a typical lasering process, pumping sources, gain materials, and resonator configurations are all essential to amplify light (Scherf et al., 2001). Under the proper excitation of light source, gain materials are stimulated to realize population inversion and the subsequent amplified oscillation by resonance. Then amplified emission of optical waves comes into being with the coherent optical field provided by resonator feedback configurations. By virtue of resonator configurations, organic lasers can be generated with low threshold and specific lasing mode. According to the optical feedback mechanism, resonator configurations for lasing action can be generally classified as distributed Bragg resonators (DBRs), Fabry–Pérot (FP) cavities, distributed feedback (DFB) resonators, whispering gallery mode (WGM) cavity, and random lasing configurations (**Figure 1A**) (Chénais and Forget, 2012). Availability of mature micro/nano-manufacturing techniques

(Holdcroft, 2001), such as prepatterned template, micromolding, photolithography, interference-holographic lithography, electron beam lithography, and nanoimprinting, allows the diverse fabrication of functional resonator configurations, which significantly accelerate the development of organic lasers.

Distributed Bragg resonators

The first introduction of microcavity lasers was realized by the group of Tessler, who fabricated a planar cavity consisting of poly (para-phenylene vinylene) (PPV) interlayer between two mirrors (Tessler et al., 1996). One of the mirrors has high reflectance (e.g., distributed Bragg reflector, DBR), and the other one is a metallic mirror that only allows partial transmission of light. The gain medium used for lasers only had a thickness of 100 nm, resulting in increasing gains and corresponding lower lasing threshold (~100 nJ). This sandwich microcavity shows a sort of Fabry–Pérot resonance property where standing-wave optical field is supported between two mirrors. The DBR resonator axis is usually perpendicular to the plane of substrate film and mirrors. The planar resonator configuration can be prepared by simple spin coating or deposition of gain polymer laser on the DBR substrate. Chen et al. designed a two-dimensional DBR resonator consisting of four Bragg mirrors, which emitted nearly diffraction-limited polymer lasers with an ultralow threshold of 17 $\mu J/cm^2$ (Huang et al., 2016). Moreover, the size parameters of DBR geometry were investigated to be 40 μm to ensure an optimal working performance. Recently, polariton lasing with a low threshold of 27.7 $\mu J/cm^2$ was observed from disordered PFO film in a DBR cavity (Wei et al., 2019). This work broadens the scope of conjugated polymers in polariton laser devices with typical features of decreased linewidth, nonlinear emission intensity, and long-range spatial coherence (**Figure 1B**). Then the threshold of polariton lasing was further decreased to an ultra-low level (17 $\mu J/cm^2$) using pentafluorene as gain materials in a planar microcavity, where SiO_2 and Ta_2O_3 layers were used for the construction of DBR microcavity, and the pentafluorene film was protected by a 10-nm buffer layer from degradation during the device fabrication process (Rajendran et al., 2019). The above work provides novel ideas for the fabrication of polaritonics.

Fabry–Pérot cavities

Most of one-dimensional microscopic wires/fibers present typical Fabry–Pérot feedback features with the body part of wire showing good waveguiding capacity and the tip parts acting as mirrors (Matino et al., 2019). Conjugated polymers with high gain properties can be fabricated to micro/nanowires *via* facile techniques such as prepatterned templating, micromolding, and self-assembly. The typical fabrication work of conjugated polymer nanowires came from the Redmond group who used the porous alumina template assisted with the melt-mold method to prepare high yields of poly(9,9-dioctylfluorene) (PFO) nanowires (O'Carroll et al., 2007a). The nanowires generally exhibit regular morphology and good dispersity with homogeneous size ranging from 250 to 300 nm in diameter. Notably, the semicrystalline PFO nanowire presents excellent waveguiding performance, and the optically pumped microlaser at 460 nm is observed (O'Carroll et al., 2007b). They subsequently used a similar templating technique to obtain poly[(9,9-dioctylfluorenyl-2,7-diyl)-co-(bithiophene)] (F8T2) nanowires, which showed superior working performance in the field of photodetectors (O'Brien et al., 2006). As for some conjugated polymers with small repeat units, uniform crystal structures tend to be formed for the lack of interference from side chains.

The self-assembly method is also a good choice to fabricate a nanofiber of conjugated polymers in low molecular weight. It has been reported that oligo (p-phenylenevinylene) (OPV) derivatives, exhibiting extended π-conjugated system, are prone to form ordered nanowire crystals with lasing action. An axially coupled microcavity system was constructed from two kinds of nanowires assembled by distinct OPV derivatives. Zhao group proposed a mutual mode selection strategy using the coupled microwires to obtain multicolor single-mode lasing generation and alternative output modulation (Zhang et al., 2017). When pumped by a proper light, gain materials can radiate laser from the microwire cavity facet, which can be coupled into the other cavity, and thus, the microwires mutually act as laser source as well as wavelength filter cavity, finally resulting in the laser mode selection and modulation (**Figure 1C**). A similar self-assembly method is employed to readily fabricate microbelts of another OPV derivative. Combined with the femtosecond laser processing technique, the microbelt can be perfectly tailored into the microfiber array along its length direction. The microfiber units are capable of presenting a similar lasing action simultaneously (Liao et al., 2015). Modulation of multicolor laser mode and multipoint lasing action provide a more comprehensive idea of the utility of organic lasers, making the assembly of FP resonators as promising candidates in full-color laser display devices as well as integrated photonic circuits.

Distributed feedback configurations

DFB geometries with diffractive periodic structures have emerged as a highly popular resonator configuration for its high optical feedback efficiency, which can efficiently avoid the large reflectivity caused by mirror or facet parts in FP cavity. When pumped by proper light, low-threshold lasering action will be generated from gain media under the interfering effect of periodic geometry (usually grating or photonic structures). According to the Bragg equation,

$$m\lambda_L = 2n_{eff}\Lambda$$

where n_{eff} is the effective refractive index of the active layer, Λ is the grating period, and m is the Bragg order. Constructive interference only occurs on lasers with specific wavelengths (λ_L).

Compared with other lasing systems, DFB configurations show special superiority in single-mode laser generation and broad-range spectral modulation by rational design of cavity parameters, such as grating period, refractive index, and thickness of gain layer (Heliotis et al., 2004; Klinkhammer et al., 2012), and the lasing spectra of conjugated polymers almost cover the whole visible region, thanks to the diverse material availability and flexible fabrication of grating parameters. A large amount of DFB laser work based on conjugated polymers have been reported during the past 20 years, mainly aiming to reduce the lasing threshold and improve the device fabrication techniques (Stehr et al., 2003).

The remarkable breakthrough on lasing threshold was achieved by the Bradley group, who intelligently proposed a mix-order (first and second order) grating strategy to reduce the lasing threshold of a polymer as low as 4 W/cm^2 (Karnutsch et al., 2007). Subsequently, a combination of improved gain properties with developed DFB geometry further reduced the lasing threshold (0.77 kW/cm^2) of conjugated polymers, making them possible to be pumped by a single LED source (Tsiminis et al., 2013). The primary DFB configuration consisted of grating templates as resonator and composite conjugated polymers as gain material. Convenient as it is, the lasing action is highly dependent on the grating substrate, which greatly limits the laser modulation capacity. In recent years, various micro/nanofabrication techniques have been employed to simplify the fabrication process and meanwhile increase the diversity and flexibility of grating configurations. The developed imprinting technique, as proposed by Prof. List, was subsequently employed to directly mold conjugated polymers into DFB gratings that presented desired lasing performance, which significantly improved the fabrication efficiency toward mass production (Gaal et al., 2003). Furthermore, advanced direct writing techniques including both electron-beam lithography (EBL), holographic polymerization technique, and laser interference ablation provided a more flexible way to achieve one-step and mass construction of one-dimensional or even complicated two-dimensional DFB lasing configurations (Kuehne et al., 2011; Zhai et al., 2011; Huang et al., 2012).

Distinct to optically driven organic lasers, electrically pumping lasers have attracted more and more attention because of its practicability and feasibility in the fields of organic laser diodes and full-color laser display. However, electrically driven laser is still confronted with serious challenges such as the extra additional loss and high lasing threshold. It has been validated that conjugated polymers with excellent charge transport capacity are ideally suitable for electrical pumping (Rothe et al., 2006). Besides, introduction of low-threshold DFB configurations into the electrically driven laser system can further reduce the pumping power intensity. Samuel et al. demonstrated an indirect electrically pumped laser configuration, in which InGaN LED was electrically driven as light source for the DFB lasing action of conjugated polymers (Yang et al., 2008). Subsequently, Heeger et al. constructed PPV-based 1D/2D grating resonators *via* nanoimprint technique to realize electrically pumped DFB laser at a low threshold (32 nJ/pulse) (Namdas et al., 2009). The electrical lasing threshold was further decreased as reported in the recent work. Oligo-(p-phenylene)-based gain materials with desirable carrier mobility were used in conjunction with DFB geometry, generating blue organic lasers at a very low threshold of only 0.16 nJ/pulse (Wei et al., 2017).

Whispering gallery mode cavities

Whispering gallery mode (WGM) resonator is a kind of typical cavity that has good optical confinement capacity for the total internal reflection effect near the structural boundary. A variety of micro-configurations has been developed to generate WGM lasers, including micro-spheres/hemispheres, microbubbles, microdisks, microrings, and microcapillaries (Yang et al., 2015). These structures usually exist in more than one axis of symmetry so that light can be readily confined in the cavity, resulting in high-quality factors and low lasing thresholds. Various WGM lasers have been reported from conjugated polymers, among which microspheres are more popular due to the superior feedback property and facile fabrication techniques. For example, Xiao et al. demonstrated a tunable optofluidic microlaser from microbubble cavities. The smooth hollow bubble filled with polymer solutions enables the low lasing threshold of 7.8 μJ/cm^2 (Tang et al., 2018). In comparison with liquid laser cavities, solid ones possess unique advantages in the miniaturization and integration of organic laser devices. Xu et al. have proposed a novel WGM random cavity to achieve double-mode lasing simultaneously (**Figure 1E**). By virtue of inkjet printing and etching method, the size of cavity can be tailored flexibly to modulate the lasing mode, which shows promising prospects in chemical sensing (Xu et al., 2020). Besides, conjugated polymers self-assemble to well-defined solid microspheres using the simple vapor diffusion precipitation method, successfully reducing lasing threshold as low as 0.37 μJ/cm^2 (Kushida et al., 2017). Very recently, Zhao et al. remarkably constructed a light-emitting electro-chemical cell micro-array consisting of conjugated polymers and electrolytes (**Figure 1F**). Every single WGM unit acted as a lasing pixel under proper optical excitation, and meanwhile, electrical driven luminance was also realized. Even though the electrical pumping laser did not realize for the additional loss in this configuration, it provides novel perspectives for the construction of electrical driven laser display devices (Liang et al., 2020).

Random lasing cavities

Conjugated polymers without specific feedback resonators can also present a lasing action, called random laser, when multiple scattering occurs in the irregular region. Random laser usually appears from gain medium with ill-defined and unordered geometries. Nanowires based on a typical π-conjugated oligophenyl material have been synthesized by the simple hot wall epitaxy method, and low-threshold random lasing action of nanowires (0.5 μJ/cm^2) was measured at ~425 nm under optical pumping (Quochi et al., 2005). Bongiovanni et al. further investigated the temperature-dependent nonlinear exciton process of the random lasing action from these nanofibers (Quochi et al., 2008). The facile fabrication techniques and high intensity of random laser enable its promising applications in sensing and optical imaging. Li et al. have taken advantage of random lasing from TiO_2 nanoparticle-doped TPA-PPV films to detect explosive vapors. The sensitivity of random laser was enhanced more than 20 times than that in spontaneous emission (Deng et al., 2010).

APPLICATIONS

As an excellent laser material, conjugated polymers in proper resonator configurations can be pumped optically or electrically to generate intense organic lasers, which is expected to play important roles in diverse practical applications, such as chemosensing, biological sensing and imaging, organic laser diode, and electrically driven multicolor laser display (Toropov et al., 2021). Microlasers with high quality factor are highly suitable for optical sensing since tiny variations of the surrounding environment and material properties will induce

drastic changes in lasing action. Explosive vapors are important analytes for conjugated polymers since their luminescent emission can be effectively quenched by explosive molecules (Yang et al., 2010). By virtue of this mechanism, Bulović et al. originally utilized the lasing behavior rather than spontaneous emission of PFO to detect explosive analytes, and the sensitivity enhanced more than 30 times. Introduction of DFB, WGM, and random lasing mode resonators allows further enhancement of sensitivity, achieving ultra-low detecting vapor pressure of 9.8 and 5 ppb for DNB and TNT, respectively (Rose et al., 2005). Xu et al. put forward a compound cavity containing PFO and Ag nanoparticles to achieve WGM random lasers, which vary in wavelength and intensity under stimuli of different liquids (**Figure 1E**) (Xu et al., 2020). This novel configuration has promising applications in laser sensing. In terms of biological applications, a DFB laser configuration combining conjugated polymers and hydrogel recognition layer has been fabricated to realize label-free and real-time measurement of avidin–biotin interaction (Heydari et al., 2014). Recently, Kuehne et al. have synthesized conjugated polymer-based microparticles, which emit both WGM lasers and Raman scattering narrow-band emission. By detecting the lasing and Raman scattering signals simultaneously, cells phagocytizing microparticles are well tracked and imaged with reduced interferences (Haehnle et al., 2020). Apart from sensing applications, electrically driven laser action also plays an important role in laser diodes and panel display, accelerating the development of integrated luminescent devices with low-cost and flexible features (Liang et al., 2020).

CONCLUSION AND OUTLOOK

In this minireview, we have focused on the organic lasing action and practical applications of conjugated polymers. Optical feedback configurations and relevant micro/nano-fabrication strategies are well summarized to provide an overall perspective on recent developments and existing problems toward polymer lasers. Even though considerable efforts have been made to simplify the fabrication techniques for resonator configurations and further reduce the lasing threshold, there still exist many bottlenecks urgently to be solved. First, it is expected that integratable lasing resonators in micro–nano scale can be further developed to ensure their practical applications in integrated laser source and full-color laser display. Besides, as a very appealing but intractable issue, electrically driven organic laser has not been totally realized in conjugated polymers due to the low carrier density and high additional losses associated with electrode absorption, polaron quenching, and triplet absorption. Even though diverse approaches focusing on the abovementioned problems have been attempted based on tailored gain material with increased carrier mobility, further efforts should be put on the optimization of resonator configurations to reduce the additional losses and achieve the electrically operated organic lasers with low threshold.

AUTHOR CONTRIBUTIONS

All authors listed have made a substantial, direct, and intellectual contribution to the work and approved it for publication.

FUNDING

This work is supported by the National Natural Science Foundation of China (Grant No. 62105096) and Doctoral Scientific Research Foundation of Henan Normal University (Grant Nos. 5101029170825 and 5101029470261).

REFERENCES

Amarasinghe, D., Ruseckas, A., Turnbull, G. A., and Samuel, I. D. W. (2009). Organic Semiconductor Optical Amplifiers. *Proc. IEEE* 97, 1637–1650. doi:10.1109/jproc.2009.2023250

Chellappan, K. V., Erden, E., and Urey, H. (2010). Laser-based Displays: a Review. *Appl. Opt.* 49, F79–F98. doi:10.1364/AO.49.000F79

Chénais, S., and Forget, S. (2012). Recent Advances in Solid-State Organic Lasers. *Polym. Int.* 61, 390–406. doi:10.1002/pi.3173

Deng, C., He, Q., He, C., Shi, L., Cheng, J., and Lin, T. (2010). Conjugated Polymer–Titania Nanoparticle Hybrid Films: Random Lasing Action and Ultrasensitive Detection of Explosive Vapors. *J. Phys. Chem. B* 114, 4725–4730. doi:10.1021/jp9117198

Gaal, M., Gadermaier, C., Plank, H., Moderegger, E., Pogantsch, A., Leising, G., et al. (2003). Imprinted Conjugated Polymer Laser. *Adv. Mater.* 15, 1165–1167. doi:10.1002/adma.200305047

Grivas, C., and Pollnau, M. (2012). Organic Solid-State Integrated Amplifiers and Lasers. *Laser Photon. Rev.* 6, 419–462. doi:10.1002/lpor.201100034

Haehnle, B., Lamla, M., Sparrer, K. M. J., Gather, M. C., and Kuehne, A. J. C. (2020). Narrow Stimulated Resonance Raman Scattering and WGM Lasing in Small Conjugated Polymer Particles for Live Cell Tagging and Tracking. *Adv. Opt. Mater.* 9, 2001553. doi:10.1002/adom.202001553

Heliotis, G., Xia, R., Turnbull, G. A., Andrew, P., Barnes, W. L., Samuel, I. D. W., et al. (2004). Emission Characteristics and Performance Comparison of Polyfluorene Lasers with One- and Two-Dimensional Distributed Feedback. *Adv. Funct. Mater.* 14, 91–97. doi:10.1002/adfm.200305504

Heydari, E., Buller, J., Wischerhoff, E., Laschewsky, A., Döring, S., and Stumpe, J. (2014). Label-Free Biosensor Based on an All-Polymer DFB Laser. *Adv. Opt. Mater.* 2, 137–141. doi:10.1002/adom.201300454

Holdcroft, S. (2001). Patterning π-Conjugated Polymers. *Adv. Mater.* 13, 1753–1765. doi:10.1002/1521-4095(200112)13:23<1753:aid-adma1753>3.0.co;2-2

Huang, W., Diao, Z., Liu, Y., Peng, Z., Yang, C., Ma, J., et al. (2012). Distributed Feedback Polymer Laser with an External Feedback Structure Fabricated by Holographic Polymerization Technique. *Org. Electron.* 13, 2307–2311. doi:10.1016/j.orgel.2012.07.004

Huang, W., Pu, D., Qiao, W., Fang, Z., Zhou, X., Ye, Y., et al. (2016). Nearly Diffraction-Limited Conjugated Polymer Microlasers Utilizing Two-Dimensional Distributed Bragg Resonators. *Org. Electron.* 38, 238–244. doi:10.1016/j.orgel.2016.08.024

Karnutsch, C., Pflumm, C., Heliotis, G., Demello, J. C., Bradley, D. D. C., Wang, J., et al. (2007). Improved Organic Semiconductor Lasers Based on a Mixed-Order Distributed Feedback Resonator Design. *Appl. Phys. Lett.* 90, 131104. doi:10.1063/1.2717518

Klinkhammer, S., Liu, X., Huska, K., Shen, Y., Vanderheiden, S., Valouch, S., et al. (2012). Continuously Tunable Solution-Processed Organic Semiconductor DFB Lasers Pumped by Laser Diode. *Opt. Express* 20, 6357–6364. doi:10.1364/OE.20.006357

Kuehne, A. J. C., and Gather, M. C. (2016). Organic Lasers: Recent Developments on Materials, Device Geometries, and Fabrication Techniques. *Chem. Rev.* 116, 12823–12864. doi:10.1021/acs.chemrev.6b00172

Kuehne, A. J. C., Kaiser, M., Mackintosh, A. R., Wallikewitz, B. H., Hertel, D., Pethrick, R. A., et al. (2011). Sub-Micrometer Patterning of Amorphous- and β-Phase in a Crosslinkable Poly(9,9-Dioctylfluorene): Dual-Wavelength Lasing from a Mixed-Morphology Device. *Adv. Funct. Mater.* 21, 2564–2570. doi:10.1002/adfm.201002553

Kushida, S., Okada, D., Sasaki, F., Lin, Z.-H., Huang, J.-S., and Yamamoto, Y. (2017). Low-Threshold Whispering Gallery Mode Lasing from Self-Assembled Microspheres of Single-Sort Conjugated Polymers. *Adv. Opt. Mater.* 5, 1700123. doi:10.1002/adom.201700123

Liang, J., Chu, M., Zhou, Z., Yan, Y., and Zhao, Y. S. (2020). Optically Pumped Lasing in Microscale Light-Emitting Electrochemical Cell Arrays for Multicolor Displays. *Nano Lett.* 20, 7116–7122. doi:10.1021/acs.nanolett.0c02378

Liao, Q., Jin, X., Zhang, H., Xu, Z., Yao, J., and Fu, H. (2015). An Organic Microlaser Array Based on a Lateral Microcavity of a Single J-Aggregation Microbelt. *Angew. Chem. Int. Ed.* 54, 7037–7041. doi:10.1002/anie.201501060

Matino, F., Persano, L., Camposeo, A., and Pisignano, D. (2019). Laser Systems and Networks with Organic Nanowires and Nanofibers. *Adv. Opt. Mater.* 7, 1900192. doi:10.1002/adom.201900192

McGehee, M. D., and Heeger, A. J. (2000). Semiconducting (Conjugated) Polymers as Materials for Solid-State Lasers. *Adv. Mater.* 12, 1655–1668. doi:10.1002/1521-4095(200011)12:22<1655:aid-adma1655>3.0.co;2-2

Moses, D. (1992). High Quantum Efficiency Luminescence from a Conducting Polymer in Solution: A Novel Polymer Laser Dye. *Appl. Phys. Lett.* 60, 3215–3216. doi:10.1063/1.106743

Namdas, E. B., Tong, M., Ledochowitsch, P., Mednick, S. R., Yuen, J. D., Moses, D., et al. (2009). Low Thresholds in Polymer Lasers on Conductive Substrates by Distributed Feedback Nanoimprinting: Progress toward Electrically Pumped Plastic Lasers. *Adv. Mater.* 21, 799–802. doi:10.1002/adma.200802436

O'Brien, G. A., Quinn, A. J., Tanner, D. A., and Redmond, G. (2006). A Single Polymer Nanowire Photodetector. *Adv. Mater.* 18, 2379–2383. doi:10.1002/adma.200601012

O'Carroll, D., Lieberwirth, I., and Redmond, G. (2007a). Melt-processed Polyfluorene Nanowires as Active Waveguides. *Small* 3, 1178–1183. doi:10.1002/smll.200600575

O'Carroll, D., Lieberwirth, I., and Redmond, G. (2007b). Microcavity Effects and Optically Pumped Lasing in Single Conjugated Polymer Nanowires. *Nat. Nanotech* 2, 180–184. doi:10.1038/nnano.2007.35

Quochi, F., Andreev, A., Cordella, F., Orrù, R., Mura, A., Bongiovanni, G., et al. (2005). Low-threshold Blue Lasing in Epitaxially Grown Para-Sexiphenyl Nanofibers. *J. Lumin.* 112, 321–324. doi:10.1016/j.jlumin.2004.09.100

Quochi, F., Saba, M., Cordella, F., Gocalinska, A., Corpino, R., Marceddu, M., et al. (2008). Temperature Tuning of Nonlinear Exciton Processes in Self-Assembled Oligophenyl Nanofibers under Laser Action. *Adv. Mater.* 20, 3017–3021. doi:10.1002/adma.200800509

Rajendran, S. K., Wei, M., Ohadi, H., Ruseckas, A., Turnbull, G. A., and Samuel, I. D. W. (2019). Low Threshold Polariton Lasing from a Solution-Processed Organic Semiconductor in a Planar Microcavity. *Adv. Opt. Mater.* 7, 1801791. doi:10.1002/adom.201801791

Rose, A., Zhu, Z., Madigan, C. F., Swager, T. M., and Bulović, V. (2005). Sensitivity Gains in Chemosensing by Lasing Action in Organic Polymers. *Nature* 434, 876–879. doi:10.1038/nature03438

Rothe, C., Galbrecht, F., Scherf, U., and Monkman, A. (2006). The β-Phase of Poly(9,9-Dioctylfluorene) as a Potential System for Electrically Pumped Organic Lasing. *Adv. Mater.* 18, 2137–2140. doi:10.1002/adma.200600901

Samuel, I. D. W., and Turnbull, G. A. (2007). Organic Semiconductor Lasers. *Chem. Rev.* 107, 1272–1295. doi:10.1021/cr050152i

Scherf, U., Riechel, S., Lemmer, U., and Mahrt, R. F. (2001). Conjugated Polymers: Lasing and Stimulated Emission. *Curr. Opin. Solid State. Mater. Sci.* 5, 143–154. doi:10.1016/s1359-0286(01)00010-9

Stehr, J., Crewett, J., Schindler, F., Sperling, R., Von Plessen, G., Lemmer, U., et al. (2003). A Low Threshold Polymer Laser Based on Metallic Nanoparticle Gratings. *Adv. Mater.* 15, 1726–1729. doi:10.1002/adma.200305221

Tang, S. J., Liu, Z., Qian, Y. J., Shi, K., Sun, Y., Wu, C., et al. (2018). A Tunable Optofluidic Microlaser in a Photostable Conjugated Polymer. *Adv. Mater.* 30, 1804556. doi:10.1002/adma.201804556

Tessler, N., Denton, G. J., and Friend, R. H. (1996). Lasing from Conjugated-Polymer Microcavities. *Nature* 382, 695–697. doi:10.1038/382695a0

Toropov, N., Cabello, G., Serrano, M. P., Gutha, R. R., Rafti, M., and Vollmer, F. (2021). Review of Biosensing with Whispering-Gallery Mode Lasers. *Light. Sci. Appl.* 10, 42. doi:10.1038/s41377-021-00471-3

Tsiminis, G., Wang, Y., Kanibolotsky, A. L., Inigo, A. R., Skabara, P. J., Samuel, I. D. W., et al. (2013). Nanoimprinted Organic Semiconductor Laser Pumped by a Light-Emitting Diode. *Adv. Mater.* 25, 2826–2830. doi:10.1002/adma.201205096

Wei, M., Rajendran, S. K., Ohadi, H., Tropf, L., Gather, M. C., Turnbull, G. A., et al. (2019). Low-threshold Polariton Lasing in a Highly Disordered Conjugated Polymer. *Optica* 6, 1124. doi:10.1364/optica.6.001124

Wei, Q., Li, Y., Liu, J., Fang, Q., Li, J., Yan, X., et al. (2017). A High Performance Deep Blue Organic Laser Gain Material. *Adv. Opt. Mater.* 5, 1601003. doi:10.1002/adom.201601003

Xia, R., Heliotis, G., and Bradley, D. D. C. (2003). Fluorene-based Polymer Gain media for Solid-State Laser Emission across the Full Visible Spectrum. *Appl. Phys. Lett.* 82, 3599–3601. doi:10.1063/1.1576906

Xia, R., Heliotis, G., and Bradley, D. D. C. (2004). Semiconducting Polyfluorenes as Materials for Solid-State Polymer Lasers across the Visible Spectrum. *Synth. Met.* 140, 117–120. doi:10.1016/s0379-6779(03)00235-2

Xu, Z., Tong, J., Shi, X., Deng, J., and Zhai, T. (2020). Tailoring Whispering Gallery Lasing and Random Lasing in A Compound Cavity. *Polymers* 12, 656. doi:10.3390/polym12030656

Yang, S., Wang, Y., and Sun, H. (2015). Advances and Prospects for Whispering Gallery Mode Microcavities. *Adv. Opt. Mater.* 3, 1136–1162. doi:10.1002/adom.201500232

Yang, Y., Turnbull, G. A., and Samuel, I. D. W. (2008). Hybrid Optoelectronics: A Polymer Laser Pumped by a Nitride Light-Emitting Diode. *Appl. Phys. Lett.* 92, 163306. doi:10.1063/1.2912433

Yang, Y., Turnbull, G. A., and Samuel, I. D. W. (2010). Sensitive Explosive Vapor Detection with Polyfluorene Lasers. *Adv. Funct. Mater.* 20, 2093–2097. doi:10.1002/adfm.200901904

Zhai, T., Zhang, X., Pang, Z., and Dou, F. (2011). Direct Writing of Polymer Lasers Using Interference Ablation. *Adv. Mater.* 23, 1860–1864. doi:10.1002/adma.201100250

Zhang, C., Zou, C.-L., Dong, H., Yan, Y., Yao, J., and Zhao, Y. S. (2017). Dual-color Single-Mode Lasing in Axially Coupled Organic Nanowire Resonators. *Sci. Adv.* 3, e1700225. doi:10.1126/sciadv.1700225

Conflict of Interest: The authors declare that the research was conducted in the absence of any commercial or financial relationships that could be construed as a potential conflict of interest.

Publisher's Note: All claims expressed in this article are solely those of the authors and do not necessarily represent those of their affiliated organizations, or those of the publisher, the editors, and the reviewers. Any product that may be evaluated in this article, or claim that may be made by its manufacturer, is not guaranteed or endorsed by the publisher.

frontiers in Chemistry

MINI REVIEW
published: 16 December 2021
doi: 10.3389/fchem.2021.823715

Micro-/Nano-Structures Fabricated by Laser Technologies for Optoelectronic Devices

Jian Yi, Hao Zhou, Wei-Hua Wei, Xing-Chen Han, Dong-Dong Han and Bing-Rong Gao**

State Key Laboratory of Integrated Optoelectronics, College of Electronic Science and Engineering, Jilin University, Changchun, China

Due to unique optical and electrical properties, micro-/nano-structures have become an essential part of optoelectronic devices. Here, we summarize the recent developments in micro-/nano-structures fabricated by laser technologies for optoelectronic devices. The fabrication of micro-/nano-structures by various laser technologies is reviewed. Micro-/nano-structures in optoelectronic devices for performance improvement are reviewed. In addition, typical optoelectronic devices with micro-nano structures are also summarized. Finally, the challenges and prospects are discussed.

Keywords: micro-/nano-structures, laser technologies, photodetector, photovoltaic cell, light-emitting diode

OPEN ACCESS

Edited by:
Yun-Fei Li,
Hebei University of Technology, China

Reviewed by:
Ziwei Li,
Hunan University, China
Wei Xin,
Northeast Normal University, China

****Correspondence:***
Dong-Dong Han
handongdong@jlu.edu.cn
Bing-Rong Gao
brgao@jlu.edu.cn

Specialty section:
This article was submitted to Nanoscience, a section of the journal Frontiers in Chemistry

Received: *28 November 2021*
Accepted: *02 December 2021*
Published: *16 December 2021*

Citation:
Yi J, Zhou H, Wei W-H, Han X-C, Han D-D and Gao B-R (2021) Micro-/Nano-Structures Fabricated by Laser Technologies for Optoelectronic Devices. Front. Chem. 9:823715. doi: 10.3389/fchem.2021.823715

INTRODUCTION

There are many animals and plants using unique micro-/nano-structures to improve their environmental adaptability (Han et al., 2016; Han et al., 2020a; Cao et al., 2020). For example, micro-/nano-structures on a lotus leaf and taro surface exhibit superhydrophobic properties (Zhang et al., 2012b; Wang et al., 2021b; Lv et al., 2021). Grating-like structures on butterfly wings trap light, leading to the colorful butterfly wing (Wang et al., 2012; Jiang et al., 2016; Zou et al., 2020). Learning from nature, micro-/nano-structures have been adopted in the various functional devices for broad applications (Han et al., 2019; Zhang et al., 2019; Zhang et al., 2021). Therefore, many researchers have focused on the fabrication and application of micro-nano structures (Zhang et al., 2012a; Han et al., 2015; Liu et al., 2021). Mainly, due to unique optical and electrical properties, micro-/nano-structures have become an essential part of optoelectronic devices.

Laser fabrication technologies show high efficiency, high precision, and low thermal effect (Li et al., 2020a; Fu et al., 2020; Ma et al., 2020; You et al., 2020; Fu et al., 2021). Laser technologies can be used to fabricate micro-/nano-structures by the interaction between laser and materials (Liu et al., 2019; Han et al., 2020b; Liu et al., 2020; Wang et al., 2021a). Especially, ultrafast lasers can fabricate broadband, transparent anti-reflection surfaces, which promote the performance of optoelectronic devices by enhancing the light absorption or introducing surface plasmon-polariton (Zhang et al., 2010; Liapis et al., 2017; Jia et al., 2020).

In this review, we summarize recent progress on micro-/nano-structures fabricated by laser technologies. Typical light trapping mechanism and surface plasmon-polariton of the micro-nano structure are discussed. Then, we outlined the typical applications, including photodetectors, photovoltaic cells, organic light-emitting devices, etc. Finally, the challenges and prospects are discussed.

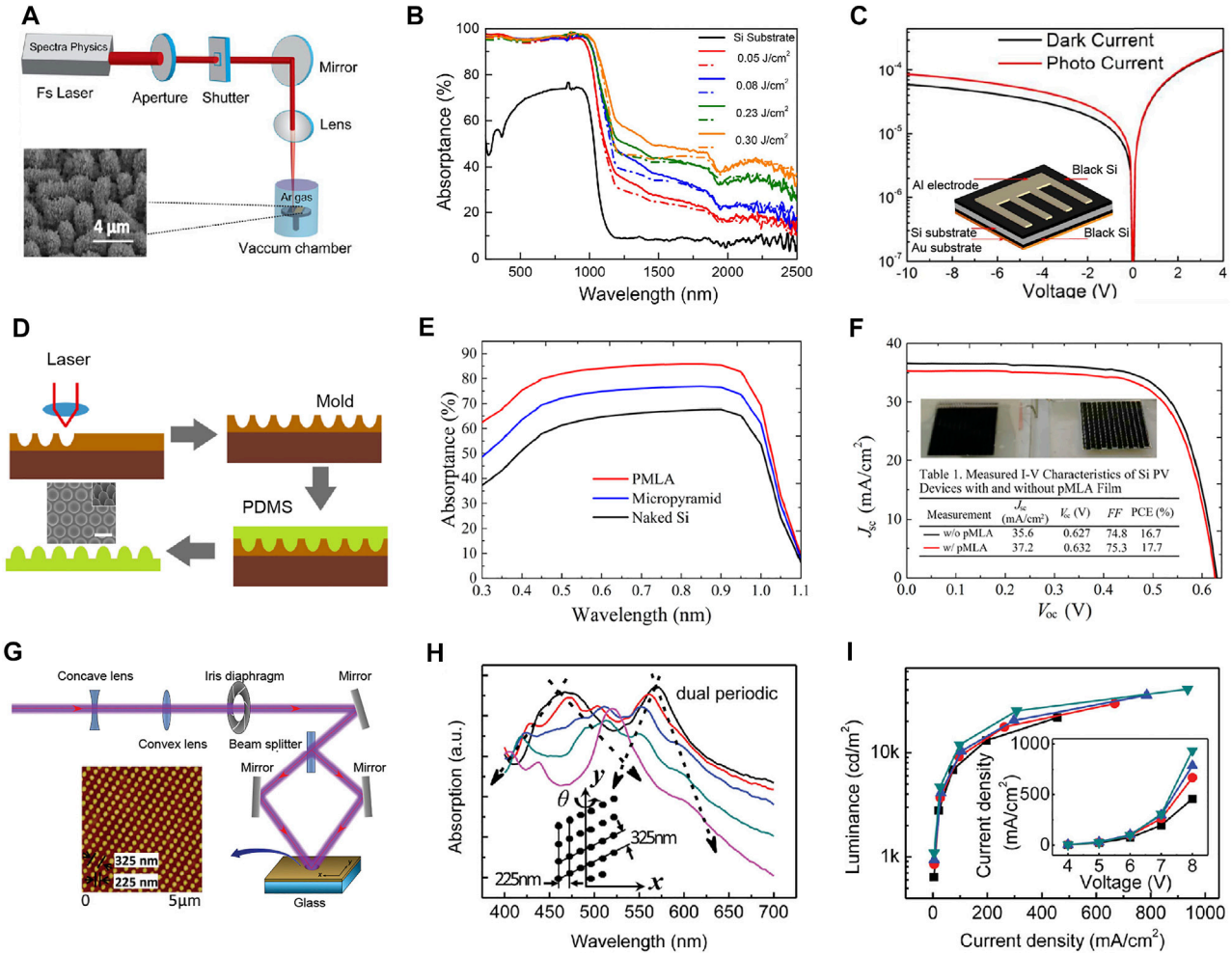

FIGURE 1 | Micro-/nano-structures fabricated by laser technologies for optoelectronic devices. **(A)** Femtosecond laser manufacturing system. Reproduced from (Yu et al., 2017) with permission of IEEE. **(B)** The corresponding absorptivity of nitrogen-doped silicon substrate. **(C)** Infrared photodetection performance. Reproduced from (Li et al., 2018) with permission of IEEE. **(D)** The preparation process of PDMS convex PMLA film. **(E)** Simulated absorption spectra of films. **(F)** Solar cell performance. Reproduced from (Fang et al., 2018) with permission of American Chemical Society. **(G)** Schematic diagram of laser two-beam interferes processing. Reproduced from (Bi et al., 2013; Jiang et al., 2014) with permission of WILEY-VCH. **(H)** Absorption spectra for WOLEDs. **(I)** Performance of WOLED. Reproduced from (Bi et al., 2013) with permission of WILEY-VCH.

MECHANISM

Introducing micro-/nano-structures inside or outside the devices can improve optoelectronic devices' performance (Ma and Cui, 2020; Na and Chew, 2020; Chen et al., 2021). Inspired by the moth-eye structure, the reflectivity is reduced by introducing micro-/nano-structures. Mainly, the light will be internally reflected many times inside the structure to form a "light trap" (Zhang et al., 2020a; Otte and Denz, 2020; Yang et al., 2021). As a result, the existence of micro-/nano-structures can improve the light absorption capacity of the optoelectronic device. Moreover, the efficiency of optoelectronic devices can be enhanced by surface plasmon-polariton (Eaton et al., 2016; Li et al., 2020b; Zhang et al., 2020b).

OPTOELECTRONIC DEVICES

Photodetector

Silicon material plays an important role in silicon-based optoelectronic integrated devices preparation. Take photodetectors as an example, the bandgap of silicon material is around 1.1–1.3 eV, limiting silicon material for infrared radiation (IR) photodetection. Therefore, many efforts, such as ion implantation or structural defects, have been developed to extend the absorption band of silicon. As a pioneer, Zhao's group (Li et al., 2017; Yu et al., 2017; Li et al., 2018) fabricated supersaturated silicon material with nitrogen, sulfur, and Au by femtosecond laser ablation (**Figure 1A**). After the femtosecond laser ablation in nitrogen (N_2) atmosphere, the surface silicon material evolved into a bead-like micro-/nano-structures with a height of 3~4 μm and a distance of

3~4 μm (Li et al., 2018). Micro-/nano-structures are beneficial for a stronger light trapping effect. Compared with the initial silicon material, laser-treated N-doped silicon material has a broader absorption (0.25–2.5 μm) and higher absorptivity (**Figure 1B**). The inset of **Figure 1C** is the device structure of the laser-treated silicon-based IR photodetector. The photo responsivity is 5.3 mA/W (V = 10 V).

Photovoltaic Cell

Photovoltaic cells convert sunlight to electric energy. Usually, light utilization efficiency is very low due to the reflection loss. To solve this problem, various anti-reflection structures have been designed. For example, Fang et al. proposed a 100% relative packing density film for enhancing photovoltaic cells performance (Fang et al., 2018). As shown in **Figure 1D**, direct-write ultraviolet (UV) laser photolithography system was employed to fabricate a paraboloidal concave photoresist pattern (master mold). Then polydimethylsiloxane (PDMS) was spin-coated onto the master mold. After thermally cured, structured PDMS was separated from the master mold for further use. **Figure 1E** is the simulated absorption spectra of films. Si substrate with paraboloidal microlens array (PMLA) film shows the highest absorption due to the suppressing reflection. It is worth noting that PMLA antireflective (AR) film indicates superhydrophobicity and self-cleaning ability. Finally, the short-circuit current density increases from 35.6 to 37.2 mA/cm^2 after integrating the PMLA AR film (**Figure 1F**). Instead of integrating the AR film on the photovoltaic cells surface, structured photoelectrodes or active layers have been fabricated by femtosecond laser ablation, interference, or laser-induced periodic surface structures for photocurrent enhancement (Zhang et al., 2015; Cui et al., 2016; Soldera et al., 2016).

Light-Emitting Diode

Bi et al. (2013) demonstrated white organic light-emitting diodes (WOLEDs) with broadband excitation by introducing two-dimensional gratings. As shown in **Figure 1G**, the grating structures were prepared by two-beam laser interference (Guo et al., 2012; Jiang et al., 2014; Yan et al., 2015). Introducing dual-period corrugations into the WOLED metal electrodes achieves broadband absorption (**Figure 1H**). In addition, broadband SPP modes lead to broadband light extraction. Significantly, broadband light extraction deeply affects the WOLEDs performance (**Figure 1I**). Compared with traditional planar devices, the current efficiency is increased by 37%, and the external quantum efficiency is increased by 48%. Recently, combining laser interference lithography and reactive ion etching, Ju et al. proposed flexible OLEDs with light extraction structure for optical efficiency improvement (Lee et al., 2019; Kim et al., 2020).

CONCLUSION AND OUTLOOK

This minireview summarizes recent progress on micro-/nano-structures fabricated by laser technologies for optoelectronic devices. The existence of micro-/nano-structures can improve the light absorption capacity and the efficiency of optoelectronic devices. Typical optoelectronic devices have been successfully designed and demonstrated the critical role of micro-/nano-structures. Significantly, new photoelectric applications, such as photoelectric dichroism, have been proposed and fabricated by laser technology based on various materials (Drevinskas et al., 2015; Jiang et al., 2020; Kuroiwa and Tatsuma, 2020; Zou et al., 2021a; Zou et al., 2021b; Xuan et al., 2021). Although successful works have demonstrated the distinguish characters, the efficiency of laser processing materials needs to improve, which benefits device preparation efficiency. With the rapid development of nanofabrication technology, advanced fundamental theories, new structural design, micro-/nano-structures will improve devices performances.

AUTHOR CONTRIBUTIONS

All authors listed have made a substantial, direct, and intellectual contribution to the work and approved it for publication.

FUNDING

This research was funded by the Strategic Priority Research Program of CAS (Grant No. XDC07030303), the National Natural Science Foundation of China (61905087), and Fundamental Research Funds for the Central Universities (2020-JCXK-18).

REFERENCES

Bi, Y.-G., Feng, J., Li, Y.-F., Zhang, X.-L., Liu, Y.-F., Jin, Y., et al. (2013). Broadband Light Extraction from white Organic Light-Emitting Devices by Employing Corrugated Metallic Electrodes with Dual Periodicity. *Adv. Mater.* 25 (48), 6969–6974. doi:10.1002/adma.201302367

Cao, J.-J., Hou, Z.-S., Tian, Z.-N., Hua, J.-G., Zhang, Y.-L., and Chen, Q.-D. (2020). Bioinspired Zoom Compound Eyes Enable Variable-Focus Imaging. *ACS Appl. Mater. Inter.* 12 (9), 10107–10117. doi:10.1021/acsami.9b21008

Chen, J., Zhou, Y., Fu, Y., Pan, J., Mohammed, O. F., and Bakr, O. M. (2021). Oriented Halide Perovskite Nanostructures and Thin Films for Optoelectronics. *Chem. Rev.* 121 (20), 12112–12180. doi:10.1021/acs.chemrev.1c00181

Cui, J., Rodríguez-Rodríguez, Á., Hernández, M., García-Gutiérrez, M.-C., Nogales, A., Castillejo, M., et al. (2016). Laser-induced Periodic Surface Structures on P3HT and on its Photovoltaic Blend with PC71BM. *ACS Appl. Mater. Inter.* 8 (46), 31894–31901. doi:10.1021/acsami.6b09053

Drevinskas, R., Beresna, M., Gecevičius, M., Khenkin, M., Kazanskii, A. G., Matulaitienė, I., et al. (2015). Giant Birefringence and Dichroism Induced by Ultrafast Laser Pulses in Hydrogenated Amorphous Silicon. *Appl. Phys. Lett.* 106 (17), 171106. doi:10.1063/1.4919538

Eaton, S. W., Fu, A., Wong, A. B., Ning, C.-Z., and Yang, P. (2016). Semiconductor Nanowire Lasers. *Nat. Rev. Mater.* 1 (6), 16028. doi:10.1038/natrevmats.2016.28

Fang, C., Zheng, J., Zhang, Y., Li, Y., Liu, S., Wang, W., et al. (2018). Antireflective Paraboloidal Microlens Film for Boosting Power Conversion Efficiency of Solar Cells. *ACS Appl. Mater. Inter.* 10 (26), 21950–21956. doi:10.1021/acsami.7b19743

Fu, X.-Y., Cai, Q., Ma, J.-N., Zhu, L., Han, D.-D., and Zhang, Y.-L. (2021). Free-standing and Flexible Graphene Supercapacitors of High Areal Capacitance Fabricated by Laser Holography Reduction of Graphene Oxide. *Appl. Phys. Lett.* 118 (7), 071601. doi:10.1063/5.0038508

Fu, X.-Y., Chen, Z.-D., Han, D.-D., Zhang, Y.-L., Xia, H., and Sun, H.-B. (2020). Laser Fabrication of Graphene-Based Supercapacitors. *Photon. Res.* 8 (4), 577–588. doi:10.1364/prj.382401

Guo, L., Jiang, H.-B., Shao, R.-Q., Zhang, Y.-L., Xie, S.-Y., Wang, J.-N., et al. (2012). Two-beam-laser Interference Mediated Reduction, Patterning and Nanostructuring of Graphene Oxide for the Production of a Flexible Humidity Sensing Device. *Carbon* 50 (4), 1667–1673. doi:10.1016/j.carbon.2011.12.011

Han, B., Zhang, Y. L., Zhu, L., Li, Y., Ma, Z. C., Liu, Y. Q., et al. (2019). Plasmonic-Assisted Graphene Oxide Artificial Muscles. *Adv. Mater.* 31 (5), 1806386. doi:10.1002/adma.201806386

Han, D.-D., Cai, Q., Chen, Z.-D., Li, J.-C., Mao, J.-W., Lv, P., et al. (2020a). Bioinspired Surfaces with Switchable Wettability. *Front. Chem.* 8, 692. doi:10.3389/fchem.2020.00692

Han, D.-D., Chen, Z.-D., Li, J.-C., Mao, J.-W., Jiao, Z.-Z., Wang, W., et al. (2020b). Airflow Enhanced Solar Evaporation Based on Janus Graphene Membranes with Stable Interfacial Floatability. *ACS Appl. Mater. Inter.* 12, 25435–25443. doi:10.1021/acsami.0c05401

Han, D.-D., Zhang, Y.-L., Liu, Y., Liu, Y.-Q., Jiang, H.-B., Han, B., et al. (2015). Bioinspired Graphene Actuators Prepared by Unilateral UV Irradiation of Graphene Oxide Papers. *Adv. Funct. Mater.* 25 (28), 4548–4557. doi:10.1002/adfm.201501511

Han, D.-D., Zhang, Y.-L., Ma, J.-N., Liu, Y.-Q., Han, B., and Sun, H.-B. (2016). Light-mediated Manufacture and Manipulation of Actuators. *Adv. Mater.* 28 (38), 8328–8343. doi:10.1002/adma.201602211

Jia, L., Zheng, W., and Huang, F. (2020). Vacuum-ultraviolet Photodetectors. *PhotoniX* 1 (1), 22. doi:10.1186/s43074-020-00022-w

Jiang, H.-B., Zhang, Y.-L., Han, D.-D., Xia, H., Feng, J., Chen, Q.-D., et al. (2014). Bioinspired Fabrication of Superhydrophobic Graphene Films by Two-Beam Laser Interference. *Adv. Funct. Mater.* 24 (29), 4595–4602. doi:10.1002/adfm.201400296

Jiang, H.-B., Zhang, Y.-L., Liu, Y., Fu, X.-Y., Li, Y.-F., Liu, Y.-Q., et al. (2016). Bioinspired Few-Layer Graphene Prepared by Chemical Vapor Deposition on Femtosecond Laser-Structured Cu Foil. *Laser Photon. Rev.* 10 (3), 441–450. doi:10.1002/lpor.201500256

Jiang, H., Zhao, B., Liu, Y., Li, S., Liu, J., Song, Y., et al. (2020). Review of Photoreduction and Synchronous Patterning of Graphene Oxide toward Advanced Applications. *J. Mater. Sci.* 55 (2), 480–497. doi:10.1007/s10853-019-03981-z

Kim, J. G., Lee, J. S., Hwang, H., Kim, E., Choi, Y., Kwak, J. H., et al. (2020). Modeling of Flexible Light Extraction Structure: Improved Flexibility and Optical Efficiency for Organic Light-Emitting Diodes. *Org. Electronics* 85, 105760. doi:10.1016/j.orgel.2020.105760

Kuroiwa, Y., and Tatsuma, T. (2020). Laser Printing of Translucent Plasmonic Full-Color Images with Transmission-Scattering Dichroism of Silver Nanoparticles. *ACS Appl. Nano Mater.* 3 (3), 2472–2479. doi:10.1021/acsanm.9b02560

Lee, J. S., Shim, Y. S., Park, C. H., Hwang, H., Park, C. H., Joo, C. W., et al. (2019). Enhanced Light Extraction from Organic Light-Emitting Diodes Using a Quasi-Periodic Nano-Structure. *Nanotechnology* 30 (8), 085302. doi:10.1088/1361-6528/aaf541

Li, C.-H., Wang, X.-P., Zhao, J.-H., Zhang, D.-Z., Yu, X.-Y., Li, X.-B., et al. (2018). Black Silicon IR Photodiode Supersaturated with Nitrogen by Femtosecond Laser Irradiation. *IEEE Sensors J.* 18 (9), 3595–3601. doi:10.1109/jsen.2018.2812730

Li, C.-H., Zhao, J.-H., Yu, X.-Y., Chen, Q.-D., Feng, J., Han, P.-D., et al. (2017). Sulfur-doped Silicon Photodiode by Ion Implantation and Femtosecond Laser Annealing. *IEEE Sensors J.* 17 (8), 2367–2371. doi:10.1109/jsen.2017.2666178

Li, Z.-Z., Wang, L., Fan, H., Yu, Y.-H., Chen, Q.-D., Juodkazis, S., et al. (2020a). O-FIB: Far-Field-Induced Near-Field Breakdown for Direct Nanowriting in an Atmospheric Environment. *Light Sci. Appl.* 9 (1), 41. doi:10.1038/s41377-020-0275-2

Li, Z., Xu, B., Liang, D., and Pan, A. (2020b). Polarization-dependent Optical Properties and Optoelectronic Devices of 2D Materials. *Research* 2020, 1–35. doi:10.34133/2020/5464258

Liapis, A. C., Rahman, A., and Black, C. T. (2017). Self-assembled Nanotextures Impart Broadband Transparency to Glass Windows and Solar Cell Encapsulants. *Appl. Phys. Lett.* 111 (18), 183901. doi:10.1063/1.5000965

Liu, Y.-Q., Chen, Z.-D., Mao, J.-W., Han, D.-D., and Sun, X. (2019). Laser Fabrication of Graphene-Based Electronic Skin. *Front. Chem.* 7, 461. doi:10.3389/fchem.2019.00461

Liu, Y.-Q., Mao, J.-W., Chen, Z.-D., Han, D.-D., Jiao, Z.-Z., Ma, J.-N., et al. (2020). Three-dimensional Micropatterning of Graphene by Femtosecond Laser Direct Writing Technology. *Opt. Lett.* 45 (1), 113–116. doi:10.1364/ol.45.000113

Liu, Y. Q., Chen, Z. D., Han, D. D., Mao, J. W., Ma, J. N., Zhang, Y. L., et al. (2021). Bioinspired Soft Robots Based on the Moisture-Responsive Graphene Oxide. *Adv. Sci.* 8, 2002464. doi:10.1002/advs.202002464

Lv, P., Zhang, Y. L., Han, D. D., and Sun, H. B. (2021). Directional Droplet Transport on Functional Surfaces with Superwettabilities. *Adv. Mater. Inter.* 8 (12), 2100043. doi:10.1002/admi.202100043

Ma, Q., and Cui, T. J. (2020). Information Metamaterials: Bridging the Physical World and Digital World. *PhotoniX* 1 (1), 1. doi:10.1186/s43074-020-00006-w

Ma, Z.-C., Zhang, Y.-L., Han, B., Hu, X.-Y., Li, C.-H., Chen, Q.-D., et al. (2020). Femtosecond Laser Programmed Artificial Musculoskeletal Systems. *Nat. Commun.* 11 (1), 4536. doi:10.1038/s41467-020-18117-0

Na, D.-Y., and Chew, W. C. (2020). Classical and Quantum Electromagnetic Interferences: What Is the Difference? *Pier* 168, 1–13. doi:10.2528/PIER20060301

Otte, E., and Denz, C. (2020). Optical Trapping Gets Structure: Structured Light for Advanced Optical Manipulation. *Appl. Phys. Rev.* 7 (4), 041308. doi:10.1063/5.0013276

Soldera, M., Taretto, K., Berger, J., and Lasagni, A. F. (2016). Potential of Photocurrent Improvement in μc-Si:H Solar Cells with TCO Substrates Structured by Direct Laser Interference Patterning. *Adv. Eng. Mater.* 18 (9), 1674–1682. doi:10.1002/adem.201600225

Wang, H., Xu, B.-B., Zhang, Y.-L., Kollipara, P. S., Liu, S., Lin, L., et al. (2021a). Light-driven Magnetic Encoding for Hybrid Magnetic Micromachines. *Nano Lett.* 21 (4), 1628–1635. doi:10.1021/acs.nanolett.0c04165

Wang, H., Zhang, Y.-L., Han, D.-D., Wang, W., and Sun, H.-B. (2021b). Laser Fabrication of Modular Superhydrophobic Chips for Reconfigurable Assembly and Self-Propelled Droplet Manipulation. *PhotoniX* 2 (1), 17. doi:10.1186/s43074-021-00033-1

Wang, J.-N., Shao, R.-Q., Zhang, Y.-L., Guo, L., Jiang, H.-B., Lu, D.-X., et al. (2012). Biomimetic Graphene Surfaces with Superhydrophobicity and Iridescence. *Chem. Asian J.* 7 (2), 301–304. doi:10.1002/asia.201100882

Xuan, Z., Li, J., Liu, Q., Yi, F., Wang, S., and Lu, W. (2021). Artificial Structural Colors and Applications. *The Innovation* 2 (1), 100081. doi:10.1016/j.xinn.2021.100081

Yan, Z.-X., Zhang, Y.-L., Wang, W., Fu, X.-Y., Jiang, H.-B., Liu, Y.-Q., et al. (2015). Superhydrophobic Sers Substrates Based on Silver-Coated Reduced Graphene Oxide Gratings Prepared by Two-Beam Laser Interference. *ACS Appl. Mater. Inter.* 7 (49), 27059–27065. doi:10.1021/acsami.5b09128

Yang, Y., Ren, Y.-X., Chen, M., Arita, Y., and Rosales-Guzmán, C. (2021). Optical Trapping with Structured Light: a Review. *Adv. Photon.* 3 (3), 034001. doi:10.1117/1.ap.3.3.034001

You, R., Liu, Y. Q., Hao, Y. L., Han, D. D., Zhang, Y. L., and You, Z. (2020). Laser Fabrication of Graphene-Based Flexible Electronics. *Adv. Mater.* 32, 1901981. doi:10.1002/adma.201901981

Yu, X.-Y., Zhao, J.-H., Li, C.-H., Chen, Q.-D., and Sun, H.-B. (2017). Gold-hyperdoped Black Silicon with High IR Absorption by Femtosecond Laser Irradiation. *IEEE Trans. Nanotechnology* 16 (3), 502–506. doi:10.1109/tnano.2017.2693691

Zhang, H. H., Wang, P. P., Zhang, S., Li, L., Li, P., Sha, W. E. I., et al. (2020a). Electromagnetic-circuital-thermal Multiphysics Simulation Method: a Review (Invited). *Pier* 169, 87–101. doi:10.2528/PIER20112801

Zhang, J., Hu, X., Chen, H., and Gao, F. (2020b). Designer Surface Plasmons Enable Terahertz Cherenkov Radiation (Invited). *Pier* 169, 25–32. doi:10.2528/PIER20102708

Zhang, X., Liu, H., Huang, X., and Jiang, H. (2015). One-step Femtosecond Laser Patterning of Light-Trapping Structure on Dye-Sensitized Solar Cell Photoelectrodes. *J. Mater. Chem. C* 3 (14), 3336–3341. doi:10.1039/c4tc02657h

Zhang, Y.-L., Chen, Q.-D., Jin, Z., Kim, E., and Sun, H.-B. (2012a). Biomimetic Graphene Films and Their Properties. *Nanoscale* 4 (16), 4858–4869. doi:10.1039/c2nr30813d

Zhang, Y.-L., Chen, Q.-D., Xia, H., and Sun, H.-B. (2010). Designable 3D Nanofabrication by Femtosecond Laser Direct Writing. *Nano Today* 5 (5), 435–448. doi:10.1016/j.nantod.2010.08.007

Zhang, Y.-L., Li, J.-C., Zhou, H., Liu, Y.-Q., Han, D.-D., and Sun, H.-B. (2021). Electro-responsive Actuators Based on Graphene. *The Innovation* 2 (4), 100168. doi:10.1016/j.xinn.2021.100168

Zhang, Y.-L., Xia, H., Kim, E., and Sun, H.-B. (2012b). Recent Developments in Superhydrophobic Surfaces with Unique Structural and Functional Properties. *Soft Matter* 8 (44), 11217–11231. doi:10.1039/c2sm26517f

Zhang, Y. L., Liu, Y. Q., Han, D. D., Ma, J. N., Wang, D., Li, X. B., et al. (2019). Quantum-Confined-Superfluidics-Enabled Moisture Actuation Based on Unilaterally Structured Graphene Oxide Papers. *Adv. Mater.* 31 (32), 1901585. doi:10.1002/adma.201901585

Zou, T., Zhao, B., Xin, W., Wang, F., Xie, H., Li, Y., et al. (2021a). Birefringent Response of Graphene Oxide Film Structurized via Femtosecond Laser. *Nano Res.* 1, 1. doi:10.1007/s12274-021-3505-x

Zou, T., Zhao, B., Xin, W., Wang, Y., Wang, B., Zheng, X., et al. (2020). High-speed Femtosecond Laser Plasmonic Lithography and Reduction of Graphene Oxide for Anisotropic Photoresponse. *Light Sci. Appl.* 9 (1), 69. doi:10.1038/s41377-020-0311-2

Zou, X., Xu, Y., and Duan, W. (2021b). 2D Materials: Rising star for Future Applications. *The Innovation* 2 (2), 100115. doi:10.1016/j.xinn.2021.100115

Conflict of Interest: The authors declare that the research was conducted in the absence of any commercial or financial relationships that could be construed as a potential conflict of interest.

Publisher's Note: All claims expressed in this article are solely those of the authors and do not necessarily represent those of their affiliated organizations, or those of the publisher, the editors and the reviewers. Any product that may be evaluated in this article, or claim that may be made by its manufacturer, is not guaranteed or endorsed by the publisher.

frontiers in Chemistry

MINI REVIEW
published: 24 December 2021
doi: 10.3389/fchem.2021.801477

Ion-Doped Photonic Crystal Fiber Lasers

Ya-Chong Hou[1,2], Yun-Fei Li[1,2], Xiao-Fan Xie[1,2], Zi-Long Kou[1,2], Yue Lu[1,2], Si-Ying Chen[1,2], Yulei Wang[1,2] and Zhiwei Lu[1,2]*

[1]Center for Advanced Laser Technology, Hebei University of Technology, Tianjin, China, [2]Hebei Key Laboratory of Advanced Laser Technology and Equipment, Tianjin, China

Compared with conventional solid-state lasers, fiber lasers have the advantages of small size, simple cooling system, and good output beam quality, enabling them an extended service lifetime in industrialized environments. Periodically arranged photonic crystals have been the most important gain medium for high-power laser applications, which overcame the problems in fiber lasers such as small mode field, low degree of nonlinearity, and non-adjustable dispersion. In this mini-review, we summarize the recent advances of typical ion-doped photonic crystal fiber lasers doped, discuss the challenges, and provide an outlook on the future developments in ion-doped photonic crystal fiber lasers.

Keywords: fiber, laser, photonic crystal, ion doping, output characteristics

OPEN ACCESS

Edited by:
Andreas Rosenkranz,
University of Chile, Chile

Reviewed by:
Ran Ding,
Hong Kong Polytechnic University,
Hong Kong SAR, China
Xiaofeng Liu,
University of California, Irvine,
United States

***Correspondence:**
Yun-Fei Li
yfli@hebut.edu.cn

Specialty section:
This article was submitted to Nanoscience, a section of the journal Frontiers in Chemistry

Received: *25 October 2021*
Accepted: *10 December 2021*
Published: *24 December 2021*

Citation:
Hou Y-C, Li Y-F, Xie X-F, Kou Z-L, Lu Y, Chen S-Y, Wang Y and Lu Z (2021) Ion-Doped Photonic Crystal Fiber Lasers. Front. Chem. 9:801477. doi: 10.3389/fchem.2021.801477

INTRODUCTION

High-quality output laser systems are constantly pursued in solid-state lasers, due to their applications in laser ranging and laser medicine (Kim et al., 2020; Miura et al., 2020; Chen et al., 2021). However, traditional solid-state lasers have severe temperature effects and generate a lot of heat, influencing the output performance. Due to the flexible structure, large mode field area (Knight et al., 1998), photonic crystal fibers maintain the superior characteristics of infinite single mode (Birks et al., 1997), low loss and adjustable dispersion (Ferrando et al., 2000; Ortigosa-Blanch et al., 2000; Zhang, 2012), overcoming the defects of conventional fibers, and have replaced the traditional YAG. So far, photonic crystal fibers have great potential for applications in fiber lasers, fiber optic communication (Han, 2010), fiber optic sensing (Kang et al., 2015) and nonlinear optics (Dudley and Taylor, 2009), so researchers have extensively studied the doping of different ions in photonic crystal fibers, and thus prepared photonic crystal fiber lasers with different output characteristics.

Currently, the power enhancement of fiber lasers is mainly affected by nonlinear effects (NLEs) (Zervas and Codemard, 2014a; Man Hu et al., 2016), photodarkening (PD) effects (Jetschke et al., 2008), and Transverse mode instability (TMI) effects (Tao et al., 2015). Large mode field fibers are usually used instead of conventional small core diameter double cladding fibers to suppress the nonlinear effects and thus increase the output power. Although increasement of the core diameter is an effective method to achieve a large mode field, this will affect the beam quality. To resolve the conflict between large mode field and beam quality, the structural design of the fiber and rare earth ion doping can be employed to suppress the photodarkening effect of the fiber (Jauregui et al., 2015; Petit et al., 2016). One of the important strategies adopted to increase the mode instability threshold is the preparation of large mode field fibers with smaller core numerical apertures. These mentioned problems can be solved by the ion doping of photonic crystal structured fibers. However, the preparation of doped photonic crystal fibers need to meet the geometric size, optical (refractive

index, homogeneity) and spectral (doping concentration, absorption and emission) performance requirements, posing a challenge for these techniques.

In this mini-review, we summarize the recent advances in doped photonic crystal fiber lasers, describe the basic structure and optical conduction mechanism of photonic crystal fibers. Several typical photonic crystal fiber lasers have been reviewed, including ytterbium ion-doped photonic crystal fiber lasers, erbium ion-doped photonic crystal fiber lasers, thulium ion-doped photonic crystal fiber lasers, and other doped types of photonic crystal fiber. In addition, the mini-review briefly discusses the challenges in the field and provides an outlook for the future.

STRUCTURE AND LIGHT CONDUCTION MECHANISM OF PHOTONIC CRYSTAL FIBERS

Photonic crystal fiber (PCF), is also known as microstructured fiber (MOF) or porous fiber (PF). Since the first photonic crystal fiber was successfully developed by Knight group in 1996, photonic crystal fibers had been hotly pursued in laser systems for years. Photonic crystal fibers have been the most important gain medium for high-power laser applications, which possess flexible structure and high optical characteristics overwhelming traditional fiber structures (Cheng et al., 2014; Li et al., 2019a; Lv et al., 2020a; Li et al., 2020). Photonic crystal fibers can be divided into total internal reflection photonic crystal fibers, photonic bandgap photonic crystal fibers, and anti-resonant photonic crystal fibers based on transmission mechanisms. Besides, they can also be divided into solid-core photonic crystal fibers and hollow-core photonic crystal fibers based on structures (Knight, 2003; Russell, 2003; Belardi and Knight, 2014). Among them, solid-core photonic crystal fiber, also known as refractive index-guided fiber, is composed of a fiber core and a cladding consisting of periodically arranged air holes around it. The light-guiding mechanism of such fiber is total internal reflection (Markos et al., 2017). Subsequently, solid-core photonic crystal fibers gradually evolve into nonlinear photonic crystal fibers, large-mode field photonic crystal fibers, and rare-earth-doped photonic crystal fibers with different structures and functions.

Hollow-core photonic crystal fibers can be divided into two types by light conduction mechanisms, namely hollow-core photonic bandgap, and hollow-core anti-resonant. The core of hollow-core photonic bandgap photonic crystal fibers is generally filled with air or other gases, whose light conduction mechanism is photonic bandgap effect, as opposed to the total internal reflection type fibers (Huang et al., 2017; Boufenar et al., 2018). In a photonic bandgap fiber, periodic structure can be formed by alternating arrangements of high and low refractive index materials, which influences the photonic bandgap. The distances between the periodically low refractive index sites are the same, resulting in the confinement of light only for a certain frequency of light in the core. Based on the band gap effect, light is only transmitted in a low refractive index core, which greatly reduces transmission losses. Moreover, the core can be adjusted according to the actual situation, which can be 3 cores, 7 cores, and other multi-core structures (Zhu et al., 2012; Xiang and Jiang, 2018; Lv et al., 2020b). The other kind is anti-resonant hollow-core photonic crystal fiber (Markos et al., 2015), whose cladding consists of only one layer of air holes. The light conduction mechanism of this fiber is different from that of hollow-core bandgap fiber; and the structure can be regarded as a resonant cavity, due to the high refractive index region on the inner wall of the cladding. In the resonant state, light leaks out of the cladding since the resonant cavity can be regarded as transparent. In the non-resonant state, the reflection coefficient of the resonant cavity has a high reflection coefficient, which limits the propagation of light within the core (Kudlinski et al., 2020). It is the flexibility and versatility of the photonic crystal fiber structure improves the output characteristics of lasers, which gives it advantages than the conventional fiber structure.

ION-DOPED PHOTONIC CRYSTAL FIBER LASERS

It is the unique advantages of photonic crystal structured fibers have stimulated research interest in the development of special lasers with various outputs. In this section, we briefly summarize the recent advances of representative ion-doped photonic crystal fiber lasers (**Figure 1**).

YTTERBIUM-DOPED IONS

In 2012, IPG achieved 10 kW single-mode fiber laser output using a large-mode-field double-clad fiber with a core diameter of about 25 μm, which became a milestone in the development of photonic crystal fiber lasers (Limpert et al., 2012). Inspired by IPG, researchers have developed a variety of photonic crystal fiber lasers. As the photodarkening effect of the fiber can be improved by doping with ions, the photonic crystal fiber structure has large-mode field properties that can withstand high power without optical damage and ensure good beam quality. Ion-doped large-mode field photonic crystal fibers have attracted significant attentions in high peak power picosecond ultrafast laser amplifiers (Zervas and Codemard, 2014b; Diouf et al., 2016; Kabir and Razzak, 2018; Li et al., 2019b). The most common doping ion in photonic crystal fiber is ytterbium ion. Specifically, Otto et al. (2014) obtained an average output power of 2 kW in an ytterbium-doped large-span photonic crystal fiber, including a peak power of 0.8 MW with a beam quality M^2 less than 3 (Wei et al., 2016). Wei et al. (2016) investigate an all-solid-state large-area ytterbium-doped quartz photonic crystal fiber, in which they achieved an all-solid-state large-mode field microstructured fiber with a core diameter of 50 μm. The fiber laser could maintain quasi-single-mode transmission characteristics in 1,064 nm and obtain a laser output of 8 W. In addition, Wang et al. (2019) also successfully developed a quasi-single-mode picosecond pulsed laser with ytterbium-doped large-mode field photonic crystal fiber, in which the inner cladding diameter was about 260 μm with outer diameter of about 450 μm, air hole diameter of about

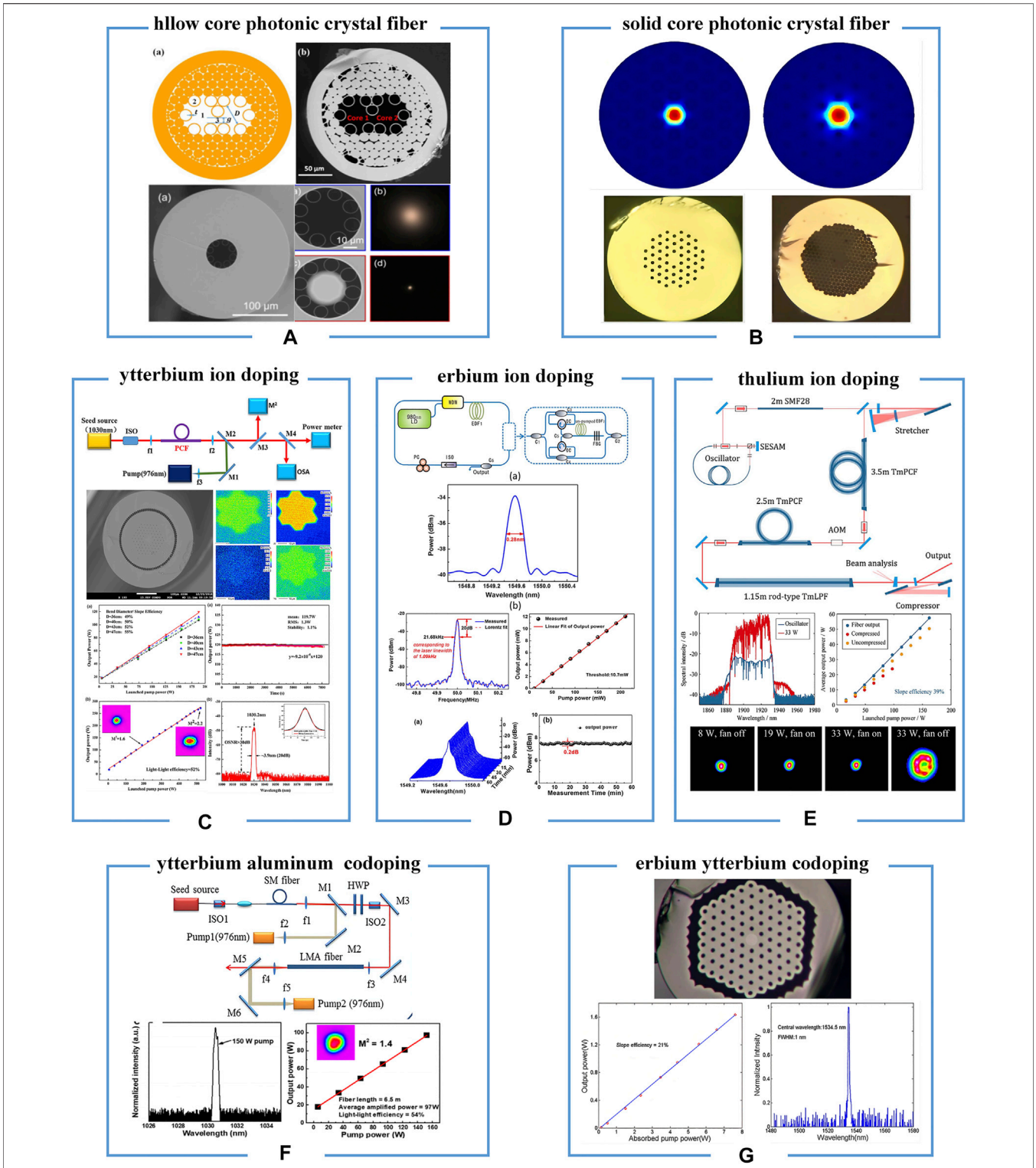

FIGURE 1 | Ion-doped photonic crystal fiber lasers. **(A,B)** Types of photonic crystal fibers. **(C–G)** Various ion-doped photonic crystal fiber lasers such as Ytterbium ion doping **(C)**, Erbium ion doping **(D)**, Thulium ion doping **(E)**, Ytterbium aluminum codoping **(F)**, and Erbium ytterbium codoping **(G)**.

2.5 μm, and the spacing of about 14 μm. At the optimal bending diameter of 47 cm and 520 W pumping power, the fiber laser achieved a maximum output power of 272 W, a single pulse energy of 5.6 μJ, and a peak power of 266 kW. However, the beam quality gradually deteriorated with the increased power, owing to the thermal accumulation of the core. The thermal accumulation

triggered the change in the refractive index of the core, leading to a mismatch in the numerical aperture of the core and further affecting the laser beam quality (Li et al., 2010). Subsequently, Wang et al. further prepared an ytterbium-doped large-mode field photonic crystal fiber laser with a core diameter of 75 μm, based on an optimized fabrication process, in which the air aperture was approximately 2 μm and the spacing was approximately 16 μm. The corresponding fiber laser obtained an average output power of 102 W with a single pulse energy of 102 μJ and a peak power of more than 1 MW at 166 W pumping power. This experiment had not observed excited stimulated Raman scattering (SRS) emission phenomenon. The Yb-doped large-mode field photonic crystal fiber lasers improved greatly in terms of picosecond pulsed laser amplification performance with the improvement of the Yb-doped core material preparation technology.

ERBIUM-DOPED IONS

Although ytterbium-doped ion photonic crystal fibers are still the mainstream of laser development, erbium-doped ion photonic crystal fiber lasers have also been extensively studied in recent years, especially in narrow linewidth output with ultrashort pulse lasers (Li et al., 2015). Li et al. (2015) obtained a three-wavelength narrow linewidth output of less than 2 kW or a six-wavelength narrow linewidth output of less than 5 kW using a tunable variable optical attenuator based on Rayleigh scattering for tunable narrow linewidth Brillouin-doped photonic crystal fiber lasers (Pourshab et al., 2017). Pourshab et al. (2017) obtained the laser output at 1,561.47 nm with an uplink linewidth of less than 1.19 kHz using an erbium-gallium co-doped photonic crystal fiber as the gain medium and a narrow-band filter, a sub-ring cavity and a cascaded anisotropic fiber as mode selection. Narrow linewidth lasers are important in a variety of fields where high precision and strong coherence are required. In addition, Elahi et al. (2017) overcame the spectral narrowing effect of erbium-doped photonic crystal fiber in the amplification process and obtained an ultrashort pulse output with a minimum pulse width of 175 fs, a repetition frequency of 43 MHz, a central wavelength of 1,550 nm, and a single pulse energy of 80 nJ in an erbium-doped photonic crystal fiber pulse amplification system.

THULIUM-DOPED IONS

At present, there are fewer reports on Nd-doped photonic crystal fiber lasers compared to Yb-doped photonic crystal fiber lasers and Erbium-doped photonic crystal fiber lasers. A chirped amplification system using a thulium-doped photonic crystal fiber with a mode field diameter of 65 μm and an air cladding of 260 μm was established by Stutzki et al. (2015) A pulsed peak power of 200 MW, an average output power of 24 W, and a pulsed energy of 120 μJ were achieved with a 790 nm laser diode backward pumping. In addition, in their study of compact thulium-doped photonic crystal fiber lasers, Lee et al. (2020) achieved a picosecond pulse output in 2 μm with an average output power of up to 25 W. This pulse was compressed by a compact multipass configuration, resulting in a maximum output pulse energy of 46.3 μJ and a maximum output pulse width of 2.8 ps.

Other Photonic Crystal Fiber Lasers

In recent years, several researchers have used chemical vapor deposition techniques to prepare photonic crystal fibers with very low numerical apertures using various co-doping ions such as $Yb^{3+}/Al^{3+}/P^{5+}$ and $Yb^{3+}/Al^{3+}/F^{-}$. For example, in their study of large-mode field photonic crystal fiber lasers, Wang et al. (2017) successfully prepared a fiber with a core diameter of 50 μm using $Yb^{3+}/Al^{3+}/P^{5+}/F^{-}$ co-doping and achieved a laser output with an average power of 97 W, a peak power of 93 kW, and a beam quality of 1.4. Since high-power fiber lasers in the 1.5 μm band have a wide range of applications and the gain medium for fiber lasers in this band is usually a double-clad erbium-ytterbium co-doped fiber, so that ytterbium-erbium co-doped photonic crystal fibers dominate among other dopant ions, Of which Wang et al. (2014) studied large-mode field fiber lasers using erbium-ytterbium co-doping in a stable laser output with a maximum power of 1.6 W and a center wavelength of 1,534.5 nm obtained in a 600 mm length photonic crystal fiber. The pump optical power was 150 mW, with the slope efficiency of 21%, and the beam quality factor M^2 less than 1.05. The co-doped photonic crystal fiber has excellent laser performance and is an important direction for future development in fiber lasers.

CONCLUSION AND OUTLOOK

In summary, optical fibers with photonic crystal structures are flexible and versatile, featuring large mode field area, infinite single mode, low loss, and hold great promise for the preparation of high-power ultrashort pulse lasers. This mini-review summarizes the recent advances in photonic crystal fiber lasers doped with different ions, including ytterbium-doped photonic crystal fiber lasers, erbium-doped photonic crystal fiber lasers, thulium-doped photonic crystal fiber lasers, and other types of photonic crystal fiber lasers. However, due to the special nature of photonic crystal structures, the major challenge at present is that the pulling of photonic crystal fibers. 3D printing microstructured optical fiber process is an effective approach to solve the problem of difficult preparation of microstructured fiber prefabricated rods and long-distance fiber drawing, paving a way to the future development of photonic crystal fiber. In addition, Compared to photonic crystal structured lasers and sensors, photonic crystal structured optical fibre communication has been less researched, but there is great potential for development due to its unique properties such as photonic band gap effect, unique waveguide properties and non-linearity making it important in areas such as optical wave transmission and control, optical information manipulation and processing and new photonic devices. In conclusion, compared with conventional optical fibers, photonic crystal

structured optical fibers possess significant research values in numerous fields.

AUTHOR CONTRIBUTIONS

All authors listed have made a substantial, direct and intellectual contribution to the work, and approved it for publication.

FUNDING

This work was supported by National Natural Science Foundation of China (Grant Nos. 62004059, 62005074, 62075056, and 61927815), Natural Science Foundation of Hebei Province (Grant Nos. F2021202047, and F2021202002), Funding Projects for the Introduction of Overseas Staff of Hebei Province (Grant No. C20210334), and Key Laboratory Fund Project (Grant No. 61421070302).

REFERENCES

Belardi, W., and Knight, J. C. (2014). Hollow Antiresonant Fibers with Reduced Attenuation. *Opt. Lett.* 39, 1853–1856. doi:10.1364/OL.39.001853

Birks, T. A., Knight, J. C., and Russell, P. S. J. (1997). Endlessly Single-Mode Photonic crystal Fiber. *Opt. Lett.* 22, 961–963. doi:10.1364/OL.22.000961

Boufenar, R., Bouamar, M., and Hocini, A. (2018). Numerical Analysis of a Temperature Sensor Based on the Photonic Band gap Effect in a Photonic crystal Fiber. *Chin. J. Phys.* 56, 1126–1132. doi:10.1016/j.cjph.2018.03.036

Chen, L., Su, Y., Zhang, J., Zhang, H., Fan, B., Shao, G., et al. (2021). Nanosecond Laser Cleaning Method to Reduce the Surface Inert Layer and Activate the Garnet Electrolyte for a Solid-State Li Metal Battery. *ACS Appl. Mater. Inter.* 13, 37082–37090. doi:10.1021/acsami.1c08509

Cheng, J., Qiu, J., and Ruan, S. (2014). Switchable Quadruple-Wavelength Erbium-Doped Photonic crystal Fiber Laser Based on a Polarization-Maintaining Photonic crystal Fiber Sagnac Loop Filter. *Opt. Laser Tech.* 58, 110–113. doi:10.1016/j.optlastec.2013.11.005

Diouf, M., Ben Salem, A., Cherif, R., Wague, A., and Zghal, M. (2016). High Power Broadband Mid-infrared Supercontinuum Fiber Laser Using a Novel Chalcogenide AsSe2 Photonic crystal Fiber. *Opt. Mater.* 55, 10–16. doi:10.1016/j.optmat.2016.03.010

Dudley, J. M., and Taylor, J. R. (2009). Ten Years of Nonlinear Optics in Photonic crystal Fibre. *Nat. Photon* 3, 85–90. doi:10.1038/NPHOTON.2008.285

Elahi, P., Kalaycıoğlu, H., Li, H., Akçaalan, Ö., and Ilday, F. Ö. (2017). 175 Fs-Long Pulses from a High-Power Single-Mode Er-Doped Fiber Laser at 1550 Nm. *Opt. Commun.* 403, 381–384. doi:10.1016/j.optcom.2017.07.072

Ferrando, A., Silvestre, E., Miret, J. J., and Andrés, p. (2000). Nearly Zero Ultraflattened Dispersion in Photonic crystal Fibers. *Opt. Lett.* 25, 790–792. doi:10.1364/OL.25.000790

Han, Y.-G. (2010). Triple-wavelength Switchable Multiwavelength Erbium-Doped Fiber Laser Based on a Highly Nonlinear Photonic crystal Fiber. *J. Korean Phy. Soc.* 56, 1251–1255. doi:10.3938/jkps.56.1251

Huang, X., Ma, J., Tang, D., and Yoo, S. (2017). Hollow-core Air-gap Anti-resonant Fiber Couplers. *Opt. Express* 25, 29296–29306. doi:10.1364/OE.25.029296

Jauregui, C., Otto, H.-J., Modsching, N., Limpert, J., and Tünnermann, A. (2015). Recent Progress in the Understanding of Mode Instabilities. *Proc. SPIE* 9344, 93440J–93446J. doi:10.1117/12.2086843

Jetschke, S., Unger, S., Schwuchow, A., Leich, M., and Kirchhof, J. (2008). Efficient Yb Laser Fibers with Low Photodarkening by Optimization of the Core Composition. *Opt. Express* 16, 15540–15545. doi:10.1364/OE.16.015540

Kabir, S., and Razzak, S. M. A. (2018). Bending Resistive Improved Effective Mode Area Fluorine Doped Quadrilateral Shaped Core Photonic crystal Fiber for High Power Fiber Lasers. *Optik* 162, 206–213. doi:10.1016/j.ijleo.2018.02.046

Kang, Z., Sun, J., Bai, Y., and Jian, S. (2015). Twin-Core Fiber-Based Erbium-Doped Fiber Laser Sensor for Decoupling Measurement of Temperature and Strain. *IEEE Sensors J.* 15, 6828–6832. doi:10.1109/JSEN.2015.2460731

Kim, W., Jang, J., Han, S., Kim, S., Oh, J. S., Kim, B. S., et al. (2020). Absolute Laser Ranging by Time-Of-Flight Measurement of Ultrashort Light Pulses [Invited]. *J. Opt. Soc. Am. A.* 37, B27–B35. doi:10.1364/JOSAA.395157

Knight, J. C., Birks, T. A., Cregan, R. F., Russell, P. S. J., and de Sandro, J.-P. (1998). Large Mode Area Photonic crystal Fibre. *Electron. Lett.* 34, 1347–1348. doi:10.1049/el_19980965

Knight, J. C. (2003). Photonic crystal Fibres. *Nature* 424, 847–851. doi:10.1038/nature01940

Kudlinski, A., Cassez, A., Vanvincq, O., Septier, D., Pastre, A., Habert, R., et al. (2020). Double Clad Tubular Anti-resonant Hollow Core Fiber for Nonlinear Microendoscopy. *Opt. Express* 28, 15062–15070. doi:10.1364/OE.389084

Lee, E., Sun, B., Sun, B., Luo, J., Singh, S., Choudhury, D., et al. (2020). Compact Pulsed Thulium-Doped Fiber Laser for Topographical Patterning of Hydrogels. *Opto-Electronic Adv.* 3, 190039. doi:10.29026/oea.2020.190039

Li, F., Yang, Z., Lv, Z., Wang, Y., Li, Q., Wei, Y., et al. (2019). High Energy Femtosecond Laser Micromachining with Hollow Core Photonic crystal Fiber Delivery. *Optik* 194, 163093. doi:10.1016/j.ijleo.2019.163093

Li, F., Yang, Z., Lv, Z., Wang, Y., Li, Q., Wei, Y., et al. (2019). High Energy Femtosecond Laser Micromachining with Hollow Core Photonic crystal Fiber Delivery. *Optik* 194, 163093. doi:10.1016/j.ijleo.2019.163093

Li, H., Huang, W., Cui, Y. L., Cui, Y., Zhou, Z., and Wang, Z. (2020). 3 W Tunable 1.65 Mm Fiber Gas Raman Laser in D2-Filled Hollow-Core Photonic crystal Fibers. *Opt. Laser Tech.* 132, 106474. doi:10.1016/j.optlastec.2020.106474

Li, J., Duan, K., Dai, Z., Ou, Z., Liu, Y., and Liu, Y. (2010). Theoretical Analysis of the Heat Dissipation Mechanism in High Power Photonic crystal Fiber Lasers. *Optik* 121, 1243–1250. doi:10.1016/j.ijleo.2009.01.015

Li, L., Zhang, M., Liu, Y., Li, Y., and Wang, Y. (2015). Stable Single-Longitudinal-Mode Erbium-Doped Fiber Laser with Narrow Linewidth Utilizing Parallel Fiber Ring Resonator Incorporating Saturable Absorber and Fiber Bragg Grating. *Appl. Opt.* 54, 4001–4005. doi:10.1364/AO.54.004001

Limpert, J., Stutzki, F., Jansen, F., Otto, H.-J., Eidam, T., Jauregui, C., et al. (2012). Yb-doped Large-Pitch Fibres: Effective Single-Mode Operation Based on Higher-Order Mode Delocalisation. *Light Sci. Appl.* 1, e8. doi:10.1038/lsa.2012.8

Lv, Y., Lou, S., Tang, Z., Liu, X., and Wang, X. (2020). Tunable C-Band and L-Band Multi-Wavelength Erbium-Doped Fiber Ring Laser Based on a Triple-Core Photonic crystal Fiber with Polarization-dependent Loss. *Opt. Laser Tech.* 128, 106269. doi:10.1016/j.optlastec.2020.106269

Lv, Y., Lou, S., Tang, Z., Liu, X., and Wang, X. (2020). Tunable C-Band and L-Band Multi-Wavelength Erbium-Doped Fiber Ring Laser Based on a Triple-Core Photonic crystal Fiber with Polarization-dependent Loss. *Opt. Laser Tech.* 128, 106269. doi:10.1016/j.optlastec.2020.106269

Man Hu, M. H., Zhao Quan, Z. Q., Jianhua Wang, J. W., Kai Liu, K. L., Xiaolong Chen, X. C., Chun Zhao, C. Z., et al. (2016). Stimulated Brillouin Scattering Threshold Dependent on Temporal Characteristics in a Kilowatt-Peak-Power, Single-Frequency Nanosecond Pulsed Fiber Amplifier. 中国光学快报 14–31407031403. doi:10.3788/COL201614.031403

Markos, C., Nielsen, K., and Bang, O. (2015). Antiresonant Guiding in a Poly(methyl-Methacrylate) Hollow-Core Optical Fiber. *J. Opt.* 17, 105603. doi:10.1088/2040-8978/17/10/105603

Markos, C., Travers, J. C., Abdolvand, A., Eggleton, B. J., and Bang, O. (2017). Hybrid Photonic-crystal Fiber. *Rev. Mod. Phys.* 89, 045003. doi:10.1103/RevModPhys.89.045003

Miura, M., Wakita, R., and Iwasaki, T. (2020). Modified Low Power Mode Laser for the Treatment of Central Serous Chorioretinopathy. *Opth* Vol. 14, 4109–4113. doi:10.2147/OPTH.S284005

Ortigosa-Blanch, A., Knight, J. C., Wadsworth, W. J., Arriaga, J., Mangan, B. J., Birks, T. A., et al. (2000). Highly Birefringent Photonic crystal Fibers. *Opt. Lett.* 25, 1325–1327. doi:10.1364/OL.25.001325

Otto, H.-J., Stutzki, F., Modsching, N., Jauregui, C., Limpert, J., and Tünnermann, A. (2014). 2 kW Average Power from a Pulsed Yb-Doped Rod-type Fiber Amplifier. *Opt. Lett.* 39, 6446–6449. doi:10.1364/OL.39.006446

Petit, V., Tumminelli, R. P., Minelly, J. D., and Khitrov, V. (2016). Extremely Low NA Yb Doped Preforms (<0.03) fabricated by MCVD. *Proc. SPIE* 9728, 97282R–97287R. doi:10.1117/12.2214546

Pourshab, N., Gholami, A., Hekmat, M. J., and Shahriyari, N. (2017). Analysis of Narrow Linewidth Fiber Laser Using Double Subring Resonators. *J. Opt. Soc. Am. B* 34, 2414–2420. doi:10.1364/JOSAB.34.002414

Russell, P. (2003). Photonic crystal Fibers. *Science* 299, 358–362. doi:10.1126/science.1079280

Stutzki, F., Gaida, C., Gebhardt, M., Jansen, F., Jauregui, C., Limpert, J., et al. (2015). Tm-based Fiber-Laser System with More Than 200 MW Peak Power. *Opt. Lett.* 40, 9–12. doi:10.1364/OL.40.000009

Tao, R., Ma, P., Wang, X., Zhou, P., and Liu, Z. (2015). 13 kW Monolithic Linearly Polarized Single-Mode Master Oscillator Power Amplifier and Strategies for Mitigating Mode Instabilities. *Photon. Res.* 3, 86–93. doi:10.1364/PRJ.3.000086

Wang, F., Hu, L., Xu, W., Wang, M., Feng, S., Ren, J., et al. (2017). Manipulating Refractive index, Homogeneity and Spectroscopy of Yb3+-Doped Silica-Core Glass towards High-Power Large Mode Area Photonic crystal Fiber Lasers. *Opt. Express* 25, 25960–25969. doi:10.1364/OE.25.025960

Wang, L., He, D., Feng, S., Yu, C., Hu, L., Qiu, J., et al. (2014). Yb/Er Co-doped Phosphate All-Solid Single-Mode Photonic crystal Fiber. *Sci. Rep.* 4, 6139. doi:10.1038/srep06139

Wang, M., Wang, F., Feng, S., Yu, C., Wang, S., Zhou, Q., et al. (2019). 272 W Quasi Single-Mode Picosecond Pulse Laser of Ytterbium-Doped Large-Mode-Area Photonic crystal Fiber. 中国光学快报 17, 071401. doi:10.3788/COL201917.071401

Wei, H., Chen, K., Yang, Y., and Li, J. (2016). All-solid Very Large Mode Area Ytterbium-Doped Silica Microstructured Fiber Based on Accurate Control on Cladding index. *Opt. Express* 24, 8978–8987. doi:10.1364/OE.24.008978

Xiang, H., and Jiang, Y. (2018). Fiber Bragg Grating Inscription in Multi-Core Photonic crystal Fiber by Femtosecond Laser. *Optik* 171, 9–14. doi:10.1016/j.ijleo.2018.06.020

Zervas, M. N., and Codemard, C. A. (2014). High Power Fiber Lasers: a Review. *IEEE J. Select. Top. Quan. Electron.* 20, 219–241. doi:10.1109/JSTQE.2014.2321279

Zervas, M. N., and Codemard, C. A. (2014). High Power Fiber Lasers: a Review. *IEEE J. Select. Top. Quan. Electron.* 20, 219–241. doi:10.1109/JSTQE.2014.2321279

Zhang, Y. (2012). Demonstration of Ultra-flattened Dispersion Low Confinement Loss in Square Lattice Structure Photonic Crystal Fibers. *J. Nanoelectronics Optoelectronics* 7, 405–409. doi:10.1166/jno.2012.1318

Zhu, T., Xiao, F., Xu, L., Liu, M., Deng, M., and Chiang, K. S. (2012). Pressure-assisted Low-Loss Fusion Splicing between Photonic crystal Fiber and Single-Mode Fiber. *Opt. Express* 20, 24465–24471. doi:10.1364/OE.20.024465

Conflict of Interest: The authors declare that the research was conducted in the absence of any commercial or financial relationships that could be construed as a potential conflict of interest.

Publisher's Note: All claims expressed in this article are solely those of the authors and do not necessarily represent those of their affiliated organizations, or those of the publisher, the editors and the reviewers. Any product that may be evaluated in this article, or claim that may be made by its manufacturer, is not guaranteed or endorsed by the publisher.

frontiers in Chemistry

MINI REVIEW
published: 24 December 2021
doi: 10.3389/fchem.2021.811074

Light-Assisted Enhancement of Gas Sensing Property for Micro-Nanostructure Electronic Device: A Mini Review

Zongtao Ma[1], *Ziying Wang*[2,3]* *and Lingxiao Gao*[2,3]*

[1]State Key Laboratory of Reliability and Intelligence Electrical Equipment, Hebei University of Technology, Tianjin, China, [2]National Engineering Research Center for Technological Innovation Method and Tool, School of Mechanical Engineering, Hebei University of Technology, Tianjin, China, [3]School of Electronics and Information Engineering, Hebei University of Technology, Tianjin, China

In recent years, gas sensing electronic devices have always attracted wide attention in the field of environment, industry, aviation and others. In order to improve the gas sensing properties, many micro- and nano-fabrication technologies have been proposed and investigated to develop high-performance gas sensing devices. It is worth noting that light irradiation is an effective strategy to enhance gas sensitivity, shorten the response and recovery time, reduce operating temperature. In this review, firstly, the latest research advances of gas sensors based on different micro-nanostructure materials under UV light and visible light activation is introduced. Then, the gas sensing mechanism of light-assisted gas sensor is discussed in detail. Finally, this review describes the present application of gas sensors with improved properties under light activation assisted conditions and the perspective of their applications.

Keywords: light irradiation, micro-nanostructure, gas sensing devices, sensor, metal oxide semiconductor

OPEN ACCESS

Edited by:
Yue-Feng Liu,
Jilin University, China

Reviewed by:
Jianxun Dai,
Dalian University of Technology, China
Jing Cao,
Tianjin Polytechnic University, China

***Correspondence:**
Ziying Wang
wangzy@hebut.edu.cn
Lingxiao Gao
lingxiao.gao@hebut.com

Specialty section:
This article was submitted to Nanoscience, a section of the journal Frontiers in Chemistry

Received: *08 November 2021*
Accepted: *24 November 2021*
Published: *24 December 2021*

Citation:
Ma Z, Wang Z and Gao L (2021) Light-Assisted Enhancement of Gas Sensing Property for Micro-Nanostructure Electronic Device: A Mini Review. Front. Chem. 9:811074. doi: 10.3389/fchem.2021.811074

INTRODUCTION

With the rapid improvement of economy and the quality of human life, people have realized that environmental pollution has caused irreparable damage to the Earth. Harmful gases from coal-fired power stations, garbage incineration, automobile exhaust and industrial waste gas not only pose a threat to the environment but also endanger human health (Cheng et al., 2021a). Therefore, the development of harmful gas detection technology is of great significance.

The metal oxide semiconductor (MOS) sensors have many advantages of small size, high response, fast response and so on, which attract great interest in real-time detection of different gases. However, the high operating temperature can reduce the life of the device and sensitivity. Consequently, researchers began to explore gas sensing devices by putting forward a large number of theoretical methods and experimental schemes, which can work at low temperature or even room temperature (RT). In recent years, with the continuous development of nanotechnology and nanomaterials, the research of RT gas sensor has also got significant progress include morphological control (Wang et al., 2021, noble metal surface modification (Wang et al., 2019a) or doping and the formation of heterostructures (Wang et al., 2019b). Furthermore, light activation is an effective method to improve the performance of MOS sensors. The optical irradiation of MOS sensor can change the surface electronic properties by adjusting the concentration of optical carriers in MOS, so as to promote the interaction between molecule and sensor layer (Kumar et al., 2020). Herein, we will summarize the latest progress of photoactivated RT MOS sensors in the past few years.

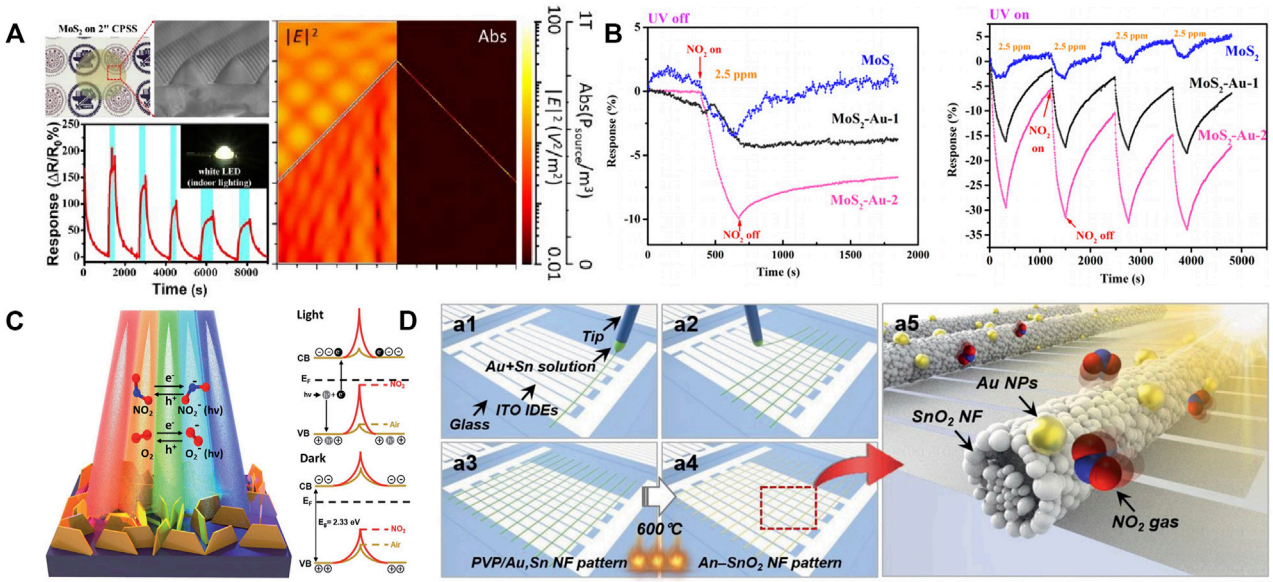

FIGURE 1 | (A) Microscopic characterization of MoS_2 and gas sensing performance under white light, Simulation results for the Flat-MoS_2 and Cone-Shaped-MoS_2 gas sensors by finite difference time domain (FDTD) illuminated by the light with the wavelength of 550 nm. Reproduced with permission from ref. 13. Copyright 2019, Royal Society of Chemistry. **(B)** Schematic illustrations of edge-enriched SnS_2 NFs for visible light activated NO_2 gas sensor. Reproduced with permission from ref. 14. Copyright 2021, Royal Society of Chemistry. **(C)** Sensing performance of MoS_2 and MoS_2-Au sensors toward NO_2 gas with no UV illumination. Reproduced with permission from ref. 17. Copyright 2018, American Institute of Physics. **(D)** Schematic illustration for (left) the experimental procedures to fabricate nanofiber pattern (NF-P) sensors via near-field electrospinning (NFES) and (right) NO_2 detection of nanofiber pattern (NF-P) sensors under visible light illumination. Reproduced with permission from ref. 18. Copyright 2021, WILEY-VCH.

Recently, many reports have confirmed that ultraviolet (UV) irradiation can indeed improve the performance of MOS sensors, including higher sensitivity, shorter recovery time and lower power consumption. UV excitation can increase the density of free electron-hole pairs and lead to photodissociation of the target gas and chemical surface adsorbents (Zhai et al., 2018; Park et al., 2014; Hyodo et al., 2017). However, the harmful effects of UV light on human skin and eyes remain an acute problem, and UV light accounts for only 5–7% of the total energy from sunlight. Therefore, additional UV-LED light sources are required, which presents a new challenge to the size design of the sensor. By contrast, visible light is superior to UV light in terms of energy acquisition and energy utilization. More importantly, it does no harm to human health. Similarly, visible light activation of narrow band gap metal oxides for RT gas sensing has been explored by numerous researchers in the past few years (Hasani et al., 2015; Li et al., 2018; Song et al., 2020). While visible light activation is an effective way to improve the performance of MOS sensors, it still faces great challenges to widely apply it in real environment.

In this paper, we discuss RT gas sensors under light assisted conditions. This review is divided into three parts: firstly, we focus on the latest progress of gas sensors based on MOS, noble metal doped MOS and MOS with heterojunction structure at room temperature by different wavelength light sources (UV light and visible light). Secondly, we describe the gas sensing mechanism under light-assisted condition. Finally, we introduce the application status and future prospects of gas sensors under light-assisted conditions.

LIGHT ACTIVATION GAS SENSORS BASED ON DIFFERENT MICRO-NANOSTRUCTURE MATERIALS

Many studies have shown that light irradiation is one of the effective ways to improve the gas sensitivity of pure MOS, noble metal doping MOS nanostructure and MOS with heterostructure can be improved under the condition of light activation, which will be described one by one below.

Gas Sensors Based on Pure Metal Oxide Nanostructure

In 2008, Costello and his colleagues firstly confirmed that UV light can improve the RT sensitivity of ZnO sensor. The ZnO sensor could detect 1 ppb of acetaldehyde and acetone and obtained adjustable sensitivity though manipulating the intensity of UV light (De Lacy Costello et al., 2008). Chen et al. demonstrated the gas sensor based 3D cone-shaped MoS_2 bilayer showed high response (~470%) and short response time (~25 s) after exposure to 1 ppm of NO under UV light (Chen et al., 2019). As shown in **Figure 1A**, it is explained that the excellent NO sensing properties is due to

the three-dimensional light scattering effect attracted by UV light, which further enhances the light absorption.

Because of the health hazards and low utilization of UV light, researchers began to explore the replacement of UV light with visible light. Li et al. prepared a highly ordered CdS nanoflakes array by using Chemical Vapor Deposition (CVD) technology and studied its gas sensing characteristics (Li et al., 2018). It is found that the sensor has good working potential under natural solar lamps and can be used for outdoor environment monitoring. The excellent gas performances are attributed to the low band gap energy (2.4 eV) and the unique morphology of CdS. These inherent properties of CdS can enhance light absorption and conductivity. Wang et al. successfully prepared SnS_2 nanoflowers by solvothermal synthesis (Eom et al., 2021). In **Figure 1B**, it is confirmed that the high absorbance of SnS_2 in the visible region triggered the generation of carriers, which could decrease the resistance and enhance the gas sensing characteristics. Friedman et al. fabricated MoS_2 by mechanical stripping and tested the sensitivity of the sensor under visible light (Friedman et al., 2014). They observed a 10-fold difference in the sensitivity of the sensors to trimethylamine before and after light exposure. The improved gas sensitivity of MoS_2 sensors comes from photoexcitation.

Gas Sensors Based on Noble Metal Doping Nanostructure

Many studies have demonstrated that the modification of noble metal and light irradiation have synergistic effect on improving the gas sensing performance of pure MOS. On one hand, Li et al. fabricated a sensor based on Au/ZnO porous octahedron (POHs). Compared with the sensor based pure ZnO POH, the response of the sensor based on Au/ZnO POHs to formaldehyde is significantly improved under UV light (Tsai et al., 2018). Zhou et al. reported a UV-assisted, recoverable, highly sensitive and selective NO_2 gas sensor based on Au-MoS_2 nanocomposite (Zhou et al., 2018a). In **Figure 1C**, the Au-MoS_2 sensor has a three-fold enhanced response to NO_2, full recovery property and good repeatability under UV light. The detection of NO_2 under UV light provides an alternative strategy for the design of single multifunctional optoelectronic devices.

On the other hand, Kim et al. reported the detection of NO_2 gas by a one-dimensional Au-SnO_2 nanofiber sensor under visible light at RT (Lim et al., 2021). The sensor shows a high degree of selectivity, sensitivity and repeatability in response to NO_2 at sub ppm levels. As shown in **Figure 1D**, the excellent RT NO_2 properties are in connection with the effects of Au nanoparticles from local surface plasmon resonance (LSPR) in visible light. This work makes the new transparent design possible for oxide gas sensors without external heaters or light sources. Additionally, Chen et al. developed a high-performance visible light activated NO_2 gas sensor based on LSPR and increased surface oxygen vacancy (Chen et al., 2020). The results show that Au NPs modification can significantly improve the visible photosensitivity of ZnO films compared with pure ZnO films. It provides an effective way to construct high-performance photoactivated gas sensor.

Gas Sensors Based on Heterojunction Nanostructure Composite

Both the construction of heterostructure and light irradiation can increase active sites and charge transfer of pure metal oxide semiconductor. The heterostructure of MOS can enhance charge transduction and adjust grain boundary potential barrier, which is beneficial to improve the gas sensitivity. For one thing, Chang et al. prepared hollow ZnO/MoS_2 nanosheets with core/shell heterostructure (Chang et al., 2020). The high acetone response and fast response/recovery rate are caused by the fast gas transport channel and the n-p heterojunction of MoS_2 nanosheets. Moreover, UV light is introduced to further improve the acetone reaction and greatly reduce the operating temperature. The optical diffraction and reflection caused by the decoration of layered MoS_2 nanosheets can significantly improve the light capture. Yang et al. successfully synthesized hollow ZnO-SnO_2 heterostructure for triethylamine (TEA) (Yang et al., 2018). Particularly, the sensor based ZnO-SnO_2 showed short response time (1.8 s) and recovery time (18 s) under UV light.

For another, Liu et al. reported hollow SnO_2@SnS_2 nanostructures prepared by one-step hydrothermal method (Liu et al., 2020). The sensor based on SnO_2@SnS_2 has a fast response rate and good recovery ability to ppb-level NO_2 under visible light at RT. The excellent sensing performance of SnO_2@SnS_2 sensor is due to the hollow and porous heterojunction structure, which is conducive to gas diffusion, especially visible light assisted to promote charge transfer and gas desorption. Chen et al. prepared gas-sensitive ZnO nanorods with sea urchin-level mesoporous structure modified by PbS quantum dots (QDs) (Chen et al., 2018). The PbS QDs have a narrow band gap shown in the Near Infrared Spectroscopy Analysis (NIR) spectrum. Compared with the original ZnO nanorods, the sensor based ZnO/PbS nanocomposites have a higher response and faster response/recovery speed to ppm level NO_2 under visible light.

SENSING MECHANISM OF LIGHT-ASSISTED GAS SENSOR

Light activation has been proved to be an effective way to improve the performance of gas sensors, but the relationship between the types of light source, the structure of materials and the improvement of gas sensing properties are not clear. The explanations for the improved gas sensitivity of UV light are as follows:

Firstly, Gong et al. proposed the gas sensor based on a novel ZnO hybrid with nanowire/optical fiber (Gong et al., 2017). The results show that UV irradiation can improve the sensitivity and shorten the response time, and the sensor also has good long-term stability. UV irradiation can respond to gas with ppb-level concentration at low temperature. The electrons in the ZnO hybrid excited by UV irradiation promote the reduction of ethanol gas, leading to the higher gas performance. Therefore, the irradiation of UV will generate more conductive electrons, improve the conductivity of the sensing materials and promote the electron transfer under UV irradiation, thus improving the

response of the gas sensor. Secondly, Zhou et al. have proposed that the increased sensitivity is ascribed to the increase in the number of active adsorption sites and the introduction of active catalysts such as Au, Ag, Pd and other noble metals (Zhou et al., 2018a). For example, Au nanoparticles can accelerate the capture of more photons, resulting in additional photoexcited carriers to promote the interaction between gas and sensing materials. The efficient separation of photoexcited carriers at the interface of MoS_2/Au also contributes to rapid and complete recovery under UV light. Finally, Zhou et al. explained that UV light can excite electron-hole pairs in ZnO (n-type) and MoS_2 (p-type) (Zhou et al., 2018b). The photoexcited electrons in the conduction band can be easily transferred to ZnO by the built-in field, which is similar to the excited hole in the valence band of ZnO to the excited hole of MoS_2. Therefore, light carriers can be effectively separated at the interface of heterojunction in order to improve the gas sensing properties.

The explanations for the improved gas sensitivity of visible light are as follows: Primarily, the explanations given by Li et al. are as follows: The photon energy of visible light greater than the band gap of semiconductor can produce electron-hole pairs. Electrons and holes cannot recombine efficiently, and the electrons of light source move to the conduction band and then are accumulated in the conduction band. This results in the high concentration of electrons in the conduction band and the high conductivity of the semiconductor. Therefore, the sensitivity of the gas sensor is significantly increased under visible light (Li et al., 2018). Posteriorly, Chen et al. developed a high-performance visible light activated NO_2 sensor based on LSPR and increased surface oxygen vacancy (Chen et al., 2020). The mechanism of visible light activated by LSPR absorption are illustrated. At the interface of metal and semiconductor, the Fermi level of ZnO is transferred to a positive charge when electrons transfer from ZnO nanorods to Au nanorods, resulting in an upward-bending band interface and a Schottky barrier. The photoexcited electrons generated in Au can overcome the blocking and injection of conduction band in ZnO, making more free electrons can participate in the chemical reaction with the surface adsorbed O_2 and NO_2 molecules. Niu et al. prepared vertically stacked MoS_2/GaSe heterojunction by all-dry transfer method (Niu et al., 2021). When the p-n junction between MoS_2 and GaSe is exposed to visible light, electron-hole pairs in both MoS_2 and GaSe layers are generated by light and tend to migrate at the interface. Due to the built-in electric field, electrons transfer to n-type MoS_2 and holes transfer to p-type GaSe, resulting in carrier separation. NO_2 has a strong electron affinity and can easily capture electrons from the conduction band of the material. In general, the separation of the light source carrier and the built-in electric field acts as a driving force to drive the gas sensing behavior.

The possible mechanism and reasons for the superior gas performance of light irradiation can be explained as follows:

1) For pure metal oxide nanostructure, the gas sensing performance depends on the amount of oxygen active substance adsorbed on the nanostructure surface. Under dark conditions, the concentration of free carriers inherent in the nanostructure is low, resulting in less utilization of the active site to produce absorbed oxygen. In contrast, with the increase of the number of free carriers under light irradiation, the surface absorption site improves the chemical activity of the surface and thus enhances the gas sensitivity.
2) For noble metal doping nanostructure, the LSPR effect not only enhances the absorption of light, but also inhibits the reorganization of electron-hole pairs produced by light. The intermediate-thermal electrons generated by LSPR absorption can overcome the Schottky barrier at the noble metal/oxide junction and inject into the oxide conduction band. Therefore, more surface adsorbed oxygen is formed on the oxide surface, leading to a stronger sensing reaction.
3) For heterojunction nanostructure composite, the formation of heterojunction can promote the separation of electron-hole pairs, effectively accelerate the electron conversion between different particles, and improve the response rate. When the heterojunction is exposed to light irradiation, electron-hole pairs in the semiconductor are generated by light and tend to migrate at the interface. Due to the built-in electric field, the electron transfer rate is enhanced, resulting in carrier separation and improving the gas sensitivity.

THE PRESENT APPLICATION OF GAS SENSORS UNDER LIGHT ACTIVATION

As essential for environmental monitoring, process control and early diagnosis of human disease, gas sensors under light activation are used to sense volatile organic compounds (VOCs). Wu et al. demonstrated a specific and highly sensitive detection of ketones using two-dimensional (2D) $MoTe_2$ (Wu et al., 2018). They also investigated the effect of UV activation on the sensing performance of VOCs. Activation of UV light results in high sensitivity, low detection limit (~0.2 ppm) to acetone and high stability even in high humidity, which is crucial for early diagnosis of diabetes. Zhao et al. demonstrated a flexible, transparent and high-performance gas sensor based In_2Se_3 using a simple pulsed laser deposition (PLD) method (Zheng et al., 2017). The gas sensor can work under the activation of visible light and shows excellent performance in detecting acetylene gas. No significant degradation of sensing performance was observed even after 100 bending cycles. The In_2Se_3 sensor has an average transmittance of 64% in the visible light range (400–800 nm). In addition, they found that the sensitivity, response and recovery rate of the sensor based In_2Se_3 depend on the light intensity. The excellent performance of In_2Se_3 sensors on flexible substrates provides a brilliant future for practical applications in wearable optoelectronic systems. Cheng et al. also prepared CuO flower-like materials (FMs) by hydrothermal method, and then obtained Au@CuO FMs by *in-situ* reduction reaction (Cheng et al., 2021b). The performance of the sensor based Au@CuO FMs was evaluated by detecting volatile and toxic gases such as ethanol, isopropanol, methanol and formaldehyde under UV light. It was found that the sensor based Au@CuO FMs had a higher response (95.3) than the sensor based CuO FMs at a

concentration of 1,000 ppm, while the sensor based Au@CuO FMs had a response of 174 under UV light. Therefore, Au@CuO FMs is a promising ethanol detection method. In summary, light irradiation as an effective means enables gas sensors to maintain better performance in environmental monitoring and human health protection.

CONCLUSION

In this paper, we first introduce the latest research progress of gas sensors with different microstructures (pure metal oxide nanostructure, noble metal doping nanostructure, heterojunction composite nanostructure) activated by UV and visible light. In the next place, we introduce the light activation mechanism of gas sensors with different structures from the perspective of microscopic mechanism. Finally, several applications of photoactivated gas sensors in environmental monitoring, process control and early diagnosis of human diseases are listed.

AUTHOR CONTRIBUTIONS

All authors listed have made a substantial, direct and intellectual contribution to the work, and approved it for publication.

FUNDING

This research work was financially supported by Natural Science Foundation of Hebei Province (F2020202050) and the National Natural Science Foundation of China (Grant No. 52104189).

REFERENCES

Chang, X., Qiao, X., Li, K., Wang, P., Xiong, Y., Li, X., et al. (2020). UV Assisted Ppb-Level Acetone Detection Based on Hollow ZnO/MoS2 Nanosheets Core/shell Heterostructures at Low Temperature. *Sensors Actuators B: Chem.* 317, 128208. doi:10.1016/j.snb.2020.128208

Chen, C., Zhang, Q., Xie, G., Yao, M., Pan, H., Du, H., et al. (2020). Enhancing Visible Light-Activated NO2 Sensing Properties of Au NPs Decorated ZnO Nanorods by Localized Surface Plasmon Resonance and Oxygen Vacancies. *Mater. Res. Express* 7, 015924. doi:10.1088/2053-1591/ab6b64

Chen, R., Wang, J., Xia, Y., and Xiang, L. (2018). Near Infrared Light Enhanced Room-Temperature NO2 Gas Sensing by Hierarchical ZnO Nanorods Functionalized with PbS Quantum Dots. *Sensors Actuators B: Chem.* 255, 2538–2545. doi:10.1016/j.snb.2017.09.059

Chen, Y.-Z., Wang, S.-W., Yang, C.-C., Chung, C.-H., Wang, Y.-C., Huang Chen, S.-W., et al. (2019). An Indoor Light-Activated 3D Cone-Shaped MoS2 Bilayer-Based NO Gas Sensor with PPb-Level Detection at Room-Temperature. *Nanoscale* 11, 10410–10419. doi:10.1039/c8nr10157d

Cheng, M., Li, W., Li, C., Wang, Q., Tan, Q., Yang, W., et al. (2021a). Photochemical Sensitive Study of Au@CuO Flower-like Materials. *Sensors Actuators B: Chem.* 348, 130644. doi:10.1016/j.snb.2021.130644

Cheng, Y., Ren, B., Xu, K., Jeerapan, I., Chen, H., Li, Z., et al. (2021b). Recent Progress in Intrinsic and Stimulated Room-Temperature Gas Sensors Enabled by Low-Dimensional Materials. *J. Mater. Chem. C* 9, 3026–3051. doi:10.1039/d0tc04196c

De Lacy Costello, B. P. J., Ewen, R. J., Ratcliffe, N. M., and Richards, M. (2008). Highly Sensitive Room Temperature Sensors Based on the UV-LED Activation of Zinc Oxide Nanoparticles. *Sensors Actuators B: Chem.* 134, 945–952. doi:10.1016/j.snb.2008.06.055

Eom, T. H., Cho, S. H., Suh, J. M., Kim, T., Lee, T. H., Jun, S. E., et al. (2021). Substantially Improved Room Temperature NO2 Sensing in 2-dimensional SnS2 Nanoflowers Enabled by Visible Light Illumination. *J. Mater. Chem. A.* 9, 11168–11178. doi:10.1039/d1ta00953b

Friedman, A. L., Keith Perkins, F., Cobas, E., Jernigan, G. G., Campbell, P. M., Hanbicki, A. T., et al. (2014). Chemical Vapor Sensing of Two-Dimensional MoS2 Field Effect Transistor Devices. *Solid-State Electro.* 101, 2–7. doi:10.1016/j.sse.2014.06.013

Gong, B., Shi, T., Zhu, W., Liao, G., Li, X., Huang, J., et al. (2017). UV Irradiation-Assisted Ethanol Detection Operated by the Gas Sensor Based on ZnONanowires/optical Fiber Hybrid Structure. *Sensors Actuators B: Chem* 245, 821–827. doi:10.1016/j.snb.2017.01.187

Hasani, A., Sharifi Dehsari, H., Amiri Zarandi, A., Salehi, A., Taromi, F. A., and Kazeroni, H. (2015). Visible Light-Assisted Photoreduction of Graphene Oxide Using CdS Nanoparticles and Gas Sensing Properties. *J. Nanomater.* 2015, 1–11. doi:10.1155/2015/930306

Hyodo, T., Urata, K., Kamada, K., Ueda, T., and Shimizu, Y. (2017). Semiconductor-type SnO2-Based NO2 Sensors Operated at Room Temperature under UV-Light Irradiation. *Sensors Actuators B: Chem.* 253, 630–640. doi:10.1016/j.snb.2017.06.155

Kumar, R., Liu, X., Zhang, J., and Kumar, M. (2020). Room-temperature Gas Sensors under Photoactivation: from Metal Oxides to 2D Materials. *Nano-micro Lett.* 12, 164. doi:10.1007/s40820-020-00503-4

Li, H.-Y., Yoon, J.-W., Lee, C.-S., Lim, K., Yoon, J.-W., and Lee, J.-H. (2018). Visible Light Assisted NO2 Sensing at Room Temperature by CdS Nanoflake Array. *Sensors Actuators B: Chem.* 255, 2963–2970. doi:10.1016/j.snb.2017.09.118

Lim, K., Jo, Y. M., Yoon, J. W., Kim, J. S., Lee, D. J., Moon, Y. K., et al. (2021). A Transparent Nanopatterned Chemiresistor: Visible-Light Plasmonic Sensor for Trace-Level NO 2 Detection at Room Temperature. *Small* 17, 2100438. doi:10.1002/smll.202100438

Liu, D., Tang, Z., and Zhang, Z. (2020). Visible Light Assisted Room-Temperature NO2 Gas Sensor Based on Hollow SnO2@SnS2 Nanostructures. *Sensors Actuators B: Chem.* 324, 128754. doi:10.1016/j.snb.2020.128754

Niu, Y., Zeng, J., Liu, X., Li, J., Wang, Q., Li, H., et al. (2021). A Photovoltaic Self-Powered Gas Sensor Based on All-Dry Transferred MoS 2 /GaSe Heterojunction for ppb-Level NO 2 Sensing at Room Temperature. *Adv. Sci.* 8, 2100472. doi:10.1002/advs.202100472

Park, S., Hong, T., Jung, J., and Lee, C. (2014). Room Temperature Hydrogen Sensing of Multiple Networked ZnO/WO3 Core-Shell Nanowire Sensors under UV Illumination. *Curr. Appl. Phys.* 14, 1171–1175. doi:10.1016/j.cap.2014.06.019

Song, Y., Zhang, Y., Ma, M., Ren, J., Liu, C., and Tan, J. (2020). Visible Light-Assisted Formaldehyde Sensor Based on HoFeO3 Nanoparticles with Sub-ppm Detection Limit. *Ceramics Int.* 46, 16337–16344. doi:10.1016/j.ceramint.2020.03.191

Tsai, Y.-T., Chang, S.-J., Ji, L.-W., Hsiao, Y.-J., Tang, I.-T., Lu, H.-Y., et al. (2018). High Sensitivity of NO Gas Sensors Based on Novel Ag-Doped ZnO Nanoflowers Enhanced with a UV Light-Emitting Diode. *ACS Omega* 3, 13798–13807. doi:10.1021/acsomega.8b01882

Wang, Z., Gao, S., Fei, T., Liu, S., and Zhang, T. (2019b). Construction of ZnO/SnO2 Heterostructure on Reduced Graphene Oxide for Enhanced Nitrogen Dioxide Sensitive Performances at Room Temperature. *ACS Sens.* 4, 2048–2057. doi:10.1021/acssensors.9b00648

Wang, Z., Sackmann, A., Gao, S., Weimar, U., Lu, G., Liu, S., et al. (2019a). Study on Highly Selective Sensing Behavior of Ppb-Level Oxidizing Gas Sensors Based on Zn2SnO4 Nanoparticles Immobilized on Reduced Graphene Oxide under Humidity Conditions. *Sensors Actuators B: Chem.* 285, 590–600. doi:10.1016/j.snb.2019.01.109

Wang, Z., Sun, J., Huo, Y., Yan, Y., Ma, Z., Bu, M., et al. (2021). Porous Co3O4 Nanocrystals Derived by Metal-Organic Frameworks on Reduced Graphene

Oxide for Efficient Room-Temperature NO2 Sensing Properties. *J. Alloys Comp.* 856, 158199. doi:10.1016/j.jallcom.2020.158199

Wu, E., Xie, Y., Yuan, B., Hao, D., An, C., Zhang, H., et al. (2018). Specific and Highly Sensitive Detection of Ketone Compounds Based on P-type MoTe2 under Ultraviolet Illumination. *ACS Appl. Mater. Inter.* 10, 35664–35669. doi:10.1021/acsami.8b14142

Yang, T., Gu, K., Zhu, M., Lu, Q., Zhai, C., Zhao, Q., et al. (2019). ZnO-SnO2 Heterojunction Nanobelts: Synthesis and Ultraviolet Light Irradiation to Improve the Triethylamine Sensing Properties. *Sensors Actuators B: Chem.* 279, 410–417. doi:10.1016/j.snb.2018.10.031

Zhai, J., Wang, T., Wang, C., and Liu, D. (2018). UV-light-assisted Ethanol Sensing Characteristics of G-C3N4/ZnO Composites at Room Temperature. *Appl. Surf. Sci.* 441026, 317–323. doi:10.1016/j.apsusc.2018.02.026

Zheng, Z., Yao, J., Wang, B., and Yang, G. (2017). A Flexible, Transparent and High-Performance Gas Sensor Based on Layer-Materials for Wearable Technology. *Nanotechnology* 28, 415501. doi:10.1088/1361-6528/aa8317

Zhou, Y., Gao, C., and Guo, Y. (2018b). UV Assisted Ultrasensitive Trace NO2gas Sensing Based on Few-Layer MoS2nanosheet-ZnO Nanowire Heterojunctions at Room Temperature. *J. Mater. Chem. A.* 6, 10286–10296. doi:10.1039/C8TA02679C

Zhou, Y., Zou, C., Lin, X., and Guo, Y. (2018a). UV Light Activated NO2gas Sensing Based on Au Nanoparticles Decorated Few-Layer MoS2thin Film at Room Temperature. *Appl. Phys. Lett.* 113, 082103–082107. doi:10.1063/1.5042061

Conflict of Interest: The authors declare that the research was conducted in the absence of any commercial or financial relationships that could be construed as a potential conflict of interest.

Publisher's Note: All claims expressed in this article are solely those of the authors and do not necessarily represent those of their affiliated organizations, or those of the publisher, the editors and the reviewers. Any product that may be evaluated in this article, or claim that may be made by its manufacturer, is not guaranteed or endorsed by the publisher.

frontiers in Chemistry

ORIGINAL RESEARCH
published: 05 January 2022
doi: 10.3389/fchem.2021.807867

Higher Light Extraction Efficiency in Organic Light-Emitting Devices by Employing 2D Periodic Corrugation

Yu Bai, Yahui Chuai, Yang Wang and Yingzhi Wang*

Changchun University of Science and Technology, Changchun, China

Photons trapped in the form of waveguide (WG) modes associated with the organic–organic interface and in the form of surface plasmon polariton (SPP) modes associated with the metallic electrode–organic interface result in a large energy loss in organic light-emitting devices (OLEDs). Introducing gratings onto the metallic electrode is especially crucial for recovering the power lost to the associated SPP modes. In our research, we demonstrate the efficient outcoupling of SPP modes in TE mode by two-dimensional (2D) grating, which cannot excited in one-dimensional (1D) grating OLED. This causes a 62.5% increase in efficiency from 2D grating OLED than 1D grating OLED. The efficient outcoupling of the WG and SPP modes is verified by the numerical simulation of both the emission spectra and the field distribution.

Keywords: OLED (organic light-emitting diode), periodic (defect) structure, SPP (surface plasmon plaritons), TE mode and TM mode, light extraction enhancement

OPEN ACCESS

Edited by:
Yue-Feng Liu,
Jilin University, China

Reviewed by:
Runda Guo,
Huazhong University of Science and Technology, China
Wang Gong,
Hebei University of Technology, China

****Correspondence:***
Yu Bai
baiyu@cust.edu.cn

Specialty section:
This article was submitted to Nanoscience, a section of the journal Frontiers in Chemistry

Received: *02 November 2021*
Accepted: *08 November 2021*
Published: *05 January 2022*

Citation:
Bai Y, Chuai Y, Wang Y and Wang Y (2022) Higher Light Extraction Efficiency in Organic Light-Emitting Devices by Employing 2D Periodic Corrugation. Front. Chem. 9:807867. doi: 10.3389/fchem.2021.807867

1 INTRODUCTION

In flat panel display and solid-state lighting, organic light-emitting devices (OLEDs) have great application potential. OLED has many advantages, such as energy efficiency, large viewing angle, low working voltage, fast response, and lightweight. Therefore, it is considered an ideal solution for future display and light sources. Although the internal quantum efficiency of OLED could nearly reach 100% now, its external quantum efficiency is still low, because of its low light extraction efficiency. Approximately 80% of the light emitted from OLED is absorbed by its internal waveguide (WG) mode, indium tin oxide (ITO) anode, and surface plasma polariton (SPP) generated between the organic layer/metallic cathode, and only 20% of the light gets to emerge out of OLED. In other words, OLED has a low light extraction efficiency. If we can solve the problem of light extraction efficiency of OLED, we can greatly enhance the external quantum efficiency of OLED (Gu et al., 1997; Erchak et al., 2001; Hobson et al., 2002; Kim et al., 2005).

One effective way of enhancing the light extraction efficiency of OLED is introducing periodic microstructures into the device. Periodic microstructures with period length between optical wavelength and subwavelength play a significant role in optical and optoelectronic devices (Moreland et al., 1982; Choi et al., 2005; Peng et al., 2005; Xie et al., 2008). Previously, we have reported that the method of laser two-beam interference can be used to directly ablate one-dimensional (1D) grating in the organic layer of OLED (Bai et al., 2011). By exciting the surface plasma effect and improving the WG effect of OLED, we can enhance its light extraction efficiency. However, for those devices that might produce surface plasma such as metallic cathodes of OLED, Worthing and Barnes (2001) pointed out that the production of surface plasma occurs in all directions of a plane, but 1D grating has directions, and only in half of the directions can surface plasma be coupled and excited; therefore, the coupling efficiency of

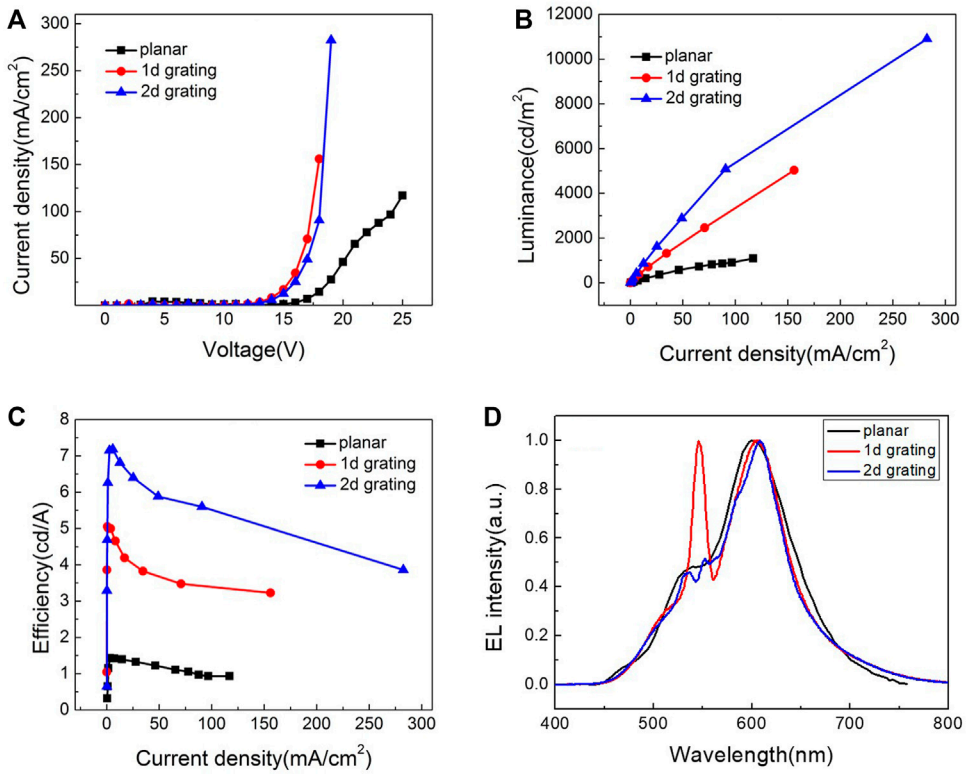

FIGURE 1 | EL performance of the 1D grating, 2D grating, and planar OLEDs. Current density–voltage **(A)**, current density–luminance **(B)**, current density–efficiency **(C)** characteristics, and the EL spectra **(D)**.

surface plasma in 1D grating is low. Furthermore, for the WG mode of OLED, 1D grating can only reduce WG loss in specific directions and cannot help in other directions.

We introduced a two-dimensional (2D) grating structure into the organic layer of OLED in this research. Taking advantage of a higher coupling efficiency of SPP and WG mode in 2D grating structure, we obtained OLED with higher light extraction efficiency (Rigneault et al., 2000; Han et al., 2003; Giannattasio and Barnes, 2005; Jing et al., 2005; Wedge et al., 2005; Yang et al., 2005; Peng et al., 2006).

2 EXPERIMENT

In previous researches, we found that 350-nm periodic grating has SPP peak position of 607 nm. In order to leverage SPP to enhance light emitting, we need to choose optical materials with peak position of approximately 607 nm. DCJTB has a peak position of 610 nm (Xu et al., 2011); therefore, it was chosen.

A conducting polymer widely used in polymer LEDs as a hole-transport material, poly(N-vinyl carbazole) (PVK), is chosen, and it is spin-coated on the ITO glass for the fabrication of the corrugated hole transporting layer (HTL) in OLEDs. 4,4′,4″-Tris(3-methylphenylphe-nylamino) triphenylamine (m-MTDATA) was doped into the PVK with a concentration of 5% by weight to enhance the hole injection and transport of the HTL. The ablation experiments used a frequency-tripled Nd:YAG laser (Spectra-Physics Company) with 3-nm pulse width, 10-ns pulse length, 10-Hz repetition rate, and 355-nm wavelength. An ITO-coated glass substrate was cleaned with acetone and ethanol. The HTL was spin-coated at 4,000 rpm/s speed for 70-nm thicknesses. The sample was prebaked in vacuum for 30 min at 60°C to evaporate the organic solvent. Then, the sample was exposed by two beams, which were split from the UV laser with a beam size of 6 mm in diameter. The microstructure fabrication was conducted in air at room temperature using a single laser pulse for 1D grating. To obtain 2D grating, we prepared 1D grating first and rotated it by 60° and then did a second laser interference ablation. The periods for 1D and 2D grating are both 350 nm.

Prepared ITO substrates coated with corrugated HTL were immediately brought into a thermal evaporation chamber. Then, the 20-nm-thick HTL of N,N0 -diphenyl-N,N0-bis(1,10-biphenyl)-4,40-diamine was evaporated. After that, 4-(dicyanomethylene)-2-t-butyl-6-(1,1,7,7-tetramethyljulolidyl-9-enyl)-4H-pyran (DCJTB) with a concentration of 1% by weight was doped into 50-nm-thick emitting layer of tris-(8-hydroxyquinoline) aluminum (Alq3) for emission layer. At

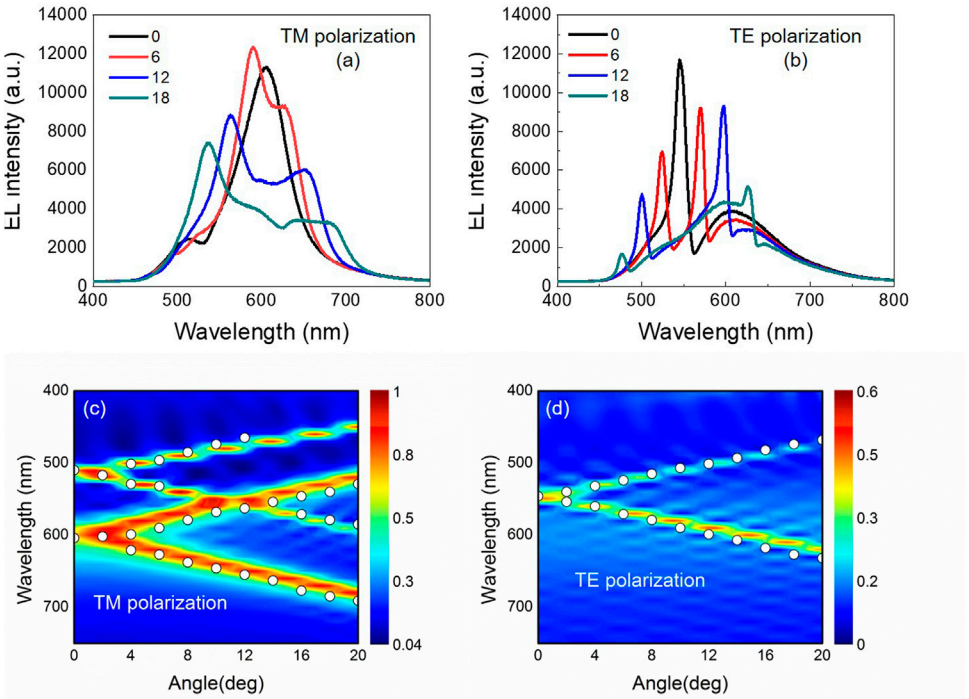

FIGURE 2 | Measured EL spectra with TM **(A)** and TE **(B)** polarization at different observation angle from the corrugated OLEDs with 1D grating, and the wavelength versus incident angle for the calculated dispersion relation of the corrugated OLEDs for TM **(C)** and TE **(D)** polarization. The measured dispersion relation extracted from the EL spectra (circles) is also shown in **(C)** and **(D)**.

last, LiF (1 nm)/Al (100 nm) for cathode was evaporated. Here, all layers were prepared by thermal evaporation in a high vacuum system with the pressure of less than 5×10^{-4} Pa. The active area of the devices was 2×2 mm^2. Their current density–voltage–luminance (J–V–L) characteristics were measured by Keithley 2400 programmable voltage–current source and Photo Research PR-655 spectrophotometer. The emission spectra at different observation angle were collected with a lens and then collimated and focused into the entrance slit of a 300-mm monochromator/spectrograph (SR-3031-A; Andor) to limit the angular acceptance to ~1°. The spectrogram of the emission was recorded using a charge coupled device (iDus; Andor). The OLEDs were placed on a rotation stage with the grooves parallel to the rotation axis. All of the measurements were conducted in air at room temperature.

3 DISCUSSION

Figure 1 shows the performance curve of the device and the EL spectra. From **Figure 1A** we can see, on both 1D and 2D devices, the current density increased significantly compared with the control flat panel device. That is because the grating microstructure increased the effective area of the device, and the laser ablation enhanced the transportation capacity of the hole-transport material. **Figures 1B,C** give the current density–luminance curve and current density–efficiency curve. We can see from them that both 1D and 2D grating devices have higher luminance and efficiency compared with flat panel devices. Between 2D and 1D grating devices, we can see the 2D device outperformed 1D device on current density, luminance, and efficiency. When the current density is 100 mA/cm^2, the luminance of 2D device is 5,000 cd/m^2, and the current efficiency is 5.53 cd/A, whereas the luminance of 1D device is 3,000 cd/m^2, and current efficiency is 3.41 cd/A. When the device structure and other conditions are matched, 2D grating device has significantly better performance than 1D grating device, and this can only be explained by 2D grating having a higher coupling efficiency when it comes to surface plasma and WG mode.

To test our deduction, we simulated the spectra and optical field of 1D and 2D grating. We employed finite-difference time-domain method to simulate light transmission in the grating of OLED (Marcuse, 1974; Gedney, 1998). We used Drude model to represent the dielectric coefficient of metal and materials, and the refractive index of material was fitted into Drude model parameters from measurements of the ellipsometer. During simulation, for directions along the grating, we adopted periodic boundary condition, and for other boundaries, we adopted perfect matching layer to cut off. For the incident wave, we used modulated Gauss impulse whose central frequency is within the visible light band of our concern. We extracted the transmission light component and reflection light component at the end of computation and used

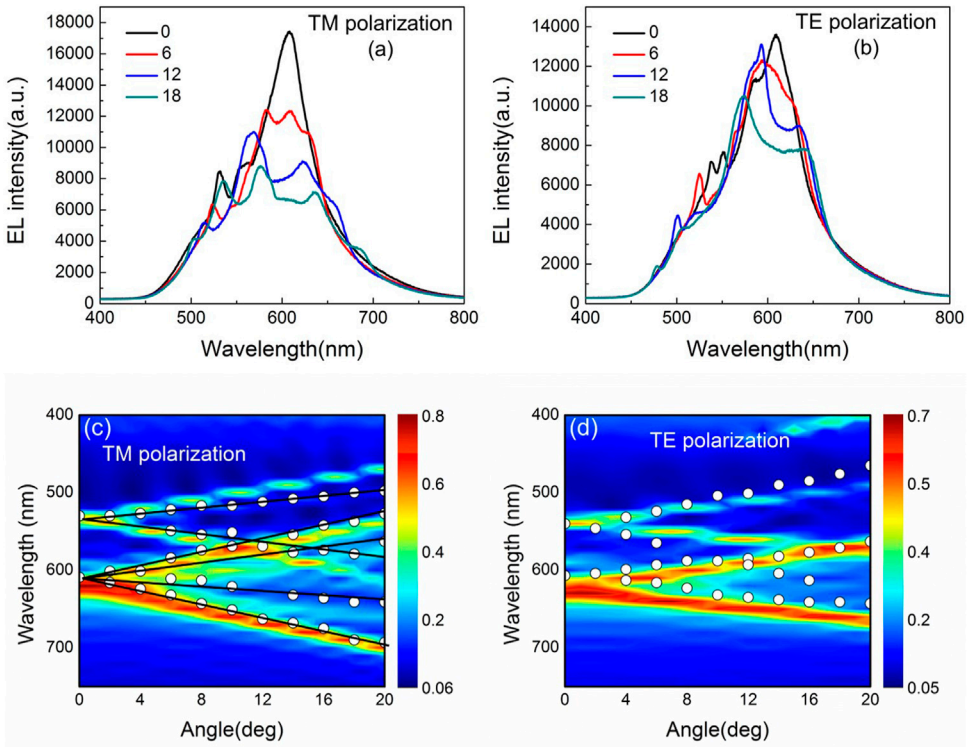

FIGURE 3 | Measured EL spectra with TM **(A)** and TE **(B)** polarization at different observation angle from the corrugated OLEDs with 2D grating. And the wavelength versus incident angle for the calculated dispersion relation of the corrugated OLEDs for TM **(C)** and TE **(D)** polarization.

the ratio of Poynting vector to represent transmission, reflection, and absorption.

Figure 2 shows the angle-dependent spectrum and dispersion curve of 1D grating OLED in TM and TE mode, whereby white circles are dispersion curve obtained from actual measurement of angle-dependent spectrum. Putting actual data and simulated curve together, we can see that the two fit very well in terms of peak position and peak width at various angles in **Figures 2C,D**. Therefore, we consider the computation method for light transmission in grating OLED correct. In **Figure 2**, apart from the peak of DCJTB itself, in TM mode of **Figure 2C**, the device gives two additional peaks: 607 and 510 nm, and in TE mode of **Figure 2D**, the device gives one more peak: 550 nm. The additional 607-nm peak in TM mode is because the grating structure excited light in surface plasma mode inside the device, and the additional 510-nm peak is because the grating structure excited light in waveguided mode inside the device. In TE mode, there is only one additional peak; that is because the surface plasma mode cannot be excited in TE mode, and the single peak comes from grating structure exciting light in WG mode inside the device. Hence, for 1D grating, because of its directionality, it can only couple and excite surface plasma in half of the transmission directions, yielding a low coupling efficiency for surface plasma. Moreover, in WG mode of OLED, 1D grating can only reduce WG loss in specific directions, not in other directions.

How about the coupling capacity for surface plasma in 2D grating? **Figure 3** shows the angle-dependent spectrum curve and dispersion curve in TM and TE mode in 2D OLED. In **Figures 3A,C** at 0°, apart from the peak of DCJTB itself, there are two additional peaks at 538 and 630 nm, among which the 630-nm peak almost superposes on the 620-nm peak of DCJTB and is wider. When the observation angle increases, the two peaks split and shift with the increase in observation angle. For 1D OLED, when its additional peak splits as the observation angle increases, each peak split into two. But for the 2D device, the 630-nm peak does not split into two, but four. In **Figures 3B,D** at 0°, there are split peaks at 540 and 640 nm, respectively, among which the 640-nm peak is wider than the 540-nm peak.

To find out the reason for the formation of these additional peaks, we simulated and analyzed the field intensity in 2D OLED at observation angle of 0°. **Figures 4A,B** show the field intensity distribution of 630-nm peak at 0° in TM mode. We can see that, in both xz and yz directions, the greatest field intensity happens on the Al/Alq interface and in directions along the interface. That tells us the 630-nm peak is formed because the grating excites surface plasma (Worthing and Barnes, 2001; Liu and Tsai, 2002; Li and Ning, 2003; Gao et al., 2006; Van Oosten et al., 2010). And because the synthesis of x and y can be seen as any direction in the plane, we can see from the simulation of field intensity distribution that, in TM mode,

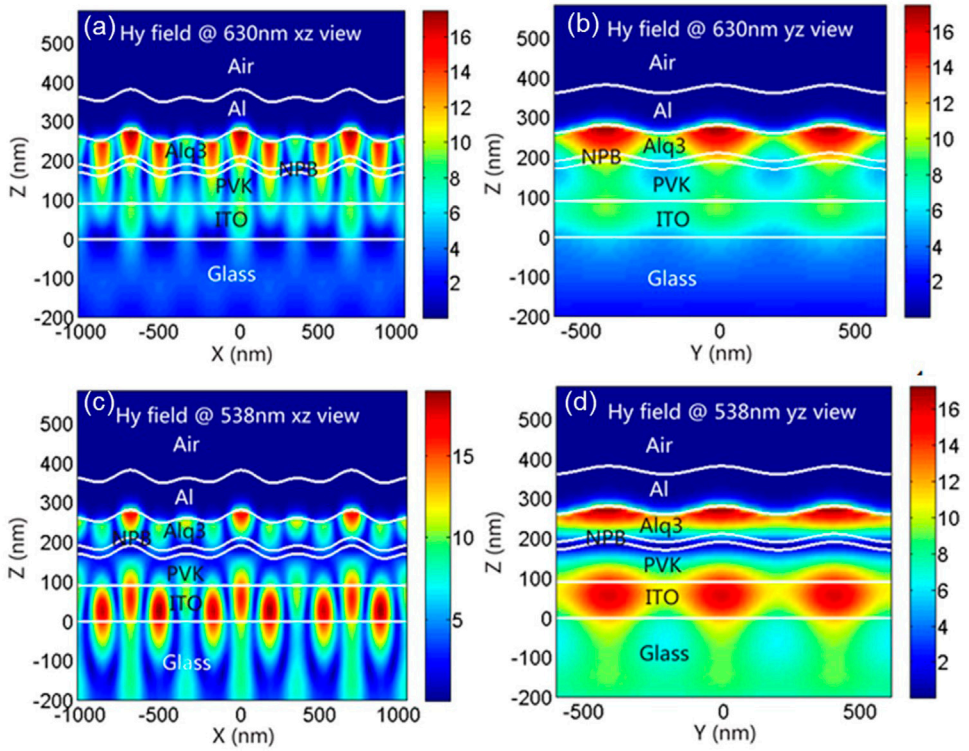

FIGURE 4 | Distribution of the magnetic field intensity in the corrugated OLEDs at the wavelength of incident polarized light of 630-nm XZ view **(A)**, 630-nm YZ view **(B)**, 538-nm XZ view **(C)**, and 538-nm YZ view **(D)**, respectively.

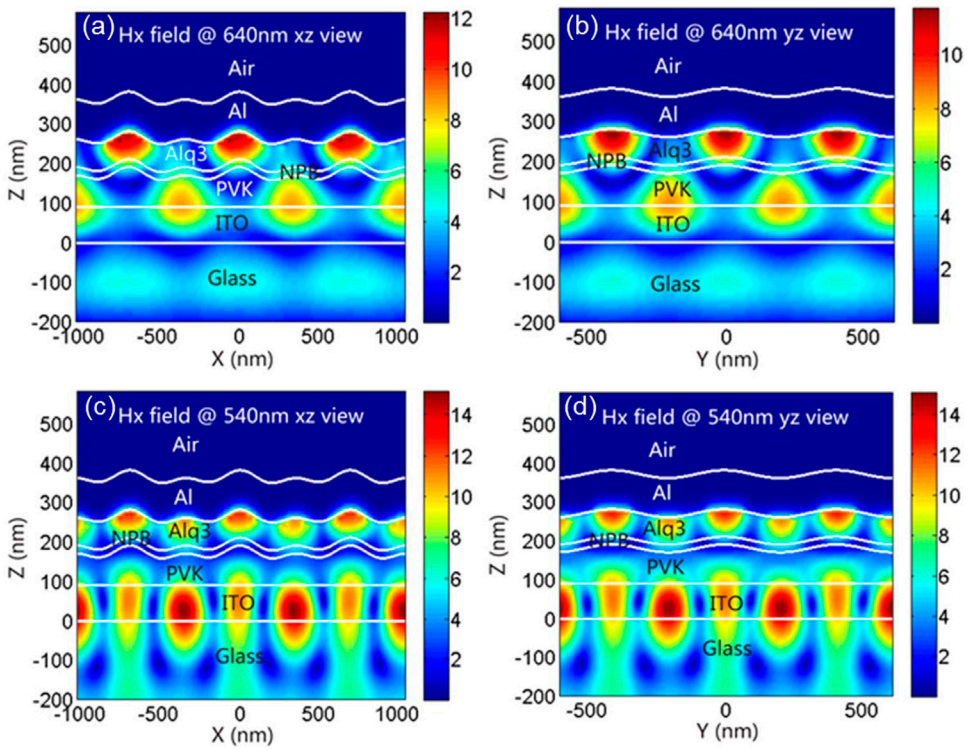

FIGURE 5 | Distribution of the magnetic field intensity in the corrugated OLEDs at the wavelength of incident polarized light of 640-nm XZ view **(A)**, 640-nm YZ view **(B)**, 540-nm XZ view **(C)**, and 540-nm YZ view **(D)**, respectively.

2D grating can couple and excite surface plasma in any direction. For the WG mode, as shown in **Figures 4C,D** in both xz and yz directions, the greatest field intensity happens in ITO and organic layers; therefore, the 538-nm peak is formed because the WG mode is excited. And as WG mode has been excited along x and y directions, it can be also considered that, in TM mode, 2D grating can couple and excite WG mode in any direction, yielding a better coupling efficiency.

Again, in TE mode, as shown in **Figures 5A,B**, in both xz and yz directions, although the field intensity is weak, the maximum intensity happens also at the Al/Alq interface and in directions along the interface, indicating that there are peaks of surface plasma in TE mode. For 1D grating OLED, surface plasma cannot be excited in TE mode; yet, we have observed surface plasma peaks in 2D grating OLED in TE mode.

We think that, for 2D grating in OLED, although one of the dimensions is in TE mode (hereby referred to as grating 1) and is incapable of exciting surface plasma mode, and the other dimension (hereby referred to as grating 2) because it intersects with grating a at 60°, we consider it, in our observation, as having two vectors: one is in parallel with grating a and the other is perpendicular to grating a. The vector parallel to grating a is in TE mode and therefore cannot excite surface plasma. But the vector perpendicular to grating a can be considered as being in TM mode and therefore can excite surface plasma. Therefore, in TE mode, weak surface plasma peaks were observed, which agrees with our actual measurement. Therefore, we think 2D grating OLED has a higher utilization efficiency for surface plasma than 1D grating OLED. In **Figures 5C,D** we can see, at peak 540 nm, the places with high field intensity concentrate in ITO and the organic layers; therefore, peak 540 nm is caused by WG mode excitation. Again, it can be excited along both x and y directions; therefore, it can also be seen as 2D grating can couple and excite WG mode in any direction, yielding a higher coupling efficiency.

4 CONCLUSION

We introduced 1D and 2D grating structures into the hole injection layer of OLED and, on that basis, obtained 1D and 2D grating OLED. Performance comparison shows that both 1D and 2D grating OLEDs yield better luminosity and efficiency than ordinary flat panel devices. At current density of 100 mA/cm^2, the luminosity and efficiency of 1D grating OLED are 3.60 and 3.63 times those of the planar OLED, and the luminosity and efficiency of 2D grating OLED are 5.75 and 5.90 times those of the planar OLED. Because 2D grating has higher coupling and excitation efficiency for surface plasma and WG mode than 1D grating, 2D grating OLED brings greater enhancement on OLED luminosity and efficiency than 1D grating OLED; the luminosity and efficiency of 2D grating OLED increased by 59.7% and 62.5% than the 1D grating OLED.

DATA AVAILABILITY STATEMENT

The original contributions presented in the study are included in the article/supplementary material, further inquiries can be directed to the corresponding author.

AUTHOR CONTRIBUTIONS

All authors listed have made a substantial, direct, and intellectual contribution to the work and approved it for publication.

FUNDING

This work is supported by the Education Department of Jilin Province for its financial support through grants numbers JJKH20190545KJ and JJKH20200754KJ, and the Jilin Province Science and Technology Development Project for the grant number 20210101182JC and 20190303034SF.

REFERENCES

Bai, Y., Feng, J., Liu, Y.-F., Song, J.-F., Simonen, J., Jin, Y., et al. (2011). Outcoupling of Trapped Optical Modes in Organic Light-Emitting Devices with One-step Fabricated Periodic Corrugation by Laser Ablation. *Org. Electron.* 12 (11), 1927–1935. doi:10.1016/j.orgel.2011.08.004

Choi, H. W., Kim, S. Y., Kim, W. K., and Lee, J. L. (2005). Enhancement of Electron Injection in Inverted Top-Emitting Organic Light-Emitting Diodes Using an Insulating Magnesium Oxide Buffer Layer. *Appl. Phys. Lett.* 87 (8), 2469. doi:10.1063/1.2033129

Erchak, A. A., Ripin, D. J., Fan, S., Rakich, P., Joannopoulos, J. D., Ippen, E. P., et al. (2001). Enhanced Coupling to Vertical Radiation Using a Two-Dimensional Photonic crystal in a Semiconductor Light-Emitting Diode. *Appl. Phys. Lett.* 78 (5), 563–565. doi:10.1063/1.1342048

Gao, H., Henzie, J., and Odom, T. W. (2006). Direct Evidence for Surface Plasmon-Mediated Enhanced Light Transmission through Metallic Nanohole Arrays. *Nano Lett.* 6 (9), 2104–2108. doi:10.1021/nl061670r

Gedney, S. D. (1998). "The Perfectly Matched Layer Absorbing Medium," in *Advances in Computational Electrodynamics* (Norwood, MA: Artech House, Inc).

Giannattasio, A., and Barnes, W. L. (2005). Direct Observation of Surface Plasmon-Polariton Dispersion. *Opt. Express* 13 (2), 428–434. doi:10.1364/OPEX.13.000428

Gu, D. Z., Garbuzov, P. E., Burrows, P. E., Venkatesh, S., Forrest, S. R., and Thompson, M. E. (1997). High-External-Quantum-Efficiency Organic Light-Emitting Devices. *Opt. Lett.* 22 (6), 396–398. doi:10.1364/ol.22.000396

Han, S., Feng, X., and Lu, Z. H. (2003). Transparent-Cathode for Top-Emission Organic Light-Emitting Diodes. *Appl. Phys. Lett.* 82 (16), 2715–2717. doi:10.1063/1.1567048

Hobson, P. A., Wedge, S., Wasey, J. A. E., Sage, I., and Barnes, W. L. (2002). Surface Plasmon Mediated Emission from Organic Light-Emitting Diodes. *Adv. Mater.* 14 (19), 1393–1396. doi:10.1002/1521-4095(20021002)14:19<1393::aid-adma1393>3.0.co;2-b

Jing, F., Okamoto, T., and Kawata, S. (2005). Enhancement of Electroluminescence through a Two-Dimensional Corrugated Metal Film by Grating-Induced Surface-Plasmon Cross Coupling. *Opt. Lett.* 30 (17), 2302–2304. doi:10.1364/ol.30.002302

Kim, D. H., Cho, C. O., Roh, Y. G., Jeon, H., Park, Y. S., and Cho, J. (2005). Enhanced Light Extraction from Gan-Based Light-Emitting Diodes with Holographically Generated Two-Dimensional Photonic crystal Patterns. *Appl. Phys. Lett.* 87 (20), 855. doi:10.1063/1.2132073

Li, J., and Ning, C. Z. (2003). Interplay of Collective Excitations in Quantum-Well Intersubband Resonances. *Phys. Rev. Lett.* 91 (9), 097401. doi:10.1103/PhysRevLett.91.097401

Liu, W. C., and Tsai, D. P. (2002). Optical Tunneling Effect of Surface Plasmon Polaritons and Localized Surface Plasmon Resonance. *Phys. Rev. B, Condensed matter* 65 (15), 155423. doi:10.1103/physrevb.65.155423

Marcuse, D. (1974). Chapter 5–Coupled Power Theory. *Theor. Dielectric Opt. Waveguides* 5, 177–250. doi:10.1016/B978-0-12-470951-5.50011-1

Moreland, J., Adams, A., and Hansma, P. K. (1982). Efficiency of Light Emission from Surface Plasmons. *Phys. Rev. B Condensed Matter* 25 (4), 2297. doi:10.1103/physrevb.25.2297

Peng, H. J., Zhu, X. L., Sun, J. X., Yu, X. M., Wong, M., and Kwok, H. S. (2006). Efficiency Improvement of Phosphorescent Organic Light-Emitting Diodes Using Semitransparent Ag as Anode. *Appl. Phys. Lett.* 88 (3), 5048. doi:10.1063/1.2164901

Peng, H., Zhu, X., Sun, J., Xie, Z., Xie, S., Wong, M., et al. (2005). Efficient Organic Light-Emitting Diode Using Semitransparent Silver as Anode. *Appl. Phys. Lett.* 87 (17), 173505. doi:10.1063/1.2115076

Rigneault, H., Lemarchand, F., and Sentenac, A. (2000). Dipole Radiation into Grating Structures. *J. Opt. Soc. Am. A.* 17 (6), 1048. doi:10.1364/josaa.17.001048

Van Oosten, D., Spasenović, M., and Kuipers, L. (2010). Nanohole Chains for Directional and Localized Surface Plasmon Excitation. *Nano Lett.* 10 (1), 286–290. doi:10.1021/nl9034863

Wedge, S., Garrett, S. H., Sage, I., and Barnes, W. L. (2005). Photoluminescence Emission through Thin Metal Films via Coupled Surface Plasmon-Polaritons. *J. Mod. Opt.* 52 (6), 833–843. doi:10.1080/09500340512331309066

Worthing, P. T., and Barnes, W. L. (2001). Efficient Coupling of Surface Plasmon Polaritons to Radiation Using a Bi-grating. *Appl. Phys. Lett.* 79 (19), 3035–3037. doi:10.1063/1.1414294

Xie, G., Meng, Y. W., Wu, F., Tao, C., Zhang, D., Liu, M., et al. (2008). Very Low Turn-On Voltage and High Brightness Tris-(8-Hydroxyquinoline) Aluminum-Based Organic Light-Emitting Diodes with a MoOx P-Doping Layer. *Appl. Phys. Lett.* 92, 093305, 2008 . Applied Physics Letters. doi:10.1063/1.2890490

Xu, D., Li, X., Ju, H., Zhu, Y., and Deng, Z. (2011). A Novel Red Organic Light-Emitting Diode with Ultrathin Dcjtb and Rubrene Layers. *Displays* 32 (2), 92–95. doi:10.1016/j.displa.2011.01.002

Yang, C. J., Lin, C. L., Wu, C. C., Yeh, Y. H., Cheng, C. C., and Kuo, Y. H. (2005). High-Contrast Top-Emitting Organic Light-Emitting Devices for Active-Matrix Displays. *Appl. Phys. Lett.* 87 (14), 913. doi:10.1063/1.2081137

Conflict of Interest: The authors declare that the research was conducted in the absence of any commercial or financial relationships that could be construed as a potential conflict of interest.

Publisher's Note: All claims expressed in this article are solely those of the authors and do not necessarily represent those of their affiliated organizations, or those of the publisher, the editors and the reviewers. Any product that may be evaluated in this article, or claim that may be made by its manufacturer, is not guaranteed or endorsed by the publisher.

frontiers in Chemistry

MINI REVIEW
published: 12 January 2022
doi: 10.3389/fchem.2021.832028

Photodetectors Based on Micro-nano Structure Material

Yu Yu[1,2], Wuyue Wang[1,2], Weihua Li[3], Gong Wang[1,2], Yulei Wang[1,2], Zhiwei Lu[1,2], Sensen Li[4], Wanli Zhao[4], Yuhai Li[4], Tongyu Liu[4] and Xiusheng Yan[4]*

[1]Center for Advanced Laser Technology, Hebei University of Technology, Tianjin, China, [2]Hebei Key Laboratory of Advanced Laser Technology and Equipment, Tianjin, China, [3]Weihai Photonics Information Technology Lab Co., Ltd., Shandong, China, [4]Science and Technology on Electro-Optical Information Security Control Laboratory, Tianjin, China

Photodetectors converting optical signals into electrical signals have been widely utilized and have received more and more attention in scientific research and industrial fields including optical interconnection, optical communication, and environmental monitoring. Herein, we summarize the latest development of photodetectors with different micro-nano structures and different materials and the performance indicators of photodetectors. Several photodetectors, such as flexible, ultraviolet two-dimensional (2D) microscale, and dual-band photodetectors, are listed in this minireview. Meanwhile, the current bottleneck and future development prospects of the photodetector are discussed.

OPEN ACCESS

Edited by:
Yue-Feng Liu,
Jilin University, China

Reviewed by:
Jingjing Zhang,
National University of Defense Technology, China
Xiaoxian Song,
Jiangsu University, China

***Correspondence:**
Yu Yu
yuyu1990@hebut.edu.cn

Specialty section:
This article was submitted to Nanoscience, a section of the journal Frontiers in Chemistry

Received: *09 December 2021*
Accepted: *24 December 2021*
Published: *12 January 2022*

Citation:
Yu Y, Wang W, Li W, Wang G, Wang Y, Lu Z, Li S, Zhao W, Li Y, Liu T and Yan X (2022) Photodetectors Based on Micro-nano Structure Material. Front. Chem. 9:832028. doi: 10.3389/fchem.2021.832028

Keywords: photodetector, micro-nano structure, performance, fabrication, applications

INTRODUCTION

Traditionally, many ordered micro-nano structures have been emerged in natural organisms. Particularly, for plants, the micro-nano structures can guide water droplets to roll freely on their leaves or stay on petals (Zhang et al., 2012a; Zhang et al., 2012b). Inspired by the micro-nano structure of organisms in nature, a growing number of researchers have focused on the application of micro-nano structures in scientific research. Micro-nano structure arrays are widely used in PDs due to their unique order-related characteristics of ordering or patterning. Photodetectors (PDs) that convert optical signals into electrical signals have been widely used and paid more and more attention in scientific research and industrial fields such as biological detection, optical communications, and environmental monitoring (Teng et al., 2018). At present, the main materials used in photodetectors for detecting ultraviolet (UV) to near-infrared spectra are crystalline-Si and III–V (Deng et al., 2015). The reason why micro-nano structure arrays can be rapidly developed in the fields of science and industry is because they can improve the efficiency of light scattering, reduce light reflection efficiency, and extract light better and surface-to-volume ratio of organic light-emitting devices (OLED) (Gao et al., 2021), resulting in the photon supersurface (Li et al., 2021). Different performances can be achieved by changing the size, distribution and different result shapes of each micro/nano structure.

At present, the production of photodetectors with different properties mainly depends on the development of nanotechnology, including template method, photolithography, self-assembly and other methods. Many new types of photodetectors have been fabricated through the above technology, such as high-sensitivity phototransistors (Hai et al., 2015), flexible photodetectors, self-powered ultraviolet detectors with heterojunction nanowire arrays, pyramid array photodetectors, and dual-band detection array van der Waals. Broadband detector, sensitive infrared photodetector (IRPD). Flexible photodetectors (PD) have received more and more attention due to their structural characteristics in many applications, such as wearable

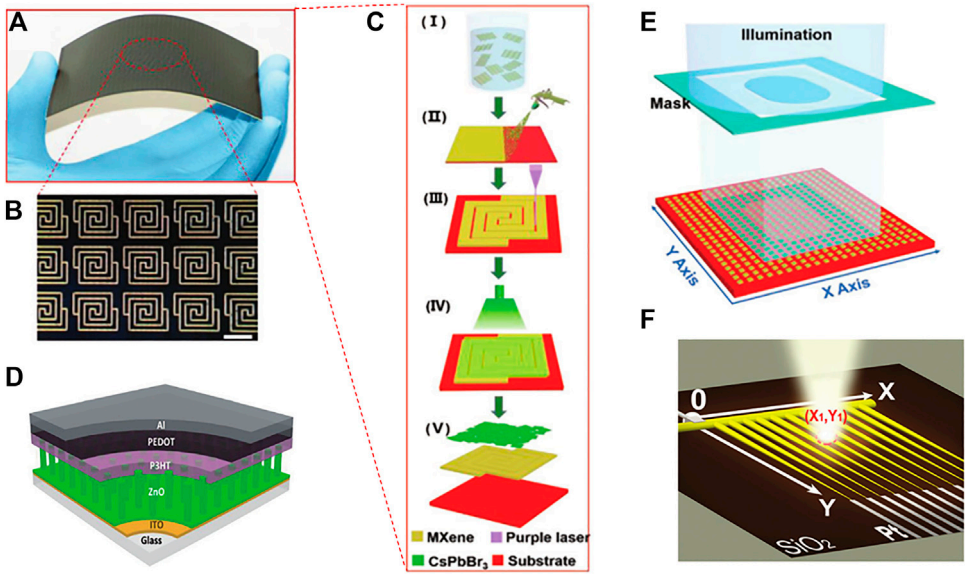

FIGURE 1 | (A) Exhibition of large-area arrays MXene electrode. (B) Micro pattern corresponding to **(A)**. **(C)** Schematic diagram of flexible photodetector processing process. **(D)** Schematic of the P3HT/ZnO heterojunction photodetector. **(E)** Schematic diagram of a digital sensor based on a large-area array photodetector. **(F)** Schematic diagram of the CdS branched photodetector.

optoelectronic devices, bendable imaging sensors and implanted optoelectronic devices (Deng et al., 2019). The self-powered photodetector array based on organic-inorganic heterojunction has unique flexibility and stability due to its special structure, which makes it widely used in optical imaging (Ouyang et al., 2017). Among them, sapphire is used as the substrate, and the pyramidal structure of MoS_2 as the material can enhance the strong interaction, thereby improving the performance of the optoelectronic device (Wang P et al., 2017). Dual-band photodetector for dual-color imaging. By introducing a strong local field, the dark current is reduced, so that the photo-generated carrier separation efficiency is increased, so that the dual-band detection capability of the broadband photodetector is improved (Wang S et al., 2017). Each structure has its own unique properties, and photodetectors of different structure types are used in different optical fields. Therefore, it is particularly important to study the characteristics of different structures in photodetectors.

In this minireview, we focus on the latest developments in the application of different structures to photodetectors. Summarized typical cases, such as flexible photodetectors, ultraviolet photodetectors, high-sensitivity ultra-fast response array photodetectors, high-performance dual-band photodetectors, are discussed the challenges faced by photodetectors and future prospects.

FLEXIBLE PHOTODETECTORS BASED ON MICRO-NANO STRUCTURE MATERIAL

Flexible photodetectors (FPDs) have received more and more attention due to their structural characteristics in many applications, such as Optical communication, industrial automatic control, medical sensor monitoring and intelligent robots and implanted optoelectronic devices. For large-scale manufacturing of FPD processing technology and its use of complex high-vacuum technology, which makes the functional function of its active materials need to achieve a good match. Traditional PDs are usually fabricated on rigid substrates, which seriously hinders their rapid development in the fields of flexible optoelectronic devices such as industrial automatic control, medical sensor monitoring, and implantable optoelectronic devices (Liu et al., 2017). In contrast to rigid PDs, FPDs can meet the needs of industrial automatic control, medical sensor monitoring, and implantable optoelectronic devices. However, it has high optoelectronic performance and good flexibility. It is integrated in an optoelectronic device, which is still a huge challenge for technical processing so far (Hossain et al., 2018). In 2019, Deng et al. demonstrated all spray processable and large area FPDs on plain paper based on two-dimensional (2D) $CsPbBr_3$ nanosheets and conductive $Ti_3C_2T_x$ (MXene) (Deng et al., 2019). **Figure 1A** is its large-area MXene electrode array, and **Figure 1B** is its microscopic model. The production process is shown in **Figure 1C**. Due to the **Figure 1C** good conductivity of MXene, the higher crystallinity of 2D $CsPbBr_3$, and their good matching with the work function, on/off current ratio of the PD reaches 2.3×10^3, and the light response reaches 18 ms. At the same time, Jones' detection rate (D*) reached 6.4×10^8 under 10 V bias and the response rate (R) reached 44.9 mA W^{-1}. In addition, the PD still has good flexibility and stability after being bent 1,500 times.

UV MICRO-NANO STRUCTURE MATERIAL PHOTODETECTORS

As an electronic sensor that converts electrical signals into light signals, ultraviolet (UV) photodetectors have good application prospects in many ways such as medicine, biology, flame monitoring, optical communication, day/night monitoring, and missile detection (Koppens et al., 2014; Chen et al., 2016; Liang et al., 2016; Esopi et al., 2017; Zhang et al., 2017). In 2017, Bangsen et al. have constructed a self-powered UV photodetector based on p-P3HT/n-ZnO nanowire array heterojunction (Ouyang et al., 2017). The schematic diagram of the photodetector is shown in **Figure 1D**. The light response of this PDs at λ = 365 nm can reach 125 μA W^{-1} to 0.84 mW cm^{-2}, and its response and recovery time are both less than 100 ms. Moreover, a photodetector array with 16 pixels is successfully demonstrated for light imaging of complex patterns, such as number-shape and cross-shape. This study provides a practical solution to achieve large-scale UV imaging by integrating inorganic–organic hybrid photodetector into self-powered array configuration.

2D MICROSCALE POSITION-SENSITIVE PHOTODETECTORS

With the continuous improvement of integration and the reduction of the size of nano-devices, two-dimensional micro-scale position sensitive detectors (PSD) have received more and more attention. Nowadays, two-dimensional materials have gradually become mainstream due to their excellent optoelectronic properties (An et al., 2013; Gan et al., 2013; Lopez-Sanchez et al., 2013; Wang et al., 2013; Baugher et al., 2014; Furchi et al., 2014a; Furchi et al., 2014b; Gong et al., 2014; Lee et al., 2014; Ross et al., 2014; Zhang et al., 2014; Li et al., 2015; Wang et al., 2015a; Wang et al., 2015b; Youngblood et al., 2015; Yue et al., 2015; Long et al., 2016). **Figure 1E** is a schematic diagram of a digital sensor based on a large area array PD. In 2018. For the first time, Chen et al. have grown a well-defined hollow spherical nanoshell array of two-dimensional transition metal aluminum dichloride (TMDC) nanomaterials for $MoSe_2$ and MoS_2 through chemical vapor deposition technology (Chen et al., 2018). The responsivity of the $MoSe_2$ hollow sphere photodetector reaches 8.9 A W^{-1}, which is about 10 times that of the $MoSe_2$ dense film (0.9 A W^{-1}). At the same time, the hollow sphere PDs has a fast response and recovery speed and λ = 365 nm irradiation good durability at wavelengths. Xu et al. designed a high-sensitivity ultra-fast response array photodetector based on a new two-dimensional lead iodide perovskite crystal (Xu et al., 2019). The array photodetector achieves high phodetectivities (6.3×10^{12} Jones) responsivities (≈47 A W^{-1}) and low dark current (≈2.4×10^{-11} A). In 2019, Li et al. developed a method capable of heterogeneous integration of atomically thin 2D crystal arrays for system-on-chip electrons on a planar patterned silicon substrate (Li et al., 2019). In addition, multi-channel devices with good optical and electrical characteristics are widely used in system-on-chip (Hao et al., 2019). Schematic diagram of CdS branch photodetector. As shown in **Figure 1F**. Hao et al. based on a highly ordered comb-shaped CdS nanowire array with tapered branches, a one-step synthesis strategy is used to achieve high-resolution 2D position-sensitive photodetection through the variable resistance of multiple lines and the variable optical response of different parts Device. The tapered branch can accurately identify the position of the incident light in each area of the nanowire array according to the change of the photocurrent. In addition to the above-mentioned traditional photodetectors, more and more complex photodetectors are gradually being used in many fields. Multicolor photodetectors have a wide range of applications in the fields of imaging, (Schermelleh et al., 2008; Sang et al., 2013), medical treatment, (Keller et al., 2001), astronomical observations (Fontana et al., 2004) and military applications (Tribolet and Destefanis, 2005). Ji et al. used interface engineering technology to develop an ultraviolet-visible multicolor photodetector based on n-Si (111)/TiO_2 nanorod array heterojunction (Tao et al., 2016). The photodetector is manufactured through continuous processes such as chemical etching, magnetron sputtering, hydrothermal growth and assembly. In the case of low reverse bias voltage (0~-2 V), only photo-generated electrons in TiO_2 can pass through the low ΔEC barrier, and the device only responds to ultraviolet light.

DUAL-BAND MICRO-NANO STRUCTURE MATERIAL PHOTODETECTORS

In the past few decades, in the field of dual-color detection technology (DCDT), people have made significant progress by introducing new materials such as quantum dots and superlattices (Martyniuk et al., 2014; Kufer et al., 2015; Lei et al., 2015; Hoang et al., 2016). Wang et al. designed a dual-band photodetector with high-performance dual-color imaging and wafer-level 2D GaSe/GaSb van der Waals vertical heterostructure based on molecular beam epitaxial growth (Wang P et al., 2017). By introducing a strong local field, the dark current is reduced, so that the photo-generated carrier separation efficiency is increased, so that the dual-band detection capability of the broadband photodetector is improved. Ultrasensitive visible and infrared specific detectivities reach up to 2.2×10^{12} and 1.3×10^{12} Jones, respectively, and an excellent external quantum efficiency up to 50% is obtained with microsecond response speed, which is expected due to its photovoltaic mechanism for free-carrier generation. This new type of heterogeneous photodiode also has the good photoresponsibility of the two-dimensional material GaSe in the visible light band and also have the excellent photodetection performance of the traditional GaSb in the infrared light band. It provides a new way for two-dimensional materials to be used in actual room temperature applications.

CONCLUSION AND OUTLOOK

In this minireview, we summarize the performance indicators of photodetectors with different structures. Such as flexible photodetectors, ultraviolet photodetectors, high-sensitivity ultra-fast response array photodetectors, and high-performance dual-band photodetectors are listed. Although these devices have

reached very good performance indicators. However, there are still many challenges to realize low-cost and large-scale preparation. However, with the rapid development of micro-nano manufacturing technology, photodetectors with good performance will be better used in electronic information, optical communications, environmental monitoring and other fields.

AUTHOR CONTRIBUTIONS

YY, GW, and WL contributed to conception and design of the study. YY, WW, YW, and ZL organized the database. SL, WZ, YL, TL, and XY performed the statistical analysis. YY and WW wrote the first draft of the manuscript. YY, GW and WW wrote sections of the manuscript. All authors contributed to manuscript revision, read, and approved the submitted version.

FUNDING

This work was supported by the National Natural Science Foundation of China (Grant Nos. 62005074, 61927815, 62075056, and 62004059), Natural Science Foundation of Hebei Province (No. F2021202002) and Key Laboratory Fund Project (No. 61421070302).

REFERENCES

An, X., Liu, F., Jung, Y. J., and Kar, S. (2013). Tunable Graphene-Silicon Heterojunctions for Ultrasensitive Photodetection. *Nano Lett.* 13, 909–916. doi:10.1021/nl303682j

Baugher, B. W. H., Churchill, H. O. H., Yang, Y., and Jarillo-Herrero, P. (2014). Optoelectronic Devices Based on Electrically Tunable P-N Diodes in a Monolayer Dichalcogenide. *Nat. Nanotech.* 9, 262–267. doi:10.1038/nnano.2014.25

Chen, H., Liu, H., Zhang, Z., Hu, K., and Fang, X. (2016). Nanostructured Photodetectors: From Ultraviolet to Terahertz. *Adv. Mater.* 28, 403–433. doi:10.1002/adma.201503534

Chen, X., Yang, H., Liu, G., Gao, F., Dai, M., Hu, Y., et al. (2018). Hollow Spherical Nanoshell Arrays of 2D Layered Semiconductor for High-Performance Photodetector Device. *Adv. Funct. Mater.* 28 (8), 1705153–117051539. doi:10.1002/adfm.201705153

Deng, H., Yang, X., Dong, D., Li, B., Yang, D., Yuan, S., et al. (2015). Flexible and Semitransparent Organolead Triiodide Perovskite Network Photodetector Arrays With High Stability. *Nano Lett.* 15, 7963–7969. doi:10.1021/acs.nanolett.5b03061

Deng, W., Huang, H, Jin, H., Li, W., Chu, X., Xiong, D., et al. (2019). All-Sprayed-Processable, Large-Area, and Flexible Perovskite/MXene-Based Photodetector Arrays for Photocommunication. *Adv. Opt. Mater.* 7 (6), 1801521. doi:10.1002/adom.201801521

Esopi, M. R., Calcagno, M., and Yu, Q. (2017). Organic Ultraviolet Photodetectors Exhibiting Photomultiplication, Low Dark Current, and High Stability. *Adv. Mater. Technol.* 2, 1700025. doi:10.1002/admt.201700025

Fontana, A., Pozzetti, L., Donnarumma, I., Renzini, A., Cimatti, A., Zamorani, G., et al. (2004). The K20 Survey. *A&A.* 424, 23–42. doi:10.1051/0004-6361:20035626

Furchi, M. M., Polyushkin, D. K., Pospischil, A., and Mueller, T. (2014a). Mechanisms of Photoconductivity in Atomically Thin MoS2. *Nano Lett.* 14, 6165–6170. doi:10.1021/nl502339q

Furchi, M. M., Pospischil, A., Libisch, F., Burgdörfer, J., and Mueller, T. (2014b). Photovoltaic Effect in an Electrically Tunable van der Waals Heterojunction. *Nano Lett.* 14, 4785–4791. doi:10.1021/nl501962c

Gan, X., Shiue, R.-J., Gao, Y., Meric, I., Heinz, T. F., Shepard, K., et al. (2013). Chip-Integrated Ultrafast Graphene Photodetector with High Responsivity. *Nat. Photon.* 7, 883–887. doi:10.1038/nphoton.2013.253

Gao, X.-m., Liu, Y. F., Liu, Y.-f., Zhang, H.-j., Zhang, T.-r., Bi, Y.-g., et al. (2021). Nanoimprinted Structures for Organic Light-Emitting Devices and Lasers. *Chin. J. Liq. Cryst. Disp.* 36 (1), 8–20. doi:10.37188/cjlcd.2020-0277

Gong, Y., Lin, J., Wang, X., Shi, G., Lei, S., Lin, Z., et al. (2014). Vertical and In-Plane Heterostructures from WS2/MoS2 Monolayers. *Nat. Mater.* 13, 1135–1142. doi:10.1038/nmat4091

Hai, H., Peng, W., Gao, Y., Wang, X., Lin, T., Wang, J., et al. (2015). Highly Sensitive Phototransistor Based on Gase Nanosheets. *Appl. Phys. Lett.* 44 (14), 699. doi:10.1063/1.4933034

Hao, Y., Guo, S., Weller, D., Zhang, M., Ding, C., Chai, K., et al. (2019). Position-sensitive Array Photodetector Based on Comb-Like Cds Nanostructure With Cone-Shape Branches. *Adv. Funct. Mater.* 29 (1), 1805967–11805967. doi:10.1002/adfm.201805967

Hoang, A. M., Dehzangi, A., Adhikary, S., and Razeghi, M. (2016). High Performance Bias-Selectable Three-Color Short-Wave/Mid-Wave/Long-Wave Infrared Photodetectors Based on Type-II InAs/GaSb/AlSb Superlattices. *Sci. Rep.* 6, 24144. doi:10.1038/srep24144

Hossain, M., Kumar, G. S., Barimar Prabhava, S. N., Sheerin, E. D., McCloskey, D., Acharya, S., et al. (2018). Transparent, Flexible Silicon Nanostructured Wire Networks with Seamless Junctions for High-Performance Photodetector Applications. *ACS Nano.* 12, 4727–4735. doi:10.1021/acsnano.8b01387

Keller, P., Toomre, D., Díaz, E., White, J., and Simons, K. (2001). Multicolour Imaging of Post-Golgi Sorting and Trafficking in Live Cells. *Nat. Cell Biol.* 3, 140–149. doi:10.1038/35055042

Koppens, F. H. L., Mueller, T., AvourisFerrari, P. A. C., Ferrari, A. C., Vitiello, M. S., and Polini, M. (2014). Photodetectors Based on Graphene, Other Two-Dimensional Materials and Hybrid Systems. *Nat. Nanotech.* 9, 780–793. doi:10.1038/nnano.2014.215

Kufer, D., Nikitskiy, I., Lasanta, T., Navickaite, G., Koppens, F. H. L., and Konstantatos, G. (2015). Hybrid 2D-0D MoS2-PbS Quantum Dot Photodetectors. *Adv. Mater.* 27, 176–180. doi:10.1002/adma.201402471

Lee, C.-H., Lee, G.-H., van der Zande, A. M., Chen, W., Li, Y., Han, M., et al. (2014). Atomically Thin p-n Junctions With van der Waals heterointerfaces. *Nat. Nanotech.* 9, 676–681. doi:10.1038/nnano.2014.150

Lei, W., Antoszewski, J., and Faraone, L. (2015). Progress, Challenges, and Opportunities for HgCdTe Infrared Materials and Detectors. *Appl. Phys. Rev.* 2, 41303. doi:10.1063/1.4936577

Li, H.-M., Lee, D., Qu, D., Liu, X., Ryu, J., Seabaugh, A., et al. (2015). Ultimate Thin Vertical P-N Junction Composed of Two-Dimensional Layered Molybdenum Disulfide. *Nat. Commun.* 6, 6564. doi:10.1038/ncomms7564

Li, H., Gu, S., Zhang, Q., Song, E., Kuang, T., Chen, F., et al. (2021). Recent Advances in Biofluid Detection with Micro/Nanostructured Bioelectronic Devices. *Nanoscale.* 13 (6), 3436–3453. doi:10.1039/d0nr07478k

Li, S. L., Zhang, L., Zhong, X., Gobbi, M., Bertolazzi, S., Guo, W., et al. (2019). Nano-subsidence Assisted Precise Integration of Patterned Two-Dimensional Materials for High-Performance Photodetector Arrays. *Acs Nano.* 13 (2), 2654–2662. doi:10.1021/acsnano.9b00889

Liang, Y., Wang, Y., Wang, J., Wu, S., Jiang, D., and Lian, J. (2016). High-Performance Flexible Photodetectors Based on Single-Crystalline Sb2Se3 Nanowires. *RSC Adv.* 6, 11501–11506. doi:10.1039/c5ra23542a

Liu, X., Yu, D., Cao, F., Li, X. J., Ji, J., Chen, J., et al. (2017). Low-Voltage Photodetectors with High Responsivity Based on Solution-Processed Micrometer-Scale All-Inorganic Perovskite Nanoplatelets. *Small.* 13, 1700364. doi:10.1002/smll.201700364

Long, M., Liu, E., Wang, P., Gao, A., Xia, H., Luo, W., et al. (2016). Broadband Photovoltaic Detectors Based on an Atomically Thin Heterostructure. *Nano Lett.* 16, 2254–2259. doi:10.1021/acs.nanolett.5b04538

Lopez-Sanchez, O., Lembke, D., Kayci, M., Radenovic, A., and Kis, A. (2013). Ultrasensitive Photodetectors Based on Monolayer MoS2. *Nat. Nanotech.* 8, 497–501. doi:10.1038/nnano.2013.100

Martyniuk, P., Antoszewski, J., Martyniuk, M., Faraone, L., and Rogalski, A. (2014). New Concepts in Infrared Photodetector Designs. *Appl. Phys. Rev.* 1, 41102. doi:10.1063/1.4896193

Ouyang, B., Zhang, K., and Yang, Y. (2017). Self-Powered UV Photodetector Array Based on P3HT/ZnO Nanowire Array Heterojunction. *Adv. Mater. Technol.* 2, 1700208. doi:10.1002/admt.201700208

Ross, J. S., Klement, P., Jones, A. M., Ghimire, N. J., Yan, J., Mandrus, D. G., et al. (2014). Electrically Tunable Excitonic Light-Emitting Diodes Based on Monolayer WSe2 P-N Junctions. *Nat. Nanotech.* 9, 268–272. doi:10.1038/nnano.2014.26

Sang, L., Hu, J., Zou, R., Koide, Y., and Liao, M. (2013). Arbitrary Multicolor Photodetection by Hetero-Integrated Semiconductor Nanostructures. *Sci. Rep.* 3, 2368. doi:10.1038/srep02368

Schermelleh, L., Carlton, P. M., Haase, S., Shao, L., Winoto, L., Kner, P., et al. (2008). Subdiffraction Multicolor Imaging of the Nuclear Periphery with 3D Structured Illumination Microscopy. *Science.* 320, 1332–1336. doi:10.1126/science.1156947

Tao, J., Qian, L., Rujia, Z., Yangang, S., Kaibing, X., Liwen, S., et al. (2016). An Interface Engineered Multicolor Photodetector Based on N-si(111)/Tio_2 Nanorod Array Heterojunction. *Adv. Funct. Mater.* 26 (9), 1400–1410. doi:10.1002/adfm.201504464

Teng, F., Hu, K., Ouyang, W., and Fang, X. (2018). Photoelectric Detectors Based on Inorganic p-Type Semiconductor Materials. *Adv. Mater.* 30, 1706262. doi:10.1002/adma.201706262

Tribolet, P., and Destefanis, G. (2005). Third Generation and Multicolor IRFPA Developments: a Unique Approach Based on DEFIR (Invited Paper). *Conf. Infrared Technol. Appl.* 5783, 350. doi:10.1117/12.607544

Wang, K., Wang, J., Fan, J., Lotya, M., O'Neill, A., Fox, D., et al. (2013). Ultrafast Saturable Absorption of Two-Dimensional MoS2 Nanosheets. *ACS Nano.* 7, 9260–9267. doi:10.1021/nn403886t

Wang, P., Liu, S., Luo, W., Fang, H., Gong, F., Guo, N., et al. (2017). Arrayed Van Der Waals Broadband Detectors for Dual-Band Detection. *Adv. Mater.* 29 (16), 1604439. doi:10.1002/adma.201604439

Wang, S., Medina, H., Hong, K.-B., Wu, C.-C., Qu, Y., Manikandan, A., et al. (2017). Thermally Strained Band Gap Engineering of Transition-Metal Dichalcogenide Bilayers with Enhanced Light-Matter Interaction toward Excellent Photodetectors. *ACS Nano* 11 (9), 8768–8776. doi:10.1021/acsnano.7b02444

Wang, X., Jiang, X., Wang, T., Shi, J., Liu, M., Zeng, Q., et al. (2015a). Electrically Configurable Graphene Field-Effect Transistors with a Graded-Potential Gate. *Nano Lett.* 15, 3212–3216. doi:10.1021/acs.nanolett.5b00396

Wang, X., Wang, P., Wang, J., Hu, W., Zhou, X., Guo, N., et al. (2015b). Ultrasensitive and Broadband MoS2Photodetector Driven by Ferroelectrics. *Adv. Mater.* 27, 6575–6581. doi:10.1002/adma.201503340

Xu, Z., Li, Y., Liu, X., Ji, C., Chen, H., Li, L., et al. (2019). Highly Sensitive and Ultrafast Responding Array Photodetector Based on a Newly Tailored 2d lead Iodide Perovskite crystal. *Adv. Opt. Mater.* 7 (11), 1900308–11900308. doi:10.1002/adom.201900308

Youngblood, N., Chen, C., Koester, S. J., and Li, M. (2015). Waveguide-Integrated Black Phosphorus Photodetector with High Responsivity and Low Dark Current. *Nat. Photon.* 9, 247–252. doi:10.1038/nphoton.2015.23

Yue, R., Barton, A. T., Azcatl, A., Pena, L. F., Wang, J., Peng, X., et al. (2015). HfSe2 Thin Films: 2D Transition Metal Dichalcogenides Grown by Molecular Beam Epitaxy. *ACS Nano.* 9, 474–480. doi:10.1021/nn5056496

Zhang, K., Peng, M., Wu, W., Guo, J., Gao, G., Liu, Y., et al. (2017). A Flexible P-CuO/n-MoS2 Heterojunction Photodetector With Enhanced Photoresponse by the Piezo-Phototronic Effect. *Mater. Horiz.* 4, 274–280. doi:10.1039/c6mh00568c

Zhang, W., Chiu, M.-H., Chen, C.-H., Chen, W., Li, L.-J., and Wee, A. T. S. (2014). Role of Metal Contacts in High-Performance Phototransistors Based on WSe2 Monolayers. *ACS Nano.* 8, 8653–8661. doi:10.1021/nn503521c

Zhang, Y.-L., Chen, Q.-D., Jin, Z., Kim, E., and Sun, H.-B. (2012a). Biomimetic Graphene Films and Their Properties. *Nanoscale.* 4 (16), 4858–4869. doi:10.1039/C2NR30813D

Zhang, Y.-L., Xia, H., Kim, E., and Sun, H.-B. (2012b). Recent Developments in Superhydrophobic Surfaces with Unique Structural and Functional Properties. *Soft Matter.* 8 (44), 11217–11231. doi:10.1039/C2SM26517F

Conflict of Interest: Author WL is employed by Weihai Photonics Information Technology Lab Co., Ltd.

The remaining authors declare that the research was conducted in the absence of any commercial or financial relationships that could be construed as a potential conflict of interest.

Publisher's Note: All claims expressed in this article are solely those of the authors and do not necessarily represent those of their affiliated organizations, or those of the publisher, the editors and the reviewers. Any product that may be evaluated in this article, or claim that may be made by its manufacturer, is not guaranteed or endorsed by the publisher.

frontiers in Chemistry

ORIGINAL RESEARCH
published: 14 January 2022
doi: 10.3389/fchem.2021.818459

Dynamics of Strong Coupling Between Free Charge Carriers in Organometal Halide Perovskites and Aluminum Plasmonic States

Yang Luo, Hai Wang, Le-Yi Zhao and Yong-Lai Zhang*

State Key Laboratory of Integrated Optoelectronics, College of Electronic Science and Engineering, Jilin University, Changchun, China

We have investigated a strong coupled system composed of a $MAPbI_xCl_{3-x}$ perovskite film and aluminum conical nanopits array. The hybrid states formed by surface plasmons and free carriers, rather than the traditional excitons, is observed in both steady-state reflection measurements and transient absorption spectra. In particular, under near upper band resonant excitation, the bleaching signal from the band edge of uncoupled perovskite was completely separated into two distinctive bleaching signals of the hybrid system, which is clear evidence for the formation of strong coupling states between the free carrier–plasmon state. Besides this, a Rabi splitting up to 260 meV is achieved. The appearance of the lower bands can compensate for the poor absorption of the perovskite in the NIR region. Finally, we found that the lifetime of the free carrier–SP hybrid states is slightly shorter than that of uncoupled perovskite film, which can be caused by the ultrafast damping of the SPs modes. These peculiar features on the strong coupled hybrid states based on free charge carriers can open new perspectives for novel plasmonic perovskite solar cells.

Keywords: strong coupling, rabi splitting, perovskite, aluminum plasmonic states, transient absorption spectra, free charge carriers

OPEN ACCESS

Edited by:
Yun-Fei Li,
Hebei University of Technology, China

Reviewed by:
Yawei Hao,
China Academy of Engineering Physics, China
Ying Jiang,
Hunan University, China

****Correspondence:***
Hai Wang
wanghai03@jlu.edu.cn

Specialty section:
This article was submitted to Nanoscience, a section of the journal Frontiers in Chemistry

Received: *19 November 2021*
Accepted: *06 December 2021*
Published: *14 January 2022*

Citation:
Luo Y, Wang H, Zhao L-Y and Zhang Y-L (2022) Dynamics of Strong Coupling Between Free Charge Carriers in Organometal Halide Perovskites and Aluminum Plasmonic States. Front. Chem. 9:818459. doi: 10.3389/fchem.2021.818459

INTRODUCTION

Organometal halide perovskites are emerging as a class of attractive materials for solution-processed optoelectronic devices with outstanding performance.(Jeon et al., 2015; Yang et al., 2015; Long et al., 2020; Chen et al., 2021; Privitera et al., 2021). Perovskites possess the same crystal structure of calcium titanate ABX_3 (D. Weber and Naturforsch, 1978), where A and B are typical organic cations (methylammonium or formamidinium) and metal cations (Pb^{2+} or Sn^{2+}) jointly bound to X, halide anions (Cl^-, Br^- or I^-). Through compositional control of such components and ratios, various perovskite materials can be realized (Zhao and Zhu, 2016; Correa-Baena et al., 2017). Owing to the specific crystal structure, perovskites show great advantages, such as high absorption coefficient, high charge-carrier mobility, low trap density, and long charge diffusion length (Stranks et al., 2013; Xing et al., 2013). Simultaneously, through improving the architecture of the photovoltaic devices, a power conversion efficiency (PCE) of up to 25.2% is achieved (Yoo et al., 2021). Methylammonium (MA) lead trihalide perovskites with the chemical composition $CH_3NH_3PbX_nY_{3-n}$ is most widely and maturely researched. Their fundamental parameters, such as photoexcited charge-carrier dynamics and carrier diffusion length, have been deeply explored. In transient absorption measurements, a

long charge diffusion length >1 μm is revealed in $CH_3NH_3PbCl_xI_{3-x}$ perovskite films (Stranks et al., 2013). Furthermore, the nature of photogenerated species has also been expounded carefully. It is confirmed that, upon photoexcitation, excitons within the perovskite can be spontaneously dissociated into free electrons and holes, namely, conventional excitons can be displaced by free charge carriers, which are identified as dominated photogenerated species in perovskite film (Manser and Kamat, 2014). These characteristics bring many distinct advantages, making the OLHP available to high-performance solar cells, light-emitting diodes, and photodetectors.

Moreover, great progress has also been made in using surface plasmons (SPs) to further enhance the performance of plasmonic devices based on OLHP (Fang et al., 2010; Bi et al., 2013; Ren et al., 2020; Juan et al., 2021; Krisnanda et al., 2021). Affected by the SPs, the optoelectronic characteristics of the perovskite film can be significantly tuned, such as enhancement of absorption, reduction of exciton binding energy, increase of charge mobility, and so on (Saliba et al., 2015; Chan et al., 2017; Ding et al., 2018; Ma et al., 2019; Mohamed Saheed et al., 2019; Krisnanda et al., 2021). However, most of the works still survive in the weak coupling regime in which the wave function of the perovskite material is unperturbed. In contrast, only a few reports have emerged on the strong coupling between SPs and OLHP. In a strong coupling regime, the excitation energy can be rapidly exchanged between SPs modes and materials with the formation of new hybrid states separated energetically by a Rabi splitting (Qian et al., 2021; Su et al., 2021; Zhao et al., 2021). In this regime, the new states are coherently superpositioned with intriguing phenomena, such as Bose–Einstein condensation (Plumhof et al., 2014) and thresholdless lasing (Ding and Ning, 2012; Wang et al., 2021). Among the variety of research, many types of excitonic materials, for instance, J-aggregates (Hao et al., 2011; Wang et al., 2016), dye molecules (Wang et al., 2017), quantum dots (Wang et al., 2016), and two-dimensional material (Liu et al., 2016; Shan et al., 2019) are realized in a strong coupling regime with SPs. In contrast, so far little is known about the coherent hybrid system generated by the interaction of free charge carriers and SPs. Particularly, there is still limited understanding on the kinetics of hybrid SP–free charge carrier states. It is also worth emphasizing again that, on account of the small exciton binding energies, free charge carriers characterized by slow recombination and relatively high mobility can be efficiently generated in OLHP (Manser and Kamat, 2014). Thus, there is a strong incentive to harness such materials for studying strong coupling between SPs and free charge carriers.

In this work, we demonstrate that strong SP–free charge carrier coupling can be achieved with $CH_3NH_3PbCl_xI_{3-x}$ perovskite film and SPs supported by Al conical nanopits arrays. Furthermore, under upper band resonant excitation, direct evidence of the formation of the hybrid free charge carrier–SP states is clearly shown in the transient absorption (TA) spectra. The result also proves that the band filling of the upper states follows the Burstein–Moss band filling model. Finally, we measured a shorter lifetime of the hybrid SP–free charge carrier states, which was accelerated by the ultrafast damping of the SPs character.

EXPERIMENTAL SECTION

The fabrication processes of the strong SP–free charge carrier coupled system is described in **Figure 1A**. First, the cleaned glasses/ITO was milled by means of a focused ion beam to define the shape of a square-like array of conical pits. Afterward, an electron beam evaporator was used for the 200-nm-thick aluminum (Al) film deposition on the patterned glasses/ITO substrates. Then, conical pit arrays with a period from 300 to 450 nm can be replicated on top of the Al film with a total area of $50 \times 50\ \mu m^2$. Al was selected not only simply for its cost-effectiveness and abundance, but also for the wide SP spectral range (Li et al., 2016). Here, the processed Al nanopits with uniform size (as shown in **Figure 1C**) show a plasmon resonance that matches with the broad absorbance spectrum of $CH_3NH_3PbCl_xI_{3-x}$ film. To obtain a strong coupled hybrid system between SPs and free charge carriers, the perovskite films were directly formed on Al conical nanopits. The perovskite precursor solution was prepared by dissolving 139.0 mg of PbI_2 and 238.5 mg of CH_3NH_3I in 2 ml N,N-dimethylformamide (DMF). Then, the samples were obtained by spin-coating these precursor solutions at 3000 rpm for 30 s and annealed at 80°C for 100 min in a nitrogen-filled glove box. **Figure 1D** provides SEM images of the morphology of the synthesized $CH_3NH_3PbI_xCl_{3-x}$ film with grain sizes ranging from 200 to 250 nm $CH_3NH_3PbCl_xI_{3-x}$ and $CH_3NH_3PbI_3$ have similar optical properties, such as absorption spectrum, bandgaps, and Fermi levels. However, it is demonstrated that the Cl-doped perovskite film has a long charge carrier diffusion length, always leading to a higher efficiency solar cell (Xing et al., 2013). Here $CH_3NH_3PbCl_xI_{3-x}$ is selected rather than $CH_3NH_3PbI_3$.

Steady-State Measurements

Figure 2A shows the reflection spectra of Al nanopit arrays with various periods. The reflection peaks display a pronounced red shift as the period of the nanopit arrays increases, showing the SP resonance region from 490 to 750 nm. In the meantime, for each nanopit array, a shoulder peak appeared on the higher energy side of the main SPs peak. The offset of the two peaks can be attributed to the difference of the refractive index of the media above and below the Al film. The reflection spectrum of the $CH_3NH_3PbCl_xI_{3-x}$ perovskite film deposited on flat Al film is also shown in **Figure 2A** as a black line. As can be seen, the perovskite film has a strong optical absorption with a band edge at 1.65 eV. Observably, all the SP bands overlap within the reflection spectrum of $CH_3NH_3PbCl_xI_{3-x}$ film. Thus, when perovskite film is formed on Al nanopit arrays, the hybrid system is prepared.

A key point to underlined here is the demonstration that free charge carriers generated in perovskite film and SPs in the hybrid system can enter the strong coupled regime. Because the initial study on strong coupling was focused on a series of J-aggregate molecules with unusually strong transition dipoles, which was

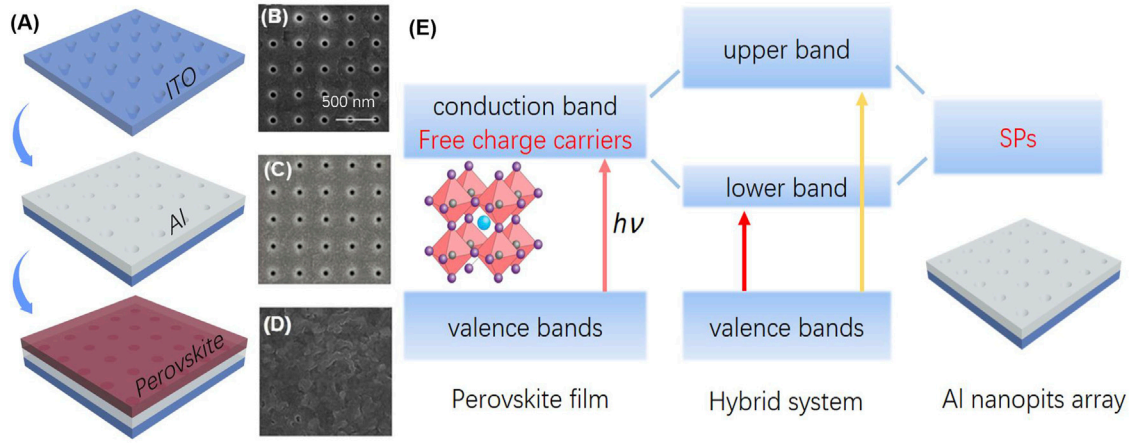

FIGURE 1 | (A) Steps of fabrication of strong free charge carrier–SP coupling system, **(B, C)** SEM image of the conical nanopits on glass/ITO and Al layer, **(D)** SEM image of perovskite layer, **(E)** the mode diagram of the hybrid free charge carrier–SP system; the inset shows the crystal structure of $CH_3NH_3PbCl_xI_{3-x}$ perovskite.

considered as the only possible candidate for strong coupling. However, moving forward, much larger Rabi splitting has also been achieved between SPs and molecules with broad absorption spectra, such as photochromic molecules and semiconductor polymer (Schwartz et al., 2011; Orgiu et al., 2015). Actually, several studies demonstrate that the vacuum Rabi splitting depends on the energy-integrated absorption of the material, namely, a larger vacuum Rabi splitting can be achieved by using material with higher absorption cross-sections (Gambino et al., 2014). Therefore, in the following part, a clear indication of strong coupling between SPs and free charge carriers in $CH_3NH_3PbCl_xI_{3-x}$ perovskite film is provided.

Figure 2B shows a series of reflection spectra of the hybrid system with different Al nanopit periods. Compared with the perovskite film on flat Al film, the reflection spectra of the hybrid systems are significantly changed. In particular, at the wavelength longer than the band edge of the perovskite, extra reflection peaks corresponding to the lower bands are shown, which can lead to overcoming the poor absorption of the $CH_3NH_3PbCl_xI_{3-x}$ film in the NIR region. On the other side, due to the strong absorption in the visible range of the perovskite film, the reflection spectra of the hybrid system at the higher energy side only changed slightly. However, it can be seen that the peak position related to the upper bands also has a red shift with the lattice period increasing as the red arrow shown in **Figure 2B**. Furthermore, the dispersion diagram of the two bands is shown in **Figure 2C**. As expected, anticrossing behavior as remarkable experimental evidence of strong coupling is clearly observed (Dintinger et al., 2005).

However, because most light is absorbed by the perovskite layer when the wavelength (λ) of the light is shorter than the band edge of $CH_3NH_3PbCl_xI_{3-x}$ ($\lambda < 760$ nm), the formation of the upper bands in the hybrid systems cannot be clearly reflected from reflection spectra. The evidence of the formation of the new hybrid SP–free charge carrier states is not comprehensive. The Rabi splitting energy cannot be revealed just from steady-state measurements. Therefore, transient absorption spectroscopy was performed to gain a further insight into the formation and dynamics of the hybrid states.

TA experiments

TA spectroscopy, also named the pump-probe technique (Gao et al., 2010; Wang et al., 2013), is an effective approach to the study of charge carrier transfer and recombination dynamics of perovskite films (Zhang et al., 2015; Zhang et al., 2016). Femtosecond reflective TA spectra was carried out by a 100 fs laser pump-probe system. A Ti:sapphire amplifier system was used to provide an 800-nm wavelength laser with 100 fs pulse width and 500 Hz repetition rate. The amplified output was split into two parts. The stronger part was sent to a β-barium borate (BBO) crystal or TOPAS system to generate the pump pulse at 400 or 560 nm while the weaker part was focused on a sapphire crystal to create a continuous white light as a probe beam. The relative delay between the pump and probe beam was controlled by an optical delay line (Newport DL325). Then, the two beams were focused on the sample by a microscope objective. The probe beam reflected from the sample was collected by an optical spectrometer (Avantes AvaSpec -ULS2048CL-EVO) while the reflected pump beam was filtered. Here, we focused on the TA spectroscopy findings on the nature of the hybrid SP–free charge carrier states. To begin with, the first part of the TA measurements were performed under nonresonant conditions by the 400 nm laser pulse. **Figure 3A** shows the TA spectra of $CH_3NH_3PbCl_xI_{3-x}$ film on flat Al film. The figure consists of a negative band at 730 nm corresponding to band edge ground state bleaching, and on both sides of the bleaching, there are two positive signals due to the photoinduced absorption of hot electrons and holes (Herz, 2016). In addition, it is worth noting that the high-energy tail of the band edge bleaching spectrum is broadened and shows a blue shift in the first 10 ps, which can be explained by a dynamic Burstein–Moss shift (Manser and Kamat, 2014). Namely, after laser excitation, the conduction and valence band edges are filled with thermalized carriers; further considering the Pauli exclusion principle, the

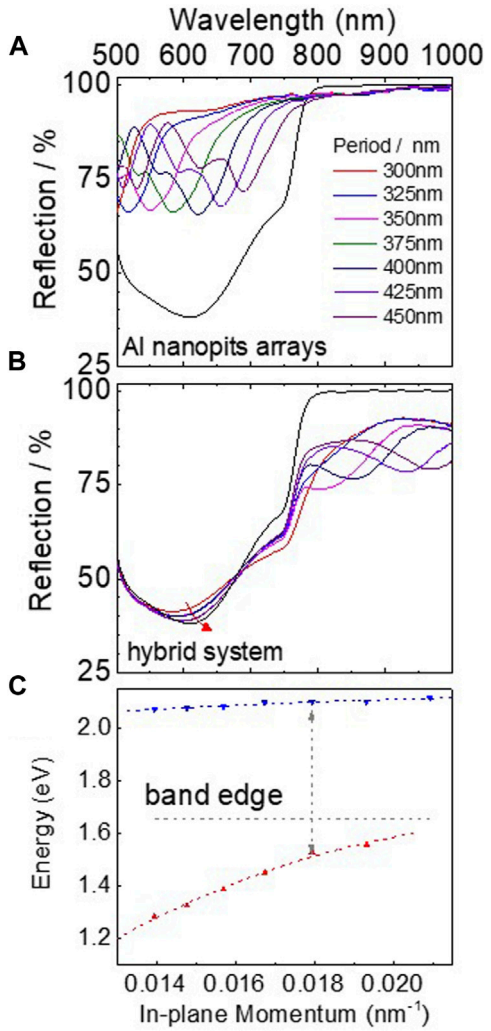

FIGURE 2 | (A) Reflection spectra of Al conical nanopit arrays covered by PMMA film. The lattice period is tuned from 300 to 450 nm. The black line shows the reflection spectrum of the $CH_3NH_3PbCl_xI_{3-x}$ perovskite film on flat Al film. **(B)** Reflection spectra of the perovskite layer on flat Al film and conical nanopit arrays. The lattice period is tuned from 300 to 450 nm. **(C)** Dispersion curve of hybrid free change carrier–SP strong coupled system. The horizontal dashed line shows the band edge of the $CH_3NH_3PbCl_xI_{3-x}$ perovskite film.

occupation of band-edge states is pushed to higher energies, leading to a dynamic Burstein–Moss band filling model.

Figures 3B–D shows the corresponding spectra of $CH_3NH_3PbCl_xI_{3-x}$ film on Al nanopit arrays with different periods of 300, 350, and 375 nm. The spectra are a little changed compared with the reference sample on flat Al film. First, for the period equal to 300 nm, the spectra show a negative signal at 760 nm and a shoulder peak at 700 nm, which are possibly corresponded to the hybrid bands. However, the separation between the two new peaks is much smaller than that measured from steady-state reflection spectra, so the strong coupling regime still cannot be clearly identified. For the period equal to 350 and 375 nm, **Figures 3C,D** shows a bleaching band around 730 nm, which is still dominated by the ground-state bleaching from uncoupled $CH_3NH_3PbCl_xI_{3-x}$ film. On the red side of the bleaching band, a positive signal is observed corresponding to the thermal effect of the SPs (Hao et al., 2011) while the bleaching signals from the upper bands are also almost undetectable. In fact, similar to the previous work under nonresonant excitation (Hao et al., 2011; Wang et al., 2016), the intrinsic photophysics of the strong coupled hybrid system cannot be observed. Under such conduction, the initial relaxation process is dominated by a state-filling process and SP thermal effect as the positive signal reported in **Supplementary Figure S1**.

To explore the nature photophysics of the hybrid SP–free charge carrier states more deeply, TA measurements were further carried out under near upper state resonant excitation by a pulsed laser at 560 nm. **Figure 4A** illustrates the TA spectra of $CH_3NH_3PbCl_xI_{3-x}$ film on flat Al film. As a reference, the plot is similar to the spectra obtained under nonresonant excitation at 400 nm. A bleaching signal around 730 nm, which also conforms to the Burstein–Moss band filling model, shows a carrier accumulation–induced blue shift (Manser and Kamat, 2014) while the small positive signals below 680 nm are assigned to photoinduced absorption. The spectra for $CH_3NH_3PbCl_xI_{3-x}$ film on different periodic nanopit arrays are reported in **Figures 4B–D**, which more clearly suggest the formation of strong coupled hybrid SP–free charge carrier states. First, when the nanopit period equals 300 nm, the spectra show a main bleaching peak at 750 nm, corresponding to the lower hybrid band. On the contrary, the amplitude of the upper hybrid band is much smaller, showing a shoulder peak around 670 nm. Under this condition, the splitting was not obvious, which suggests the coupling strength is low. This can be further proved by the dynamic behaver of the hybrid states (see **Figure 5**), which is still similar to the bleaching recovery of pure perovskite film.

More importantly, when the nanopit period equals 350 nm, the SP resonance of Al nanopits can resonate with the free charge carriers in perovskite film. With respect to the reference sample, the TA spectra of the hybrid system show completely different properties. The band edge transition bleaching is completely separated into two bleaching signals at around 700 and 820 nm, which can be attributed to the upper and lower hybrid SP–free charge carrier states with observation of Rabi splitting energy up to 260 meV. Such behavior provides more objective, precise evidence than that observed from steady-state reflection measurements. With the period further increased to 375 nm, as shown in **Figure 4D**, the bleaching peak of the upper state is a little red shifted while the bleaching band of the lower state also experiences a red shift almost extending out of the detection window. By comprehensive analysis of the three different period hybrid systems, the simultaneous shifting of both upper and lower hybrid states is consistent with the characteristic strong coupling: anticrossing behavior, which further remarkably underlines the formation of the coherent hybrid SP–free charge carrier states. Another important observation that needs to be stressed here is that, under upper band resonant excitation, the lower band bleaching signal is narrowing with time. Such distinguishable narrowing of the

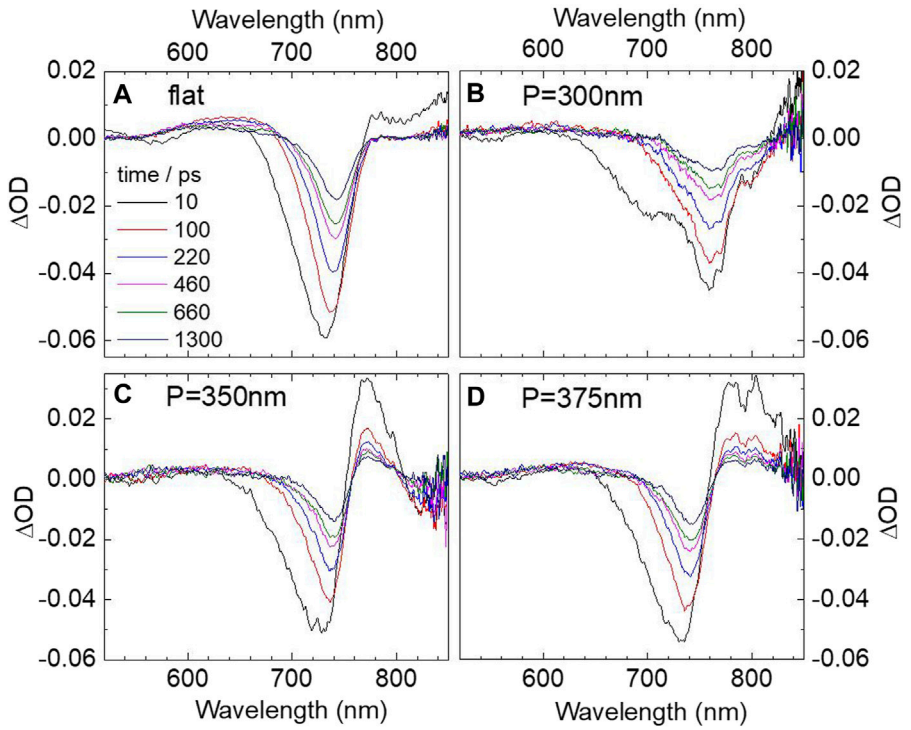

FIGURE 3 | Transient absorption spectra of $CH_3NH_3PbCl_xI_{3-x}$ perovskite film on flat **(A)** Al film and **(B–D)** different Al nanopit arrays with periods of 300, 350, and 375 nm under 400 nm excitation. The spectra are recorded at 10, 100, 220, 460, 660, and 1300 ps.

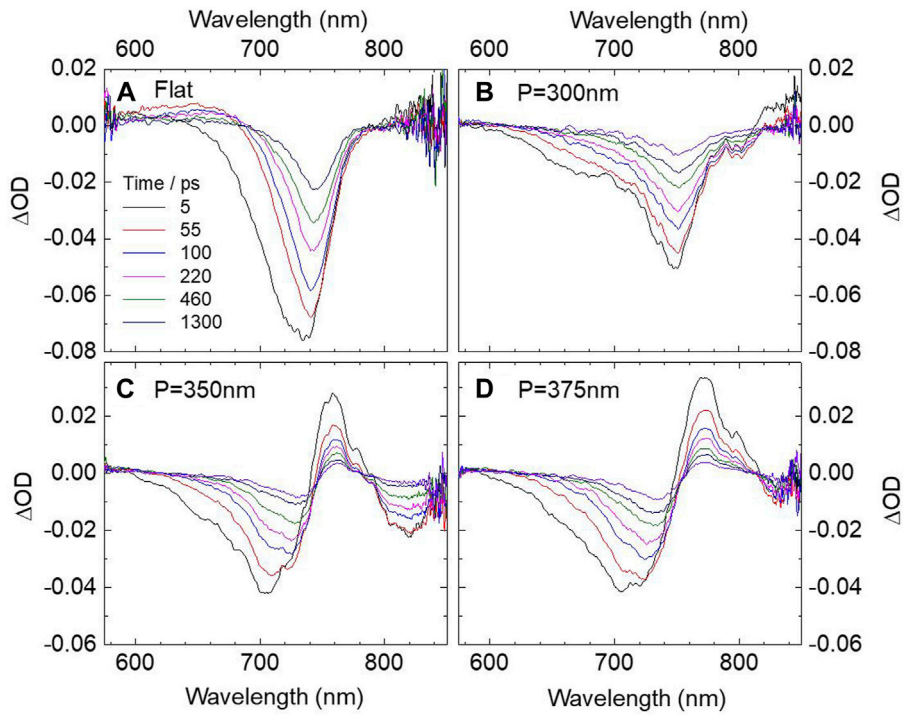

FIGURE 4 | Transient absorption spectra of $CH_3NH_3PbCl_xI_{3-x}$ perovskite film on flat **(A)** Al film and **(B–D)** different Al nanopit arrays with periods of 300, 350, and 375 nm under 560 nm excitation. The spectra are recorded at 5, 55, 100, 220, 460, and 1300 ps.

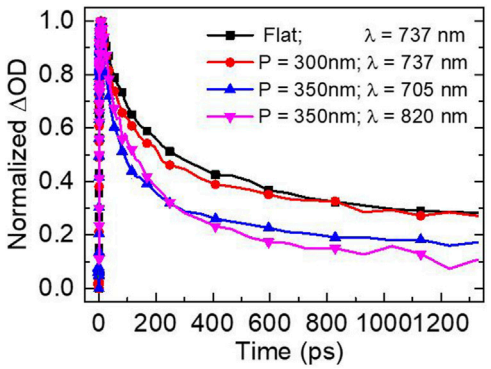

FIGURE 5 | Normalized bleaching dynamics under 560 nm resonant excitation of $CH_3NH_3PbCl_xI_{3-x}$ perovskite film on a flat Al film (measured at 737 nm) and on Al nanopit arrays with periods of 350 nm (measured at the hybrid bands of 705 and 820 nm) and 300 nm (measured at the upper band of 737 nm).

lower band can also be described by the Burstein–Moss effect. On the other hand, the shape of the lower hybrid states does not change with the time. We, therefore, attribute that free carriers are accumulated at the lower bands of the hybrid states after 560 nm laser excitation. The understanding presented here provides new mechanisms of strong coupling between SPs and free charge carriers, which serve to shed light on designing novel ultrafast plasmonic devices.

Finally, the kinetic process of the hybrid SP–free charge carrier states is analyzed. In **Figure 5**, we plot the amplitude-normalized dynamics of the lower and upper hybrid bands of the coupled sample with a nanopit period of 350 nm compared with the dynamics of the band edge bleaching of perovskite film on a flat Al film. As shown, under upper band resonant excitation, the population dynamics of the hybrid states are shorter than the bleaching recovery of free charge carriers in pure perovskite film. This result show interesting differences from the lifetime measured from hybrid states composed of traditional excitons and SPs. Previous experiments confirm that the longer lifetimes of the hybrid states is intrinsic and can be even longer than the lifetime of bare excitons, which is accorded with a non-Markovian regime (Canaguier-Durand et al., 2015). However, here we should emphasize that, again, the excited-state population in $CH_3NH_3PbCl_xI_{3-x}$ film is dominated by free charge carriers. The ultrafast damping plasmon character (Pelton et al., 2008; Hartland, 2011) reduces the lifetime of the coherent hybrid SP–free charge carrier states. Namely, the relaxation of such new hybrid states can be expedited by SPs, leading to a shorter lifetime.

CONCLUSION

In summary, we construct a hybrid structure comprising an Al subwavelength nanopit array and perovskite film. In steady-state measurements, the reflection spectra profile of the hybrid systems characterized by two distinct bands, whose dispersions show the typical signature of strong coupling. These results experimentally demonstrate that strong coupling can be achieved with SPs and free charge carriers generated in $CH_3NH_3PbCl_xI_{3-x}$ film. Moreover, the nature photophysics of the new hybrid SP–free charge carrier states was studied by TA spectroscopy. Under nonresonant excitation by a 400-nm laser, the initial relaxation process is dominated by a state-filling effect, which still cannot provide the intrinsic dynamics of the hybrid state. Furthermore, under near upper band resonant excitation, the TA spectra remarkably displayed the formation of the hybrid SP–free charge carrier state, in which the upper bands can be well ascribed to the dynamic Burstein–Moss effect. We have also found that the lifetime of the hybrid SP–free charge carrier states is shorter than the bleaching recovery of pure $CH_3NH_3PbCl_xI_{3-x}$ film, which is different from that observed in a strong coupling system with traditional excitons conformed to a non-Markovian regime. As a possible explanation, we assume that the ultrafast damping of the SP modes accelerates the relaxation of the hybrid SP–free charge carrier states. To conclude, these new insights on strong coupling with hybrid organic-inorganic perovskites provide a new framework to develop low-cost photovoltaic and light-emitting devices and nanolasers (Sanvitto and Kena Cohen, 2016). New developments on nanoplasmonic devices working in a strong coupling regime with free charge carriers are surely on the horizon.

DATA AVAILABILITY STATEMENT

The original contributions presented in the study are included in the article/**Supplementary Material**, further inquiries can be directed to the corresponding author.

AUTHOR CONTRIBUTIONS

YL, HW, and Y-LZ conceived the research. YL and HW fabricated the samples. YL and L-YZ performed the measurements. All authors discussed the data and wrote the manuscript.

FUNDING

This work was supported by the National Key Research and Development Program of China and the National Natural Science Foundation of China (NSFC) under Grants 21903035, 22073037, and 21773087.

SUPPLEMENTARY MATERIAL

The Supplementary Material for this article can be found online at: https://www.frontiersin.org/articles/10.3389/fchem.2021.818459/full#supplementary-material

REFERENCES

Bi, Y.-G., Feng, J., Li, Y.-F., Zhang, X.-L., Liu, Y.-F., Jin, Y., et al. (2013). Broadband Light Extraction from White Organic Light-Emitting Devices by Employing Corrugated Metallic Electrodes with Dual Periodicity. *Adv. Mater.* 25, 6969–6974. doi:10.1002/adma.201302367

Canaguier-Durand, A., Genet, C., Lambrecht, A., Ebbesen, T. W., and Reynaud, S. (2015). Non-Markovian Polariton Dynamics in Organic Strong Coupling. *Eur. Phys. J. D* 69, 1–7. doi:10.1140/epjd/e2014-50539-x

Chan, K., Wright, M., Elumalai, N., Uddin, A., and Pillai, S. (2017). Plasmonics in Organic and Perovskite Solar Cells: Optical and Electrical Effects. *Adv. Opt. Mater.* 5, 1600698. doi:10.1002/adom.201600698

Chen, J., Zhou, Y., Fu, Y., Pan, J., Mohammed, O. F., and Bakr, O. M. (2021). Oriented Halide Perovskite Nanostructures and Thin Films for Optoelectronics. *Chem. Rev.* 121, 12112–12180. doi:10.1021/acs.chemrev.1c00181

Correa-Baena, J.-P., Abate, A., Saliba, M., Tress, W., Jesper Jacobsson, T., Grätzel, M., et al. (2017). The Rapid Evolution of Highly Efficient Perovskite Solar Cells. *Energy Environ. Sci.* 10, 710–727. doi:10.1039/C6EE03397K

Ding, K., and Ning, C. Z. (2012). Metallic Subwavelength-Cavity Semiconductor Nanolasers. *Light Sci. Appl.* 1–e20. doi:10.1038/lsa.2012.20

Ding, R., Wang, X.-P., Feng, J., Li, X.-B., Dong, F.-X., Tian, W.-Q., et al. (2018). Clarification of the Molecular Doping Mechanism in Organic Single-Crystalline Semiconductors and Their Application in Color-Tunable Light-Emitting Devices. *Adv. Mater.* 30, 1801078. doi:10.1002/adma.201801078

Dintinger, J., Klein, S., Bustos, F., Barnes, W. L., and Ebbesen, T. W. (2005). Strong Coupling between Surface Plasmon-Polaritons and Organic Molecules in Subwavelength Hole Arrays. *Phys. Rev. B* 71, 035424. doi:10.1103/physrevb.71.035424

Fang, H.-H., Yang, J., Ding, R., Chen, Q.-D., Wang, L., Xia, H., et al. (2010). Polarization Dependent Two-Photon Properties in an Organic Crystal. *Appl. Phys. Lett.* 97, 101101. doi:10.1063/1.3486683

Gambino, S., Mazzeo, M., Genco, A., Di Stefano, O., Savasta, S., Patanè, S., et al. (2014). Exploring Light-Matter Interaction Phenomena under Ultrastrong Coupling Regime. *ACS Photon.* 1, 1042–1048. doi:10.1021/ph500266d

Gao, B.-R., Wang, H.-Y., Hao, Y.-W., Fu, L.-M., Fang, H.-H., Jiang, Y., et al. (2010). Time-Resolved Fluorescence Study of Aggregation-Induced Emission Enhancement by Restriction of Intramolecular Charge Transfer State. *J. Phys. Chem. B* 114, 128–134. doi:10.1021/jp909063d

Hao, Y.-W., Wang, H.-Y., Jiang, Y., Chen, Q.-D., Ueno, K., Wang, W.-Q., et al. (2011). Hybrid-State Dynamics of Gold Nanorods/Dye J-Aggregates under Strong Coupling. *Angew. Chem.* 123, 7970–7974. doi:10.1002/ange.201101699

Hartland, G. V. (2011). Optical Studies of Dynamics in Noble Metal Nanostructures. *Chem. Rev.* 111, 3858–3887. doi:10.1021/cr1002547

Herz, L. M. (2016). Charge-Carrier Dynamics in Organic-Inorganic Metal Halide Perovskites. *Annu. Rev. Phys. Chem.* 67, 65–89. doi:10.1146/annurev-physchem-040215-112222

Jeon, N. J., Noh, J. H., Yang, W. S., Kim, Y. C., Ryu, S., Seo, J., et al. (2015). Compositional Engineering of Perovskite Materials for High-Performance Solar Cells. *Nature* 517, 476–480. doi:10.1038/nature14133

Juan, F., Wu, Y., Shi, B., Wang, M., Wang, M., Xu, F., et al. (2021). Plasmonic Au Nanooctahedrons Enhance Light Harvesting and Photocarrier Extraction in Perovskite Solar Cell. *ACS Appl. Energ. Mater.* 4, 3201–3209. doi:10.1021/acsaem.0c02973

Krisnanda, T., Zhang, Q., Dini, K., Giovanni, D., Liew, T. C. H., and Sum, T. C. (2021). Room Temperature Light-Mediated Long-Range Coupling of Excitons in Perovskites. *Adv. Opt. Mater.* 9, 2001835. doi:10.1002/adom.202001835

Li, J., Ueno, K., Uehara, H., Guo, J., Oshikiri, T., and Misawa, H. (2016). Dual Strong Couplings between Tpps J-Aggregates and Aluminum Plasmonic States. *J. Phys. Chem. Lett.* 7, 2786–2791. doi:10.1021/acs.jpclett.6b01224

Liu, W., Lee, B., Naylor, C. H., Ee, H.-S., Park, J., Johnson, A. T. C., et al. (2016). Strong Exciton-Plasmon Coupling in MoS2 Coupled with Plasmonic Lattice. *Nano Lett.* 16, 1262–1269. doi:10.1021/acs.nanolett.5b04588

Long, G., Sabatini, R., Saidaminov, M. I., Lakhwani, G., Rasmita, A., Liu, X., et al. (2020). Chiral-Perovskite Optoelectronics. *Nat. Rev. Mater.* 5, 423–439. doi:10.1038/s41578-020-0181-5

Ma, C., Liu, C., Huang, J., Ma, Y., Liu, Z., Li, L.-J., et al. (2019). Plasmonic-Enhanced Light Harvesting and Perovskite Solar Cell Performance Using Au Biometric Dimers with Broadband Structural Darkness. *Sol. RRL* 3, 1900138. doi:10.1002/solr.201900138

Manser, J. S., and Kamat, P. V. (2014). Band Filling with Free Charge Carriers in Organometal Halide Perovskites. *Nat. Photon* 8, 737–743. doi:10.1038/nphoton.2014.171

Mohamed Saheed, M. S., Mohamed, N. M., Mahinder Singh, B. S., and Jose, R. (2019). Surface Plasmon Assisted Electron-Hole Migration for High Photocurrent Density Generation in a Perovskite Solar Cell. *ACS Appl. Energ. Mater.* 2, 8707–8714. doi:10.1021/acsaem.9b01675

Orgiu, E., George, J., Hutchison, J. A., Devaux, E., Dayen, J. F., Doudin, B., et al. (2015). Conductivity in Organic Semiconductors Hybridized with the Vacuum Field. *Nat. Mater* 14, 1123–1129. doi:10.1038/nmat4392

Pelton, M., Aizpurua, J., and Bryant, G. (2008). Metal-nanoparticle Plasmonics. *Laser Photon. Rev.* 2, 136–159. doi:10.1002/lpor.200810003

Plumhof, J. D., Stöferle, T., Mai, L., Scherf, U., and Mahrt, R. F. (2014). Room-temperature Bose-Einstein Condensation of Cavity Exciton-Polaritons in a Polymer. *Nat. Mater* 13, 247–252. doi:10.1038/nmat3825

Privitera, A., Righetto, M., Cacialli, F., and Riede, M. K. (2021). Perspectives of Organic and Perovskite-Based Spintronics. *Adv. Opt. Mater.* 9, 2100215. doi:10.1002/adom.202100215

Qian, Z., Shan, L., Zhang, X., Liu, Q., Ma, Y., Gong, Q., et al. (2021). Spontaneous Emission in Micro- or Nanophotonic Structures. *PhotoniX* 2, 21. doi:10.1186/s43074-021-00043-z

Ren, H., Ren, X., Niu, K., Wang, S., Huang, Z., and Wu, X. (2020). Optical-Electrical-Thermal Optimization of Plasmon-Enhanced Perovskite Solar Cells. *Phys. Chem. Chem. Phys.* 22, 17068–17074. doi:10.1039/D0CP02220A

Saliba, M., Zhang, W., Burlakov, V. M., Stranks, S. D., Sun, Y., Ball, J. M., et al. (2015). Plasmonic-Induced Photon Recycling in Metal Halide Perovskite Solar Cells. *Adv. Funct. Mater.* 25, 5038–5046. doi:10.1002/adfm.201500669

Sanvitto, D., and Kéna-Cohen, S. (2016). The Road towards Polaritonic Devices. *Nat. Mater* 15, 1061–1073. doi:10.1038/nmat4668

Schwartz, T., Hutchison, J. A., Genet, C., and Ebbesen, T. W. (2011). Reversible Switching of Ultrastrong Light-Molecule Coupling. *Phys. Rev. Lett.* 106, 196405. doi:10.1103/physrevlett.106.196405

Shan, H., Yu, Y., Wang, X., Luo, Y., Zu, S., Du, B., et al. (2019). Direct Observation of Ultrafast Plasmonic Hot Electron Transfer in the Strong Coupling Regime. *Light Sci. Appl.* 8, 9. doi:10.1038/s41377-019-0121-6

Stranks, S. D., Eperon, G. E., Grancini, G., Menelaou, C., Alcocer, M. J. P., Leijtens, T., et al. (2013). Electron-Hole Diffusion Lengths Exceeding 1 Micrometer in an Organometal Trihalide Perovskite Absorber. *Science* 342, 341–344. doi:10.1126/science.1243982

Su, R., Fieramosca, A., Zhang, Q., Nguyen, H. S., Deleporte, E., Chen, Z., et al. (2021). Perovskite Semiconductors for Room-Temperature Exciton-Polaritonics. *Nat. Mater.* 20, 1315–1324. doi:10.1038/s41563-021-01035-x

Wang, H., Toma, A., Wang, H.-Y., Bozzola, A., Miele, E., Haddadpour, A., et al. (2016). The Role of Rabi Splitting Tuning in the Dynamics of Strongly Coupled J-Aggregates and Surface Plasmon Polaritons in Nanohole Arrays. *Nanoscale* 8, 13445–13453. doi:10.1039/C6NR01588C

Wang, H., Wang, H.-Y., Bozzola, A., Toma, A., Panaro, S., Raja, W., et al. (2016). Dynamics of Strong Coupling between J-Aggregates and Surface Plasmon Polaritons in Subwavelength Hole Arrays. *Adv. Funct. Mater.* 26, 6198–6205. doi:10.1002/adfm.201601452

Wang, H., Wang, H.-Y., Toma, A., Yano, T.-a., Chen, Q.-D., Xu, H.-L., et al. (2016). Dynamics of Strong Coupling between Cdse Quantum Dots and Surface Plasmon Polaritons in Subwavelength Hole Array. *J. Phys. Chem. Lett.* 7, 4648–4654. doi:10.1021/acs.jpclett.6b02059

Wang, H., Wang, H. Y., Wang, L., Chen, Q. D., Xu, H. L., Carrara, A., et al. (2017). Multimode Coherent Hybrid States: Ultrafast Investigation of Double Rabi Splitting between Surface Plasmons and Sulforhodamine 101 Dyes. *Adv. Opt. Mater.* 5, 1600857. doi:10.1002/adom.201600857

Wang, J., Xu, H., Su, R., Peng, Y., Wu, J., Liew, T. C. H., et al. (2021). Spontaneously Coherent Orbital Coupling of Counterrotating Exciton Polaritons in Annular Perovskite Microcavities. *Light Sci. Appl.* 10, 45. doi:10.1038/s41377-021-00478-w

Wang, L., Zhu, S.-J., Wang, H.-Y., Wang, Y.-F., Hao, Y.-W., Zhang, J.-H., et al. (2013). Unraveling Bright Molecule-like State and Dark Intrinsic State in

Green-Fluorescence Graphene Quantum Dots via Ultrafast Spectroscopy. *Adv. Opt. Mater.* 1, 264–271. doi:10.1002/adom.201200020

Weber, D., and Naturforsch, Z. (1978). CH3NH3SnBrxI3-x (x = 0-3), ein Sn(II)-System mit kubischer Perowskitstruktur/CH3NH3SnBrxI3-x(x = 0-3), a Sn(II)-System with Cubic Perovskite Structure. *B: J. Chem. Sci.* 33, 862–865. doi:10.1515/znb-1978-0809

Xing, G., Mathews, N., Sun, S., Lim, S. S., Lam, Y. M., Grätzel, M., et al. (2013). Long-Range Balanced Electron- and Hole-Transport Lengths in Organic-Inorganic CH 3 NH 3 PbI 3. *Science* 342, 344–347. doi:10.1126/science.1243167

Yang, W. S., Noh, J. H., Jeon, N. J., Kim, Y. C., Ryu, S., Seo, J., et al. (2015). High-Performance Photovoltaic Perovskite Layers Fabricated through Intramolecular Exchange. *Science* 348, 1234–1237. doi:10.1126/science.aaa9272

Yoo, J. J., Seo, G., Chua, M. R., Park, T. G., Lu, Y., Rotermund, F., et al. (2021). Efficient Perovskite Solar Cells via Improved Carrier Management. *Nature* 590, 587–593. doi:10.1038/s41586-021-03285-w

Zhang, Z.-Y., Chen, X., Wang, H.-Y., Xu, M., Gao, B.-R., Chen, Q.-D., et al. (2015). Elucidating the Band Structure and Free Charge Carrier Dynamics of Pure and Impurities Doped CH3NH3PbI3−xClx Perovskite Thin Films. *Phys. Chem. Chem. Phys.* 17, 30084–30089. doi:10.1039/C5CP04333F

Zhang, Z.-Y., Wang, H.-Y., Zhang, Y.-X., Hao, Y.-W., Sun, C., Zhang, Y., et al. (2016). The Role of Trap-Assisted Recombination in Luminescent Properties of Organometal Halide Ch3nh3pbbr3 Perovskite Films and Quantum Dots. *Sci. Rep.* 6, 27286. doi:10.1038/srep27286

Zhao, Y., Yang, Y., and Sun, H.-B. (2021). Nonlinear Meta-Optics towards Applications. *PhotoniX* 2, 3. doi:10.1186/s43074-021-00025-1

Zhao, Y., and Zhu, K. (2016). Organic-Inorganic Hybrid Lead Halide Perovskites for Optoelectronic and Electronic Applications. *Chem. Soc. Rev.* 45, 655–689. doi:10.1039/C4CS00458B

Conflict of Interest: The authors declare that the research was conducted in the absence of any commercial or financial relationships that could be construed as a potential conflict of interest.

Publisher's Note: All claims expressed in this article are solely those of the authors and do not necessarily represent those of their affiliated organizations, or those of the publisher, the editors, and the reviewers. Any product that may be evaluated in this article, or claim that may be made by its manufacturer, is not guaranteed or endorsed by the publisher.

frontiers in Chemistry

ORIGINAL RESEARCH
published: 25 January 2022
doi: 10.3389/fchem.2022.847972

Epitaxial Growth of Bi_2Se_3 Infrared Transparent Conductive Film and Heterojunction Diode by Molecular Beam Epitaxy

Ya-Hui Chuai[1], *Chao Zhu*[1], *Dan Yue*[1] *and Yu Bai*[2]*

[1]Institute of Physics, Changchun University of Science and Technology, Changchun, China, [2]College of Electronical and Information Engineering, Changchun University of Science and Technology, Changchun, China

Epitaxial *n*-type infrared transparent conductive Bi_2Se_3 thin film was cultivated by molecular beam epitaxy (MBE) method on Al_2O_3 (001) substrate. The orientation between Bi_2Se_3 and the substrate is $Bi_2Se_3(001)//Al_2O_3(1\ \bar{2}\ 10)$. Conducting mechanism ensued the small-polaron hopping mechanism, with an activation energy of 34 meV. The film demonstrates conductivity of *n*-type, and the resistivity is 7×10^{-4} Ωcm at room temperature. The Film exhibits an excellent carrier mobility of 1,015 cm^2/Vs at room temperature and retains optical transparency in the near-infrared (>70%) and far-infrared (>85%) ranges. To the best of our knowledge, the Bi_2Se_3 film yields the best result in the realm of *n*-type Infrared transparent conductive thin films generated through either physical or chemical methods. To demonstrate the application of such films, we produced N-Bi_2Se_3/P-$CuScO_2$ heterojunction diode device, the ~3.3 V threshold voltage of which conformed fairly well with the $CuScO_2$ bandgap value. The high optical transparency and conductivity of Bi_2Se_3 film make it very promising for optoelectronic applications, where a wide wavelength range from near-infrared to far-infrared is required.

Keywords: thin film, Bi2Se3, optical property, electronic property, N-Bi2Se3/P-CuScO2 heterojunction

OPEN ACCESS

Edited by:
Yue-Feng Liu,
Jilin University, China

Reviewed by:
Ziqi Yan,
Shanghai Maritime University, China
Ziying Wang,
Hebei University of Technology, China

***Correspondence:**
Yu Bai
baiyu@cust.edu.cn

Specialty section:
This article was submitted to Nanoscience, a section of the journal Frontiers in Chemistry

Received: *03 January 2022*
Accepted: *10 January 2022*
Published: *25 January 2022*

Citation:
Chuai Y-H, Zhu C, Yue D and Bai Y (2022) Epitaxial Growth of Bi_2Se_3 Infrared Transparent Conductive Film and Heterojunction Diode by Molecular Beam Epitaxy. Front. Chem. 10:847972. doi: 10.3389/fchem.2022.847972

INTRODUCTION

Infrared transparent conductive film is widely used in military and civilian infrared detectors, such as Infrared guidance, Infrared imaging, Infrared detection and Infrared methane/CO detector etc. (Zhang et al., 2021), because of its remarkable optical transmittance in the Infrared light range and strong electromagnetic shielding ability. However, the traditional wide band gap oxide transparent conductive film such as ITO (Sn-doped In_2O_3) and AZO (Al-doped ZnO) (Jain et al., 2020; Khan et al., 2020), can only transmit visible light and near-infrared light, and has low transmittance in the mid- and far-infrared bands. At present, infrared detectors are developing in the direction of all-weather high sensitivity, such as dual-use day and night, wider infrared spectrum detection range (mid-to-far infrared band), and adaptability to complex electromagnetic interference signal environments (Zhang et al., 2020; Sizov et al., 2021). Therefore, it is particularly important to develop a wide-band infrared transparent conductive film.

Up to now, a few infrared transparent conductive films have been developed by researchers. T. Chen from Yale University reported a doped In_2O_3-based infrared transparent conductive film for the first time, which has a transmittance of 40% in the 2.5–12 μm band and a resistance of 30 Ω/□ (Chen et al., 1983). N. Lipkin prepared In_xO_y thin films by using reactive ion evaporation

and controlled oxygen defects, achieving a mid- and far-infrared transmittance of up to 72%, but the thin-film resistance reached 40 Ω/□ (Lipkin et al., 2001). E. Aydin reduced the resistance of the In_2O_3-based film to 18 Ω/□ through Zr doping by magnetron sputtering, while the transmission band is blue-shifted to the near-infrared region of 0.25–2.5 μm (Aydin et al., 2019). L. Johnson prepared $Cu_xAl_yO_z$ and $Cu_xCr_yO_z$ amorphous films that deviate from the stoichiometric ratio by asymmetric bipolar pulsed DC magnetron sputtering method. The former has 70% transmittance in the mid-infrared band and the sheet resistance is 26 Ω/□, and the latter has a transmittance of 55% in the far infrared band (Johnson and Moran, 2001). Jicai Han prepared Ru-doped Y_2O_3 film on a ZnS substrate by plasma bombardment assisted magnetron sputtering, the transmittance of the film is 65% in the 3.5–12 μm infrared band, and the resistance is 3.36×10^2 Ω/□ (Yang et al., 2013). The author has also developed a series of P-type doped $CuFeO_2$ and $CuScO_2$ based infrared transparent conductive films. The highest transmittance in the 0.78–5 μm near mid-infrared band is 90%, and the lowest resistivity is 2.25×10^3 Ω/□ (Chuai et al., 2015a; Chuai et al., 2015b; Chuai et al., 2016a; Chuai et al., 2016b; Chuai et al., 2019). In summary, the classic design strategy of infrared transparent conductive film is mainly to prepare the wide band gap semiconductor oxide by element doping and stoichiometric deviation film preparation, and adjust the composition to improve the infrared transmittance and conductivity of the film at the same time. However, doping tends to cause a blue shift in the infrared transmission band of the oxide, and the film that deviates from the stoichiometric ratio has poor crystallinity and high resistance. Therefore, wide band gap semiconductor oxide is not an ideal mid- and far-infrared transparent conductive material.

Bismuth chalcogenides materials Bi_2Se_3 has gained attention due to its unique physical properties as a three-dimensional topological insulator, and potential applications in spintronics, optoelectronics and quantum computing (Xia et al., 2009; Qi and Zhang, 2011; Jash et al., 2020). Bi_2Se_3 has a body state (with an insulator band gap) and a surface state (without a band gap). The surface state can exist stably because of the protection of the time reversal symmetry. Therefore, it is externally conductive on the surface and insulated on the inside. Bi_2Se_3 is a typical V-VI compound semiconductor, belonging to the hexagonal crystal system, space group D5 3d (R3m), with a narrow band gap energy about 0.5 eV (Zhang et al., 2009). Bi_2Se_3 has a layered structure, each unit contains 5 atomic layers, oriented along the *Z* axis, and the stacking sequence is Se1-Bi1-Se2-Bi1′-Se1′, defined as 1 Quintuple Layer (QL), each QL The thickness is about 0.995 nm. There is a strong chemical bond between the two atomic layers inside a QL, while the bond between QLs is weak ---van der Waals force. The basic feature of the Bi_2Se_3 three-dimensional topological insulator is that there are four time-reversed symmetry points in the Brillouin zone of its surface state. Kramers degeneracy occurs at these points, thus forming Dirac cones. The apex of the Dirac cone is called the Dirac point, and the dispersion relationship between energy and momentum near the apex is linear (not quadratic). Due to the spin-coupling effect, the spin direction of the surface state is always perpendicular to the direction of momentum, so that electrons travel on the surface with low loss (or lossless) at a speed similar to photons (surface mobility $\mu_s \approx 6000\ cm^2/Vs$), the inside is in an insulator state (Hasan and Kane, 2010). Therefore, the band gap of Bi_2Se_3 yields a low free-carrier plasma oscillation cut-off frequency, and high transparency in the infrared (IR) range. Excellent surface mobility makes it also have high electrical conductivity which make it an ideal wide-band high infrared transmittance and conductivity film.

Though Bi_2Se_3 film can be fabricated by magnetron sputtering, chemical vapor deposition, and electrodeposition method. But still unable to prepare Bi_2Se_3 film with stoichiometric ratio. Because selenium (Se) is highly volatile, Bi_2Se_3 tends to form Se vacancies which act as donors to give a rather high carrier concentration and low carrier mobility (Richardella et al., 2010; Liu et al., 2015). During thin-film growth, when Se-atoms are lost to a greater extent at elevated substrate temperatures, pure phase Bi_2Se_3 film can barely survive, and the films obtained might present impure phases or turn into another phase all together. The high carrier concentration will blue shift the infrared transmission band, which will shorten the infrared transmission area. The low carrier mobility will cause the resistivity of the film to decrease. To counter this problem and achieve stoichiometric Bi_2Se_3 single crystal thin film with greater quality, we employed molecular beam epitaxy (MBE) to make the single crystal film at standard stoichiometric ratios.

In this letter, we use molecular beam epitaxy (MBE) to prepare high-quality Bi_2Se_3 single crystal thin film on Al_2O_3 (001) substrate. The main advantages of MBE are as follows: The film can grow at a low growth temperature and a slow growth rate, and it is easier to fine-tune the beam intensity, and timely adjust the composition of the film according to the change of the source, and single crystal films with a thickness of dozens of atomic layers can be prepared. Thus, the Se vacancy defect density in the thin film is reduced, and the body electron concentration is reduced. As far as we know, this is the first time that the infrared transmission characteristics of Bi_2Se_3 film is reported. We expect that the present results are greatly helpful for the practical usage of Bi_2Se_3 as novel wide band infrared transparent conductive film.

EXPERIMENT AND CALCULATION

Preparation of Bi_2Se_3 Thin Film

Molecular beam epitaxy (MBE) was employed to prepare Bi_2Se_3 thin film on Al_2O_3 (001) substrate. Before film growth, the substrate was cleaned in UHV at 300°C for 15 min. Bi was sourced from high purity bismuth (Bi, 99.999%), and Se from selenium (Se, 99.999%). In order to obtain Bi and Se vapour, Bi and Se were put into the effusion tank for co-evaporation. The beam flux ratio of Bi and Se was 1:20, and the growth rate was ~0.4 quintuple layer (QL) per minute. The total pressure was kept constant at 30 Pa. To enhance the crystalline property of the film, we adopted a two-step growth method. This method can increase the nucleation density of crystal grains on the substrate without causing tex-turing of the film (Park et al., 2016). In the first step, the substrate was heated to 170°C, and then deposited the initial

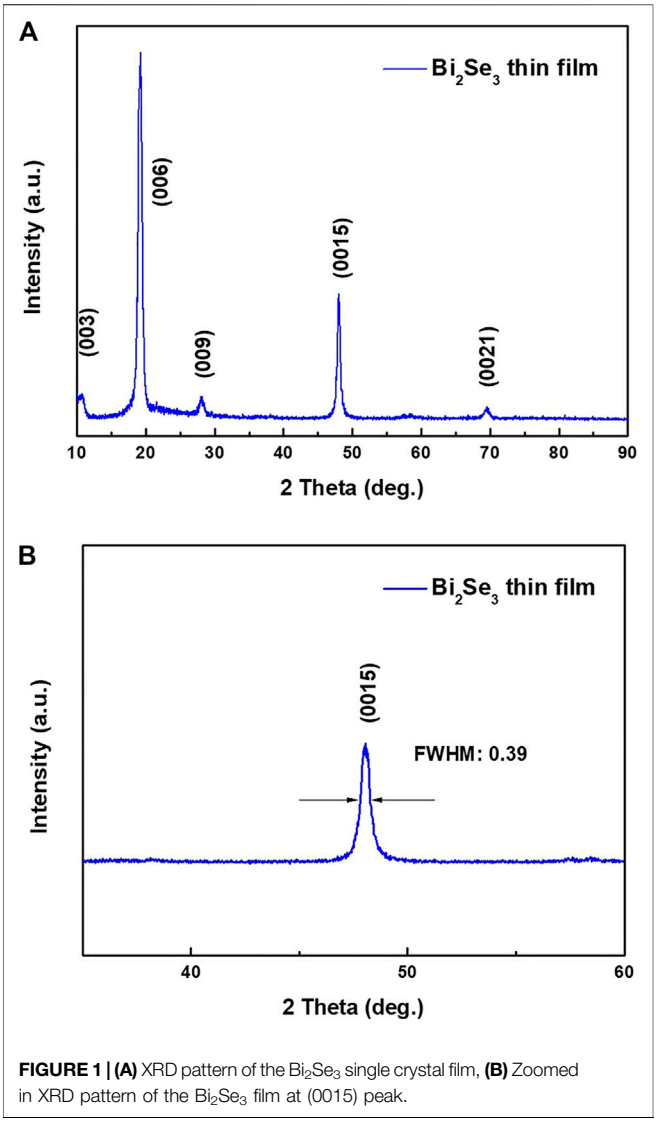

FIGURE 1 | (A) XRD pattern of the Bi_2Se_3 single crystal film, **(B)** Zoomed in XRD pattern of the Bi_2Se_3 film at (0015) peak.

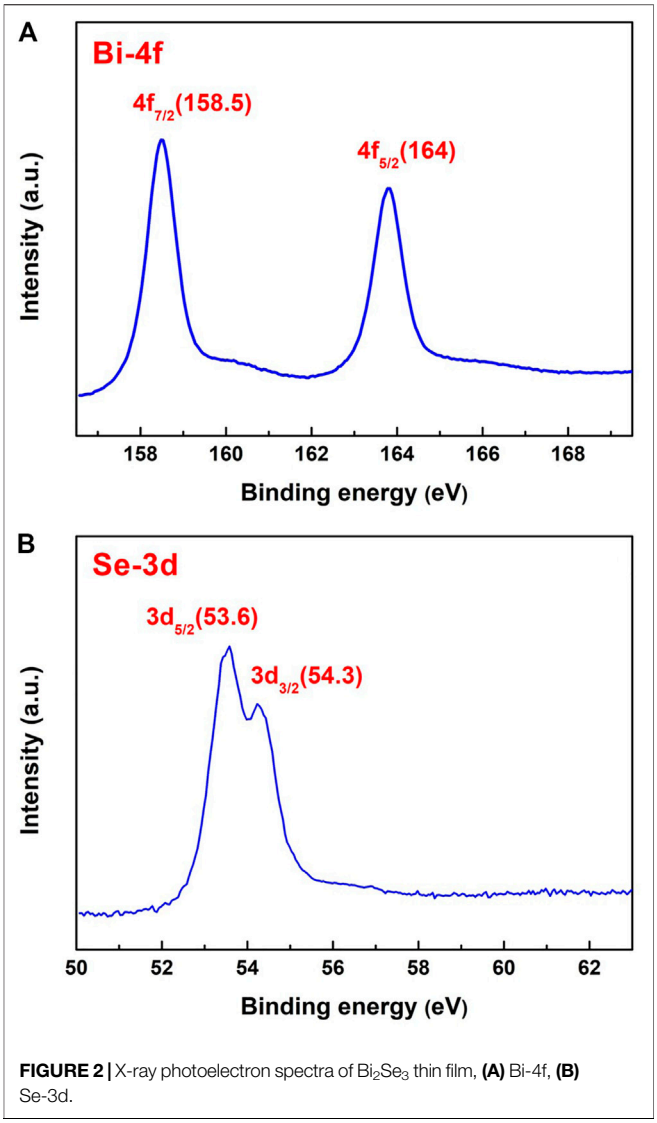

FIGURE 2 | X-ray photoelectron spectra of Bi_2Se_3 thin film, **(A)** Bi-4f, **(B)** Se-3d.

3–4 QLs of Bi_2Se_3 thin film. Then the obtained ultra-thin film was annealed at 300°C in H_2 atmosphere for 30 min. In the second step, the substrate temperature was raised to 350°C at a rate of 4°C per minute. Then continue to grow to the predetermined thickness of the film. To assess the stability and antioxidant capacity of the Bi_2Se_3 film, all the tests were carried out after 2 weeks of air exposure.

Characterization and Measurement

Conventional X-ray diffraction (XRD) technique was employed to represent the crystallographic orientation of the Bi_2Se_3 film on a Bruker D8 Advance X, Pert diffractometer (Cu-Ka: $\lambda = 1.540$ A). A scanning speed of 8° per min was chosen, ranging from 10° to 90°. X-ray photoelectron spectroscopy (XPS, ESCALAB 250) was used to determine the valence states of the elements. To detect the surface morphology of the film, feld emission scanning electron microscope (FE-SEM JSM-7500F) and atomic force microscope instrument (AFM Veeco DI-3100) were used. To further investigate the atomic arrangement of the film, a high-resolution transmission electron microscope (HRTEM, TEM 2010F) was used. To measure the optical properties of the film, such as transmission and absorption, a UV-vis-NIR spectrophotometer (Shimazu UV-3600PC) was used working in the wavelength range of 250–3,000 nm, plus a Fourier transform infrared spectrometer (FTIR) working in the range of 2.5–12 μm. To examine the electrical properties, a Hall-effect measurement system (ACCENT HL55OOPC) was introduced, the test range was between 90 and 300 K.

RESULTS AND DISCUSSION

Structural and Chemical Valence Characteristics

Figure 1A shows the XRD patterns of the resulting Bi_2Se_3 film. The only peaks observed in the scanned range are clearly defined and high intensity reflections [(003), (006), (009), (0015), (0021)]. The appearance of only (001) diffraction peaks indicates that the

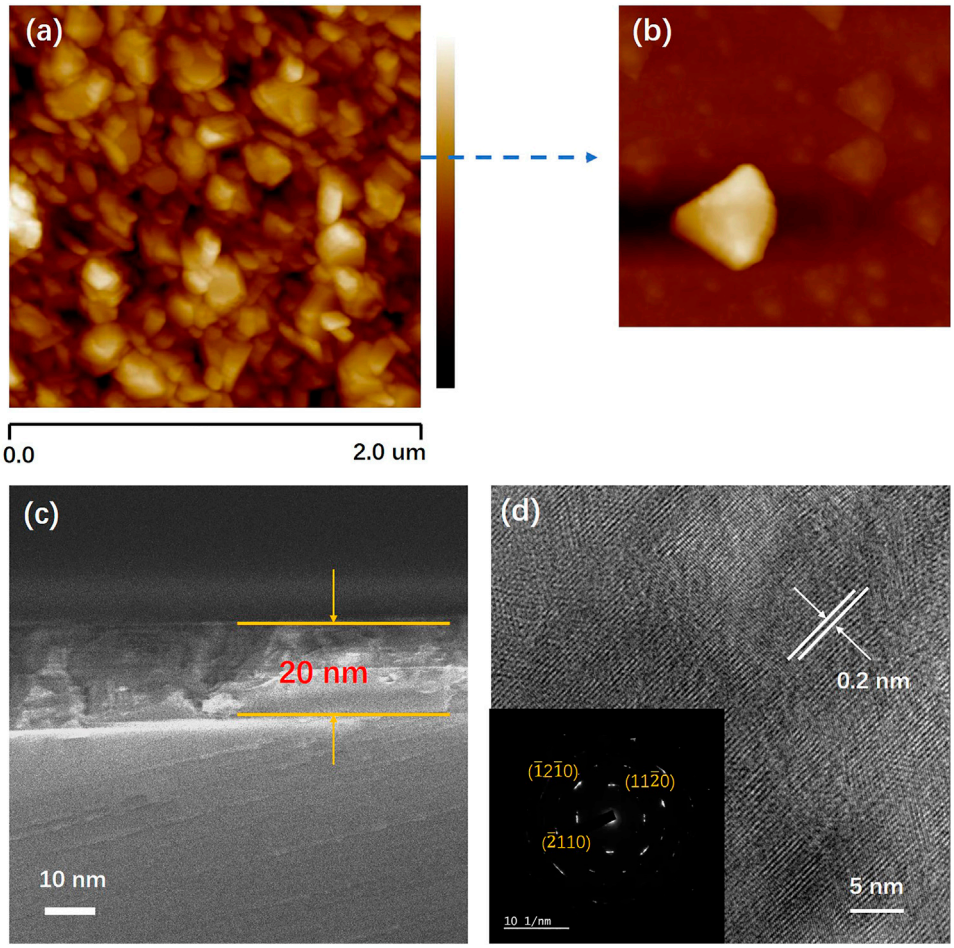

FIGURE 3 | (A) 2 μm × 2 μm atomic force microscope images of the Bi_2Se_3 thin film, **(B)** Enlarged image of Bi_2Se_3 grain, **(C)** Cross-sectional SEM image of Bi_2Se_3 (001) thin film close to the interface of the substrate, **(D)** Surface HRTEM image and SAED pattern of Bi_2Se_3 thin film.

film is preferentially oriented along the *c*-axis perpendicular to the substrate surface. Further, the layered structures of Bi and Se atoms in the form of Se(1)-Bi-Se (2)-Bi-Se(1) are normal to the *c*-axis. The width of the half-maximum (FWHM) of the (0015) rocking curve (**Figure 1B**) is about 0.39°, indicating good crystallinity of the film. From the d-spacing's of the (0015) peak, the lattice parameters of the Bi_2Se_3 film were determined as $a = b = 4.138$ (3) Å and $c = 28.666$ (2) Å, which conforms well to the reported standard card data file (No. 01-089-2008).

Figure 2 shows the X-ray photoelectron spectra (XPS) of Bi-4f and Se-3d of Bi_2Se_3 thin film. In the Bi-4f spectrum, two distinct peaks Bi-$4f_{7/2}$ = 158.5 eV and Bi-$4f_{5/2}$ = 164 eV are observed, both are intense and with binding energy. This is consistent with the Bi_2O_3 (Bi^{3+}) phase, which leads to the conclusion that the Bi ions are in the tervalent state. **Figure 2B** reveals two adjacent sharp peaks in the Se-$3d_{5/2}$ spectrum at 53.6 and 54.3 eV on $3d_{3/2}$ peaks, respectively. Compare with the X-ray Photoelectron Spectroscopy Database of the National Institute of Standards and Technology (NIST), and it can be inferred that the valence state of the Se ions is −2. XPS analysis reveals the valence states of Bi and Se to be +3 and −2 in the Bi_2Se_3 film, which is conducive to the formation of a pure Bi_2Se_3 phase. The atomic content of Bi and Se on the surface of the film is 0.47 and 0.53 respectively. The deviation of the surface stoichiometric ratio is due to the lower vapor pressure of the Se element, so Se is prone to volatilization during the growth process, especially on the surface of the film.

Morphologies and Microstructure of the Bi_2Se_3 Film

Figure 3A shows the film's surface morphology atomic force microscope (AFM) image. It shows that the nano-particles is uniform and arrange orderly with an average size of 120 nm. As shown in **Figure 3B**, a higher-magnification view of the surface revealed triangular crystal facets and terrace structures of the Bi_2Se_3 thin film. The root-mean-square (RMS) roughness value for the 2 μm × 2 μm area is 0.9 nm. The thickness of Bi_2Se_3 film is shown in **Figure 3C**. The image indicates that the Bi_2Se_3 film thickness is uniform and tightly bonded to the substrate. No lattice defects such as threading dislocations are observed at the interface. In **Figure 3D**, the interplanar d spacing between lattice fringes is measured to be 0.2 nm, in conformance with the

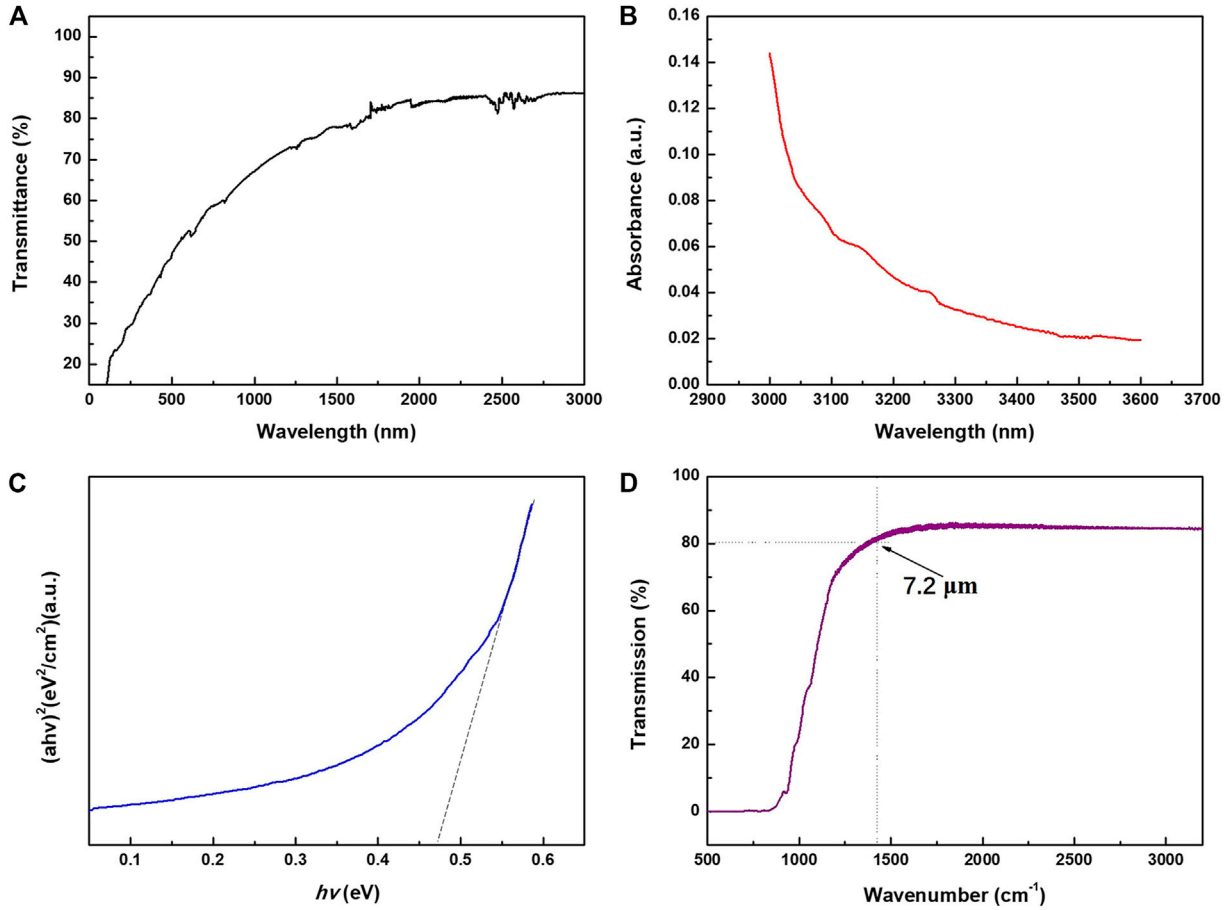

FIGURE 4 | (A) Optical transmission spectrum of Bi_2Se_3 thin film, **(B)** Absorption spectrum of Bi_2Se_3 thin film, **(C)** $(ahv)^2$ versus hv plot, and **(D)** Infrared transmission spectra of Bi_2Se_3 thin film.

d-spacing of the (11 $\bar{2}$ 0) planes in the pdf file No. 01-089- 2008. Selected area electron diffraction pattern (SAED) of Bi_2Se_3 film shows three different diffraction spacings ([11 $\bar{2}$ 0] [$\bar{1}$ 2 $\bar{1}$ 0] and [$\bar{2}$ 110]) indexed as a 6-fold symmetric [001] zone axis pattern, conforming to the layered structure along the *c*-axis orientation. The above conclusions indicate that the Bi_2Se_3 film is a single crystal film, and it preferentially grows along the *c*-axis direction.

Optical Properties of Bi_2Se_3 Thin Film

Figure 4A gives the optical transmission spectrum of the Bi_2Se_3 film in visible light-near infrared band. All the measured data have been deducted from the influence of the substrate. The film exhibits a transmittance of 50–70% in the entire visible light band, and a higher transmittance of 70–85% in the near-infrared band. **Figure 4B** gives the absorption spectrum of Bi_2Se_3 thin film. At 3,000 nm wavelength stands a sharp absorption edge. It is the fundamental absorption which energy corresponds to the energy required for the electron to transition from the top of the valence band to the bottom of the conduction band. Therefore, this absorption edge has been widely adopted to determine the forbidden band width. The optical absorption coefficient (a) and photon energy (hv) has a relation as such:

$$\alpha h\nu = A\left(h\nu - E_g\right)^m \quad (1)$$

Where E_g is the optical bandgap of the materials, A is a constant, and m hinges on the type of transition: m = 1/2 when band transition is indirect, and m = 2 when band transition is direct (Deng et al., 2013). **Figure 4C** delineates the linear relationship between $(ahv)^2$ and hv, it indicates that the Bi_2Se_3 thin film has a direct bandgap structure. Extend the straight portion of the curve and the bandgap can be estimated as 0.47 eV. This value is a bit smaller than previously reported in the literature of 0.5 eV. Generally, the relationship between the forbidden band width and the carrier concentration can be expressed as such a linear relationship $\Delta E = \Delta E\ (0) - kn^{1/3}$, where n is carrier concentration. During the growth of Bi_2Se_3 thin film, high-temperature annealing will cause the absence of Se atoms, which will create Se vacancies in the film, forming a natural *n*-type semiconductor. The bulk carrier concentration n increases, so the actual measured band gap is lower than the theoretical value. **Figure 4D** shows the infrared transmission spectrum of the Bi_2Se_3 thin film. The total transmittance of Bi_2Se_3 film in the wavelength range of 3.2 (3,125 wavenumber) −7.2 (1,400 wavenumber) μm is as high

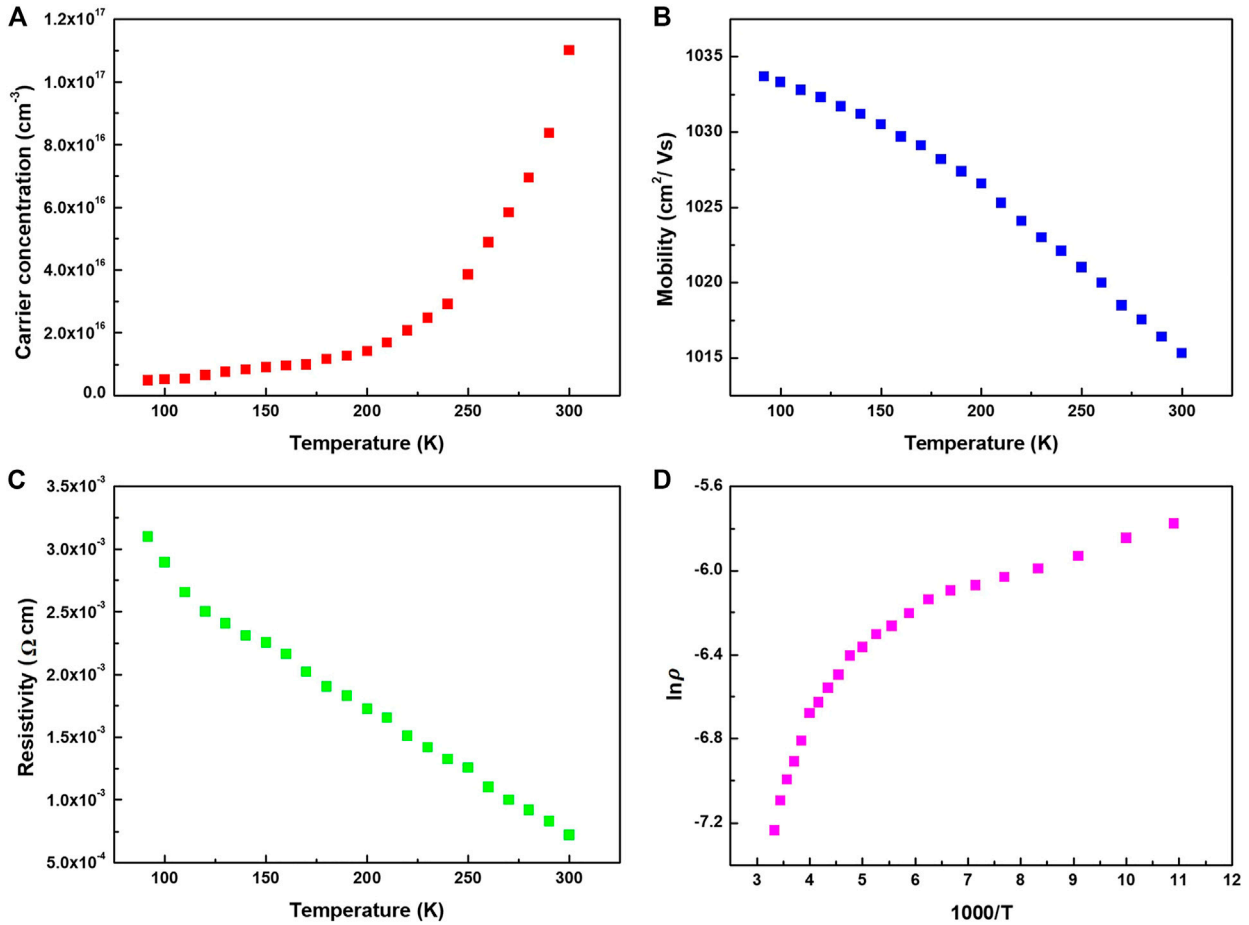

FIGURE 5 | (A) Temperature dependence of: **(A)** Carrier concentration, **(B)** Hall mobility, **(C)** electrical resistivity **(D)** lnρ plotted as function of 1,000/T for the Bi_2Se_3 thin film.

as 85% with no obvious characteristic absorption peak. The high transmittance (or low absorptivity), especially in the infrared band, is primarily attributed to the free carrier plasma edge around the far-infrared frequency. Due to the collective oscillation of conduction band electrons, called plasma oscillation, the transmittance of the film decreases at 7.2 μm suddenly. According to Drude's free electron theory, the plasma oscillation frequency ω_p of the material determines the upper limit of the transmission wavelength. When the incident light frequency $\omega < \omega_p$, the film exhibits strong reflectivity; when $\omega > \omega_p$, the film exhibits transmittance. Thus, ω_p sets the low cutoff frequency of the transmission band.

Electrical Characteristics of Bi_2Se_3 Thin Film

In order to further analyze the electrical characteristics and transmission characteristics of Bi_2Se_3 thin films. Multiple temperature Hall effect measurement were carried out for the low temperature range. The influences of temperature on the resistivity, carrier density and mobility were investigated. As well as high transmittance in infrared band, the Bi_2Se_3 thin film also exhibits excellent electrical properties. The graphics of temperature dependent carrier concentration, Hall mobility and resistivity are shown in **Figures 5A–C**. The electron concentration of the film increases as the temperature rises, and the bulk electron concentration of the film at room temperature is about $1.15\times10^{17}cm^{-3}$. The Hall mobility decreases as the temperature rises, and the Hall mobility at room temperature is as high as 1,015 cm^2/Vs, which is two orders of magnitude higher than the copper-iron ore series *p*-type infrared transparent conductive film we prepared previously. The reason for the high mobility is that Bi_2Se_3 belongs to a three-dimensional topological insulator structure. The basic feature of the structure is that there are four time-reversed symmetry points in the Brillouin zone of its surface state with Kramers degenerate phenomenon, which form the Dirac Cone. The apex of the Dirac cone is called the Dirac point, and the dispersion relationship between energy and momentum near the apex is linear. Due to the spin-coupling effect, the spin direction of the surface state is always perpendicular to the direction of momentum, so that electrons travel on the surface with low loss (or lossless) at a speed similar to the photon. The Hall coefficient of Bi_2Se_3 film is $-7.8\ cm^3C^{-1}$ at room temperature, which

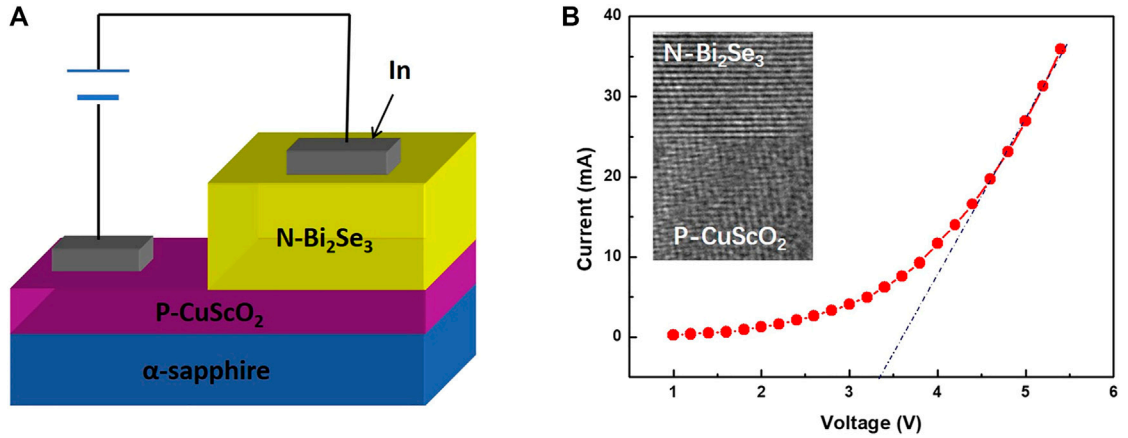

FIGURE 6 | (A) Schematic structure of N-Bi_2Se_3/P-$CuScO_2$ heterojunction diode device. **(B)** Current (*I*)—voltage (*V*) characteristics of N-Bi_2Se_3/P-$CuScO_2$ diode device. The inset in **(B)** shows the cross-sectional HREM image of N-Bi_2Se_3/P-$CuScO_2$ interface.

indicates characteristic of n-type conduction. The room temperature conductivity of the film is 7×10^{-4} Ωcm. As shown in **Figure 5D**, Bi_2Se_3 film shows thermal activation behavior at room temperature, because the plots of $\ln\rho$ ~1,000/T show a linear relation. The conductivity can be expressed by $^1/_\rho = Aexp[-E_a/(k_BT)]$, where A is constant, Ea is the thermal activation energy, and kB is Boltzmann constant. As temperature increases, electrical conductivity of the material increases, confirmative of the semiconductor nature of Bi_2Se_3 thin film in our study. The estimated E_a is 34 meV, which is less than 10% of the optical bandgap ($E_g \approx 0.47$ eV) of Bi_2Se_3, indicating the electronic transport is thermally activated by a donor in the conduction band.

Preparation and Measurement of Infrared Transparent Diode Device

In order demonstrate the application of our thin film, we made N-Bi_2Se_3/P-$CuScO_2$ infrared transparent heterojunction diode, the schematic diagram of which is shown in **Figure 6A**. The schematic diagram of this diode is shown in **Figure 6A**. First, we use the polymer-assisted deposition method to grow the $CuScO_2$ film with a thickness of about 200 nm on a sapphire substrate, and then deposit a layer of Bi_2Se_3 thin film with a thickness of 150 nm by MBE. Finally, we evaporate In on the surface of the device as the electrode. **Figure 6B** shows the *I–V* curve of the heterojunction diode. It can be easily found the rectifying characteristic through the curve, accompanied by a threshold voltage of 3.3 V, which is consistent with the forbidden band width of $CuScO_2$ (3.3–3.5 eV). Thus, hetero-epitaxial growth at the $CuScO_2$ (lower part) and Bi_2Se_3 (upper part) interface is demonstrated.

CONCLUSION

In this paper, we used molecular beam deposition (MBE) method to epitaxial grow Bi_2Se_3 thin film, which was then incorporated into N-Bi_2Se_3/P-$CuScO_2$ infrared transparent heterojunction diodes. The unique growth and processing design of MBE underpins the high quality, epitaxial growth of the film. The Bi_2Se_3 thin film thus produced displayed remarkable optical transparency in IR region, and great *n*-type electrical conductivity. The $CuScO_2$ film-based infrared transparent heterojunction diode has an abrupt interface, exhibits rectifying I—V characteristics with the threshold voltage of ~3.3V. The results prove that the Bi_2Se_3 film has excellent optical and electrical properties in the wide-band infrared range. Such photoelectric properties make it a great candidate for window electrodes of infrared detectors, as well as other scenarios in the wide infrared wavelength range.

DATA AVAILABILITY STATEMENT

The original contributions presented in the study are included in the article/Supplementary Material, further inquiries can be directed to the corresponding authors.

AUTHOR CONTRIBUTIONS

All authors listed have made a substantial, direct, and intellectual contribution to the work and approved it for publication.

ACKNOWLEDGMENTS

Authors would like to express their gratitude to the Scientific Research Project of Jilin Provincial Department of Education (20190545KJ), National Natural Science Foundation of China (NSFC) (61905023); The Fourth Lifting Project of Young Science and Technology Talents in Jilin Province (QT202026); Natural Science Foundation of Jilin Province Science and Technology Department (20210101182JC).

REFERENCES

Aydin, E., De Bastiani, M., Yang, X., Sajjad, M., Aljamaan, F., Smirnov, Y., et al. (2019). Zr-Doped Indium Oxide (IZRO) Transparent Electrodes for Perovskite-Based Tandem Solar Cells. *Adv. Funct. Mater.* 29, 1901741. doi:10.1002/adfm.201901741

Chen, T. c., Ma, T. p., and Barker, R. C. (1983). Infrared Transparent and Electrically Conductive Thin Film of In2O3. *Appl. Phys. Lett.* 43 (10), 901–903. doi:10.1063/1.94199

Chuai, Y.-H., Hu, B., Li, Y.-D., Shen, H.-Z., Zheng, C.-T., and Wang, Y.-D. (2015). Effect of Sn Substitution on the Structure, Morphology and Photoelectricity Properties of High C-axis Oriented CuFe1−xSnxO2 Thin Film. *J. Alloys Compd.* 627, 299–306. doi:10.1016/j.jallcom.2014.12.118

Chuai, Y.-H., Shen, H.-Z., Li, Y.-D., Hu, B., Zhang, Y., Zheng, C.-T., et al. (2015). Epitaxial Growth of Highly Infrared-Transparent and Conductive CuScO2 Thin Film by Polymer-Assisted-Deposition Method. *RSC Adv.* 5, 49301–49307. doi:10.1039/c5ra07743e

Chuai, Y.-H., Wang, X., Shen, H.-Z., Li, Y.-D., Zheng, C.-T., and Wang, Y.-D. (2016). Effects of Zn-Doping on Structure and Electrical Properties of P-type Conductive CuCr1−x Zn X O2 Delafossite Oxide. *J. Mater. Sci.* 51, 3592–3599. doi:10.1007/s10853-015-9679-4

Chuai, Y. H., Bai, Y., Zheng, C. T., Liu, C. Y., Wang, X., and Yue, D. (2019). Chemical Modulation of Valence Band and Photoelectric Properties of Epitaxial P-type Infrared Transparent Conducting $CuScO_2$ Thin Films. *Mater. Res. Express* 6, 126460. doi:10.1088/2053-1591/ab78c8

Chuai, Y., Wang, X., Zheng, C., Zhang, Y., Shen, H., and Wang, Y. (2016). Highly Infrared-Transparent and P-type Conductive CuSc1−xSnxO2 Thin Films and a P-CuScO2:Sn/n-ZnO Heterojunction Fabricated by the Polymer-Assisted Deposition Method. *RSC Adv.* 6, 31726–31731. doi:10.1039/c6ra00919k

Deng, Z., Fang, X., Wu, S., Zhao, Y., Dong, W., Shao, J., et al. (2013). Structure and Optoelectronic Properties of Mg-Doped CuFeO2 Thin Films Prepared by Sol-Gel Method. *J. Alloys Compd.* 577, 658–662. doi:10.1016/j.jallcom.2013.06.155

Hasan, M. Z., and Kane, C. L. (2010). Colloquium: Topological Insulators. *Rev. Mod. Phys.* 82, 3045–3067. doi:10.1103/revmodphys.82.3045

Jain, P., Nakabayashi, Y., Haga, K.-i., and Tokumitsu, E. (2020). Electrical Properties of In2O3 and ITO Thin Films Formed by Solution Process Using In(acac)3 Precursors. *Jpn. J. Appl. Phys.* 59, SCCB12. doi:10.7567/1347-4065/ab4a89

Jash, A., Ghosh, S., Bharathi, A., and Banerjee, S. S. (2020). Coupling-decoupling of Conducting Topological Surface States in Thick Bi2Se3 Single Crystals. *Phys. Rev. B* 101, 165119. doi:10.1103/physrevb.101.165119

Johnson, L., and Moran, M. (2001). "Infrared Transparent Conductive Oxides," in *SPIE Proceedings,Window and Dome Technologies and Materials VII*,289 4375.

Khan, A., Rahman, F., Nongjai, R., and Asokan, K. (2020). Structural, Optical and Electrical Transport Properties of Sn Doped In2O3. *Solid State. Sci.* 109, 106436. doi:10.1016/j.solidstatesciences.2020.106436

Lipkin, N., Zipin, H., Yadin, Y., Klein, Z., Dagan, L., and Marcovitch, O. (2001). "Dual Band Transparent Conductive Coating," in *Proc. SPIE 4375, Window and Dome Technologies and Materials VII*, 315 4375. doi:10.1117/12.439190

Liu, F., Liu, M., Liu, A., Yang, C., Chen, C., Zhang, C., et al. (2015). The Effect of Temperature on Bi2Se3 Nanostructures Synthesized *via* Chemical Vapor Deposition. *J. Mater. Sci. Mater. Electron.* 26 (6), 3881–3886. doi:10.1007/s10854-015-2915-5

Park, J. Y., Lee, G.-H., Jo, J., Cheng, A. K., Yoon, H., Watanabe, K., et al. (2016). Molecular Beam Epitaxial Growth and Electronic Transport Properties of High Quality Topological Insulator Bi 2 Se 3 Thin Films on Hexagonal boron Nitride. *2d Mater.* 3, 035029. doi:10.1088/2053-1583/3/3/035029

Qi, X.-L., and Zhang, S.-C. (2011). Topological Insulators and Superconductors. *Rev. Mod. Phys.* 83, 1057–1110. doi:10.1103/revmodphys.83.1057

Richardella, A., Zhang, D. M., Lee, J. S., Koser, A., Rench, D. W., Yeats, A. L., et al. (2010). Coherent Heteroepitaxy of Bi2Se3 on GaAs (111)B. *Appl. Phys. Lett.* 97, 262104. doi:10.1063/1.3532845

Sizov, F., Vuichyk, M., Svezhentsova, K., Tsybrii, Z., Stariy, S., and Smolii, M. (2021). CdTe Thin Films as Protective Surface Passivation to HgCdTe Layers for the IR and THz Detectors. *Mater. Sci. Semiconductor Process.* 124, 105577. doi:10.1016/j.mssp.2020.105577

Xia, Y., Qian, D., Hsieh, D., Wray, L., Pal, A., Lin, H., et al. (2009). Observation of a Large-gap Topological-Insulator Class with a Single Dirac Cone on the Surface. *Nat. Phys* 5 (6), 398–402. doi:10.1038/nphys1274

Yang, L., Han, J., Zhu, J., Zhu, Y., and Schlaberg, H. I. (2013). Chemical Bonding and Optoelectrical Properties of Ruthenium Doped Yttrium Oxide Thin Films. *Mater. Res. Bull.* 48, 4486–4490. doi:10.1016/j.materresbull.2013.07.039

Zhang, H., Liu, C.-X., Qi, X.-L., Dai, X., Fang, Z., and Zhang, S.-C. (2009). Topological Insulators in Bi2Se3, Bi2Te3 and Sb2Te3 with a Single Dirac Cone on the Surface. *Nat. Phys* 5 (6), 438–442. doi:10.1038/nphys1270

Zhang, L., Wang, B., Zhou, Y., Wang, C., Chen, X., and Zhang, H. (2020). Synthesis Techniques, Optoelectronic Properties, and Broadband Photodetection of Thin-Film Black Phosphorus. *Adv. Opt. Mater.* 8, 2000045. doi:10.1002/adom.202000045

Zhang, W., Chen, H., and Ding, R. (2021). Readout Integrated Circuit with Multi-Mode Background Suppression for Long Wavelength Infrared Focal Plane Arrays. *Opt. Quant. Electron.* 53, 4. doi:10.1007/s11082-020-02644-7

Conflict of Interest: The authors declare that the research was conducted in the absence of any commercial or financial relationships that could be construed as a potential conflict of interest.

frontiers in Chemistry

MINI REVIEW
published: 10 March 2022
doi: 10.3389/fchem.2022.864186

Recent Advances in Silver Nanowires Electrodes for Flexible Organic/Perovskite Light-Emitting Diodes

Shuping Hou[1], Jie Liu[1], Feipeng Shi[1], Guo-Xu Zhao[2,3], Jia-Wei Tan[2,3] and Gong Wang[2,3]**

[1]School of Information Engineering, Tianjin University of Commerce, Tianjin, China, [2]Center for Advanced Laser Technology, Hebei University of Technology, Tianjin, China, [3]Hebei Key Laboratory of Advanced Laser Technology and Equipment, Tianjin, China

Flexible organic light-emitting diodes and perovskite light-emitting diodes (PeLEDs) have been investigated as an innovative category of revolutionary LED devices for next-generation flat display and lighting applications. A transparent conductive electrode is a key component in flexible OLEDs and PeLEDs, and has been the limitation of the development in this area. Silver nanowires (AgNWs) have been regarded as the most suitable alternative material in TCEs, due to the economical solution synthesis and compatibility with roll-to-roll technology. This mini-review addresses the advances in silver nanowires electrodes for flexible organic/perovskite light-emitting diodes, and the relationship between electrode optimization and device performance is demonstrated. Moreover, the potential strategies and perspectives for their further development of AgNWs-based flexible OLEDs and PeLEDs are presented.

Keywords: silver nanowires, organic light-emitting diodes, perovskite light-emitting diodes, flexible electronics, transparent conductive electrode

OPEN ACCESS

Edited by:
Yue-Feng Liu,
Jilin University, China

Reviewed by:
Bing Han,
Shanghai Jiao Tong University, China
Jia-Nan Ma,
Taiyuan University of Technology, China

****Correspondence:***
Shuping Hou
houshuping@tjcu.edu.cn
Gong Wang
wanggong@hebut.edu.cn

Specialty section:
This article was submitted to Nanoscience, a section of the journal Frontiers in Chemistry

Received: *28 January 2022*
Accepted: *15 February 2022*
Published: *10 March 2022*

Citation:
Hou S, Liu J, Shi F, Zhao G-X, Tan J-W and Wang G (2022) Recent Advances in Silver Nanowires Electrodes for Flexible Organic/Perovskite Light-Emitting Diodes. Front. Chem. 10:864186. doi: 10.3389/fchem.2022.864186

INTRODUCTION

Wearable electronics are revolutionizing how people interact with the world and each other (Afroj et al., 2020). Within the last 2 decades, the market trend of wearable electronics has stepped away from bulky, heavy, and wired electronics, and consumers are experiencing a world where devices are becoming smaller, lighter, and wirelessly connected with advanced smart technologies. (Han et al., 2019; Ma et al., 2020; Shi et al., 2021). Much of these changes were enabled by the successful development of novel electronic materials and miniaturization of electronic devices (N.Sgourou et al., 2017). To further enhance the functionality, practicality, and aesthetics of the next generation of wearable electronic products, soft and elastic flexible electronic products are needed. (Yuvaraja et al., 2020). In recent years, flexible organic light-emitting diodes (OLEDs) have become a promising technology for flat panel displays and solid-state lighting applications, thanks to their high efficiency, that could significantly reduce the energy consumption for lighting and information display (Xu et al., 2016; Lee J et al., 2017; Zou et al., 2020). Besides, metal halide perovskites (MHPs) are mechanically soft and process superior optoelectronic properties, and therefore show potential applications in next-generation wearable displays (Wang et al., 2020; Zhou et al., 2020).

Current OLEDs and PeLEDs rely heavily on the cost prohibitive component: ITO electrode (Khan et al., 2019). However, the ITO electrodes always suffer from degradation or failure if subjected to repeated bending, stretching, or other types of deformation in flexible electronics, which influence the efficiency and stability of the devices (S.Datta et al., 2020). Therefore, it is necessary to develop alternatives to ITO as the transparent conductive electrodes (TCEs) in flexible electronics (Yu et al.,

2021). Silver nanowires (AgNWs) have been investigated as a potential ITO replacement, as the AgNW network can reproduce the high surface conductivity and visual transparency of ITO, and have the superior mechanical performance meanwhile (M.Abbasi et al., 2015; Tan et al., 2020). This mini-review focuses on the characteristics of AgNWs electrodes and their advantages overwhelming other flexible TCEs. Besides, the evolution of device performance of AgNWs-based flexible OLEDs and PeLEDs are summarized. Moreover, the future development of silver nanowires electrodes for flexible organic/perovskite light-emitting diodes is prospected.

Silver Nanowires Electrodes

A transparent electrode is a key component in flexible/stretchable organic light-emitting diodes and perovskite light-emitting diodes (Zhu et al., 2019). Indium-tin oxide (ITO) has been more or less the only option for the transparent electrodes. ITO coated on glass is predominantly employed, whereas ITO coated on plastic substrates such as polyethylene terephthlate (PET) are used whenever flexibility is required (Lee S. M. et al., 2017). However, owing to the limited supply of indium, ITO becomes more and more expensive. In addition, ITO also has other inherent drawbacks due to the material's properties, such as a lack of flexibility of the ITO layer, lack of chemical stability, fragility, and the toxicity of indium. All of the above-mentioned problems point to the urgent need to develop alternatives to ITO, especially for flexible/stretchable electronic devices (Sannicolo et al., 2016).

A number of alternative transparent electrodes have been investigated, the most notable ones include: 1) Conductive polymers represented by poly (3,4-ethylenedioxythiophene): poly (styrene sulfonate) (PEDOT:PSS). The conductivity of PEDOT:PSS can reach 1000 S/cm. PEDOT thin films can be transparent in the visible spectrum. However, PEDOT is unstable, the conductivity is still much lower than the ITO electrode, and the synthesis of the polymer is costly (Ma et al., 2021). 2) Carbon nanotubes (CNTs) appear to be a better solution because the conductivity of CNTs is higher than that of PEDOT. Ultrathin CNT coatings have been used to fabricate LEDs (He and Ye, 2015). However, CNTs are rather expensive and it is difficult to obtain uniform dispersions suitable for processing. The sheet resistance cannot be reduced to below 100 Ω/sq without significant loss of transparency. 3) Transparent conducting oxides other than ITO, such as alumina doped zinc oxide, gallium doped zinc oxide, etc. Aluminum doped zinc oxide is attractive as a less expensive and nontoxic alternative to ITO. However, the fabrication process still requires high vacuum physical sputtering or evaporation, and the coatings either do not have sufficiently low sheet resistance or low surface smoothness for processing into ultrathin organic films (Seok et al., 2019). 4) Graphene has also been investigated as transparent electrode. The best result is ~30 Ω/sq at ~90% transparency in which the graphene was synthesized through chemical vapor deposition and chemically p-doped by nitric acid. The stability of the doped electrode might be of concern due to the evaporation and migration of the nitric acid dopant (Liu et al., 2019). 5) Silver has a higher conductivity than conducting polymers, CNTs and doped ZnO. Based on calculations, the solar photon flux-weighted transmission versus sheet resistance for silver nanowires has a figure of merit exceeding 85% transmission at 10 Ω/sq sheet resistance versus 80% transmission for 10 Ω/sq ITO/glass substrate. Large-scale coating of silver nanowires has been demonstrated, and the transmittance at 550 nm can be over 80% (including the substrate) for 9 Ω/sq silver nanowire electrodes. Silver nanowires are highly attractive for transparent electrodes; however, improved processing techniques must be developed to form ultrathin coatings with low surface roughness (Guo et al., 2013).

Compared with other typical electrodes, the major advantages of silver nanowire transparent electrodes are the following: 1) The conductivity of silver is one to two orders of magnitude higher than ITO, doped ZnO, conducting polymers, and CNTs. An ultrathin coating of silver nanowires can form a highly conductive network. A high aspect ratio of nanowire length to diameter is essential for the network formation at low silver content per surface area. Besides, proper post-treatments are always used to improve the physical contact between adjacent AgNWs (Langley et al., 2013; Seo et al., 2021). 2) The polymer substrates for the silver nanowires are conventional polymers such as epoxies and polyacrylates, whose manufacturing cost is lower than that of glass. Furthermore, lamination is an effective approach to make the metal nanowires connect more closely with the polymer substrate and further reduce the roughness, which improve the quality of AgNWs (Kim et al., 2020; Kumar et al., 2021). 3) The silver nanowire/polymer substrate fabrication involves solution-based processing, which can be scaled up to roll-to-roll production for lowered cost. 4) The silver nanowire/polymer substrates are flexible and stable. Choosing the appropriate substrate polymer, one can fabricate highly flexible or even stretchable electronic devices under large deformations (Xiong et al., 2013). 5) The materials are nontoxic. The devices may be recycled or safely disposed to significantly reduce the overall environmental impact from electronic waste.

Flexible Organic Light-Emitting Diodes

Flexible organic light-emitting diodes (FOLEDs) have been a promising technology for displays in wearable devices; however, the high manufacturing cost still hamper their large-scale applications (Li et al., 2013; Zhang et al., 2021). The manufacturing cost is mainly attributed to the high cost associated with substrate, electrode, and light-extraction structure (LES). AgNWs can be integrated in a streamlined solution-based process which is well-matched with Roll-to-Roll production for high throughput, which is an ideal approach to decrease the fabrication cost of FOLEDs. Besides, silver nanowires (AgNWs) have been investigated as a potential ITO replacement, as the AgNW network can reproduce the high surface conductivity and visual transparency of ITO (Zhang and Engholm, 2018).

In 2013, Gaynor et al. reported an ITO-free white OLED based on solution-processed AgNWs/PMMA electrodes, which showed a high power efficiency of 54 lm/W (Gaynor et al., 2013). In this work, the solution-possessed AgNW electrodes exhibited great

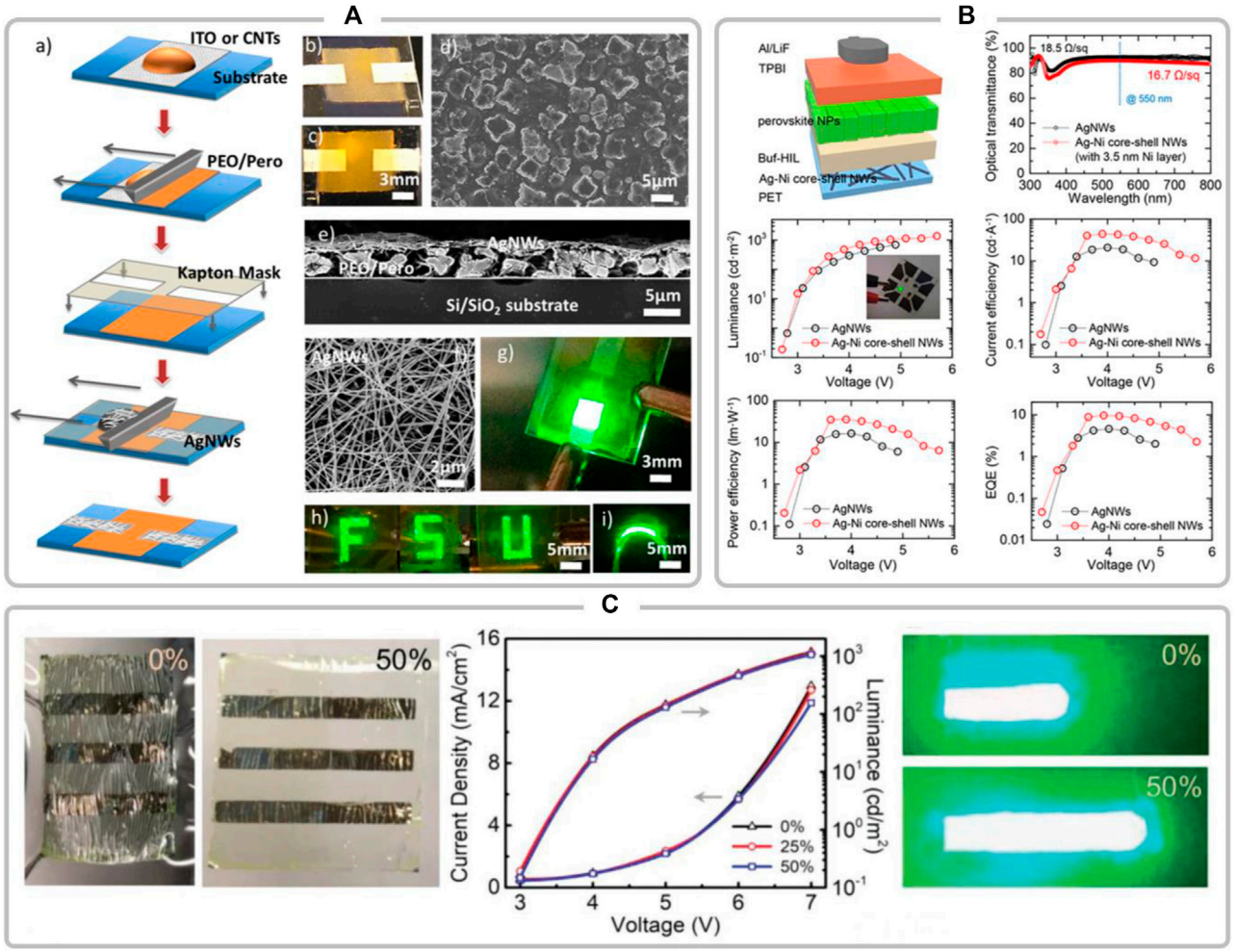

FIGURE 1 | (A) Fully Printed Halide Perovskite Light-Emitting Diodes with Silver Nanowire Electrodes; reproduced with permission from R.Bade et al. (2016) **(B)** Electroplated Silver-Nickel Core-Shell Nanowire Network Electrodes for Highly Efficient Perovskite Nanoparticle Light-Emitting Diodes; reproduced with permission from Kang et al. (2020) **(C)** Stretchable Organometal-Halide-Perovskite Quantum-Dot Light-Emitting Diodes; reproduced with permission from Li et al. (2019).

advantages with commercial roll-to-roll production, demonstrating significant potentials to fabricate low-cost FOLED. Lee et al. developed a highly efficient OLED based on AgNW electrode, showing a low turn-on voltage of 3.6 V, a high current efficiency of 44.5 cd/A, and power efficiency of 35.8 lm/W (Lee et al., 2014). Chang et al. investigated a solution-processed s-MoO_x-treated AgNW electrode with transmittance up to 95.9%, and low R_s of 29.8 Ω/sq (Chang et al., 2015). The resulting ITO-free FOLEDs exhibited a superior performance with power efficiency of 29.2 lm/W and EQE of 10.3%. Wei et al. constructed a highly conductive, smooth and transparent AgNW/PEDOT:PSS hybrid electrode with a resulting maximum current efficiency of 58.2 cd/A in 2017 (Wei et al., 2017).

Flexible Perovskite Light-Emitting Diodes

Perovskites have been hotly pursued in recent years owing to their high photoluminescence quantum yield, long carrier diffusion length, strong light absorption, adjustable bandgap, and high carrier mobility (Song et al., 2019). After perovskite was first employed in light-emitting diodes, a slurry of research efforts has since been devoted in flexible PeLEDs (Kumawat et al., 2019). Flexible PeLEDs combine the excellent optoelectronic properties of perovskites with the potential of highly flexible electronics have come out as a novel category of revolutionary LED for panel displays and solid-state lighting applications (Lim et al., 2021; Rhee et al., 2021). To enable flexible applications of perovskite light-emitting diodes, flexible electrodes should satisfy the requirements of transparency, conductivity, and robustness. AgNWs electrode is an ideal choice for the flexible electrode and is widely applied in flexible and even stretchable PeLEDs. Besides, the perovskite active layer should feature good mechanical stability, and further engineering technology for perovskite film is important.

As shown in **Figure 1A**, Bade et al. first reported the fully printed PeLEDs in 2016 with AgNWs as the cathode, and a printed composite film consisting of metal halide perovskites (MPHs) and poly (ethylene oxide) (PEO) as the emissive layer (R.Bade et al., 2016). The flexible PeLED can survive 5 mm radius

of curvature without affection of the device performance. Subsequently, Chen et al. developed a morphology-controlled $CsPbBr_3$-based PeLEDs fabricated on AgNWs/PET substrate in 2018 (Cheng et al., 2019). The flexible device showed a maximum current efficiency of 31.0 cd/A, and a maximum external quantum efficiency (EQE) of 10.1%. Later on, Kang et al. fabricated Ag-Ni core-shell nanowires by solution-electroplating to decrease the resistance, increase the work function of the electrodes, and prevent the reaction of AgNWs with the overlying perovskite nanoparticles (Kang et al., 2020). The PeLEDs based on Ag-Ni core-shell NW electrodes and $FAPbBr_3$ nanoparticles exhibited an EQE of 9.67% (**Figure 1B**). Moreover, stretchable PeLEDs were also constructed on AgNWs/PI electrode with a luminescent efficiency up to 9.2 cd/A in **Figure 1C** (Li et al., 2019).

CONCLUSION AND OUTLOOK

The cost-effective AgNWs-based OLEDs and PeLEDs take a big stride to the large-area and low-cost fabrication of flat displays in wearable devices. AgNWs with high aspect ratio process high transmittance and conductivity after proper post-treatments. Besides, lamination effectively make the close connect between AgNWs and polymer substrate and further reduce the roughness of electrode. Moreover, AgNWs/polymer substrate exhibit superior flexibility and stability even under repeated bending, enabling their applications in OLEDs and PeLEDs. As a result, the flexible AgNWs-based OLEDs and PeLEDs demonstrate good device performance and stability under deformations. Further efforts are also required to elucidate the physical mechanisms in flexible OLEDs and PeLEDs, especially when they are in bending condition. Furthermore, the encapsulation approach should be further discussed for their commercial applications.

AUTHOR CONTRIBUTIONS

All authors listed have made a substantial, direct and intellectual contribution to the work, and approved it for publication.

FUNDING

This work was supported by the National Natural Science Foundation of China (Grant No. 62004059) and Natural Science Foundation of Hebei Province (No. F2021202047).

REFERENCES

Afroj, S., Tan, S., Abdelkader, A. M., Novoselov, K. S., and Karim, N. (2020). Highly Conductive, Scalable, and Machine Washable Graphene-Based E-Textiles for Multifunctional Wearable Electronic Applications. *Adv. Funct. Mater.* 30 (23), 2000293. doi:10.1002/adfm.202000293

Bade, S. G. R., Li, J., Shan, X., Ling, Y., Tian, Y., Dilbeck, T., et al. (2016). Fully Printed Halide Perovskite Light-Emitting Diodes with Silver Nanowire Electrodes. *ACS Nano* 10 (2), 1795–1801. doi:10.1021/acsnano.5b07506

Chang, J.-H., Chiang, K.-M., Kang, H.-W., Chi, W.-J., Chang, J.-H., Wu, C.-I., et al. (2015). A Solution-Processed Molybdenum Oxide Treated Silver Nanowire Network: a Highly Conductive Transparent Conducting Electrode with superior Mechanical and Hole Injection Properties. *Nanoscale* 7 (10), 4572–4579. doi:10.1039/c4nr06805j

Cheng, L.-P., Huang, J.-S., Shen, Y., Li, G.-P., Liu, X.-K., Li, W., et al. (2019). Efficient CsPbBr3 Perovskite Light-Emitting Diodes Enabled by Synergetic Morphology Control. *Adv. Opt. Mater.* 7 (4), 1801534. doi:10.1002/adom.201801534

Datta, R. S., Syed, N., Zavabeti, A., Jannat, A., Mohiuddin, M., Rokunuzzaman, M., et al. (2020). Flexible Two-Dimensional Indium Tin Oxide Fabricated Using a Liquid Metal Printing Technique. *Nat. Electron.* 3 (1), 51–58. doi:10.1038/s41928-019-0353-8

Gaynor, W., Hofmann, S., Christoforo, M. G., Sachse, C., Mehra, S., Salleo, A., et al. (2013). Color in the Corners: ITO-free White OLEDs with Angular Color Stability. *Adv. Mater.* 25 (29), 4006–4013. doi:10.1002/adma.201300923

Guo, X., Ma, Y., Wang, Y., and Tong, L. (2013). Nanowire Plasmonic Waveguides, Circuits and Devices. *Laser Photon. Rev.* 7 (6), 855–881. doi:10.1002/lpor.201200067

Han, B., Zhang, Y. L., Zhu, L., Li, Y., Ma, Z. C., Liu, Y. Q., et al. (2019). Plasmonic-Assisted Graphene Oxide Artificial Muscles. *Adv. Mater.* 31 (5), 1806386. doi:10.1002/adma.201806386

He, W., and Ye, C. (2015). Flexible Transparent Conductive Films on the Basis of Ag Nanowires: Design and Applications: A Review. *J. Mater. Sci. Technol.* 31 (6), 581–588. doi:10.1016/j.jmst.2014.11.020

Kang, H., Choi, S.-R., Kim, Y.-H., Kim, J. S., Kim, S., An, B.-S., et al. (2020). Electroplated Silver-Nickel Core-Shell Nanowire Network Electrodes for Highly Efficient Perovskite Nanoparticle Light-Emitting Diodes. *ACS Appl. Mater. Inter.* 12 (35), 39479–39486. doi:10.1021/acsami.0c10386

Khan, Q., Subramanian, A., Yu, G., Maaz, K., Li, D., Sagar, R. U. R., et al. (2019). Structure Optimization of Perovskite Quantum Dot Light-Emitting Diodes. *Nanoscale* 11 (11), 5021–5029. doi:10.1039/c8nr09864f

Kim, C.-L., Lee, J.-Y., Shin, D.-G., Yeo, J.-S., and Kim, D.-E. (2020). Mechanism of Heat-Induced Fusion of Silver Nanowires. *Sci. Rep.* 10 (1), 9271. doi:10.1038/s41598-020-66304-2

Kumar, A., Shaikh, M. O., and Chuang, C.-H. (2021). Silver Nanowire Synthesis and Strategies for Fabricating Transparent Conducting Electrodes. *Nanomaterials* 11 (3), 693. doi:10.3390/nano11030693

Kumawat, N. K., Liu, X.-K., Kabra, D., and Gao, F. (2019). Blue Perovskite Light-Emitting Diodes: Progress, Challenges and Future Directions. *Nanoscale* 11 (5), 2109–2120. doi:10.1039/c8nr09885a

Langley, D., Giusti, G., Mayousse, C., Celle, C., Bellet, D., and Simonato, J.-P. (2013). Flexible Transparent Conductive Materials Based on Silver Nanowire Networks: a Review. *Nanotechnology* 24 (45), 452001. doi:10.1088/0957-4484/24/45/452001

Lee, H., Lee, D., Ahn, Y., Lee, E.-W., Park, L. S., and Lee, Y. (2014). Highly Efficient and Low Voltage Silver Nanowire-Based OLEDs Employing a N-type Hole Injection Layer. *Nanoscale* 6 (15), 8565–8570. doi:10.1039/c4nr01768d

Lee, J., An, K., Won, P., Ka, Y., Hwang, H., Moon, H., et al. (2017). A Dual-Scale Metal Nanowire Network Transparent Conductor for Highly Efficient and Flexible Organic Light Emitting Diodes. *Nanoscale* 9 (5), 1978–1985. doi:10.1039/c6nr09902e

Lee, S.-M., Kwon, J. H., Kwon, S., and Choi, K. C. (2017). A Review of Flexible OLEDs toward Highly Durable Unusual Displays. *IEEE Trans. Electron. Devices* 64 (5), 1922–1931. doi:10.1109/TED.2017.2647964

Li, N., Oida, S., Tulevski, G. S., Han, S.-J., Hannon, J. B., Sadana, D. K., et al. (2013). Efficient and Bright Organic Light-Emitting Diodes on Single-Layer Graphene Electrodes. *Nat. Commun.* 4, 2294. doi:10.1038/ncomms3294

Li, Y. F., Chou, S. Y., Huang, P., Xiao, C., Liu, X., Xie, Y., et al. (2019). Stretchable Organometal-Halide-Perovskite Quantum-Dot Light-Emitting Diodes. *Adv. Mater.* 31 (22), 1807516. doi:10.1002/adma.201807516

Lim, K.-G., Han, T.-H., and Lee, T.-W. (2021). Engineering Electrodes and Metal Halide Perovskite Materials for Flexible/stretchable Perovskite Solar Cells and

Light-Emitting Diodes. *Energy Environ. Sci.* 14 (4), 2009–2035. doi:10.1039/d0ee02996c

Liu, Y.-Q., Chen, Z.-D., Mao, J.-W., Han, D.-D., and Sun, X.-Y. (2019). Laser Fabrication of Graphene-Based Electronic Skin. *Front. Chem.* 7, 416. doi:10.3389/fchem.2019.00461

Ma, C., Liu, Y.-F., Bi, Y.-G., Zhang, X.-L., Yin, D., Feng, J., et al. (2021). Recent Progress in post Treatment of Silver Nanowire Electrodes for Optoelectronic Device Applications. *Nanoscale* 13 (29), 12423–12437. doi:10.1039/d1nr02917g

Ma, Z.-C., Zhang, Y.-L., Han, B., Hu, X.-Y., Li, C.-H., Chen, Q.-D., et al. (2020). Femtosecond Laser Programmed Artificial Musculoskeletal Systems. *Nat. Commun.* 11 (1), 4536. doi:10.1038/s41467-020-18117-0

M.Abbasi, N. M., Yu, H., Wang, L., Zain-ul-Abdin, Z.-U., Amer, W. A., Akram, M., et al. (2015). Preparation of Silver Nanowires and Their Application in Conducting Polymer Nanocomposites. *Mater. Chem. Phys.* 166, 1–15. doi:10.1016/j.matchemphys.2015.08.056

Rhee, S., An, K., and Kang, K.-T. (2021). Recent Advances and Challenges in Halide Perovskite Crystals in Optoelectronic Devices from Solar Cells to Other Applications. *Crystals* 11 (1), 39. doi:10.3390/cryst11010039

Sannicolo, T., Lagrange, M., Cabos, A., Celle, C., Simonato, J.-P., and Bellet, D. (2016). Metallic Nanowire-Based Transparent Electrodes for Next Generation Flexible Devices: a Review. *Small* 12 (44), 6052–6075. doi:10.1002/smll.201602581

Seo, Y., Ha, H., Matteini, P., and Hwang, B. (2021). A Review on the Deformation Behavior of Silver Nanowire Networks under Many Bending Cycles. *Appl. Sci.* 11 (10), 4515. doi:10.3390/app11104515

Seok, H. J., Lee, J. H., Park, J. H., Lim, S. H., and Kim, H. K. (2019). Transparent Conducting Electrodes for Quantum Dots Light Emitting Diodes. *Isr. J. Chem.* 59 (8), 729–746. doi:10.1002/ijch.201900045

Sgourou, E., Panayiotatos, Y., Vovk, R., and Chroneos, A. (2017). Toward Defect Engineering Strategies to Optimize Energy and Electronic Materials. *Appl. Sci.* 7 (7), 674. doi:10.3390/app7070674

Shi, X., Zuo, Y., Zhai, P., Shen, J., Yang, Y., Gao, Z., et al. (2021). Large-area Display Textiles Integrated with Functional Systems. *Nature* 591 (7849), 240–245. doi:10.1038/s41586-021-03295-8

Song, Z., Zhao, J., and Liu, Q. (2019). Luminescent Perovskites: Recent Advances in Theory and Experiments. *Inorg. Chem. Front.* 6 (11), 2969–3011. doi:10.1039/c9qi00777f

Tan, D., Jiang, C., Li, Q., Bi, S., and Song, J. (2020). Silver Nanowire Networks with Preparations and Applications: a Review. *J. Mater. Sci. Mater. Electron.* 31 (18), 15669–15696. doi:10.1007/s10854-020-04131-x

Wang, H. P., Li, S., Liu, X., Shi, Z., Fang, X., and He, J. H. (2020). Low-Dimensional Metal Halide Perovskite Photodetectors. *Adv. Mater.* 33 (7), 2003309. doi:10.1002/adma.202003309

Wei, B., Wu, X., Lian, L., Yang, S., Dong, D., Feng, D., et al. (2017). A Highly Conductive and Smooth AgNW/PEDOT:PSS Film Treated by Hot-Pressing as Electrode for Organic Light Emitting Diode. *Org. Electron.* 43, 182–188. doi:10.1016/j.orgel.2017.01.030

Xiong, X., Zou, C.-L., Ren, X.-F., Liu, A.-P., Ye, Y.-X., Sun, F.-W., et al. (2013). Silver Nanowires for Photonics Applications. *Laser Photon. Rev.* 7 (6), 901–919. doi:10.1002/lpor.201200076

Xu, L.-H., Ou, Q.-D., Li, Y.-Q., Zhang, Y.-B., Zhao, X.-D., Xiang, H.-Y., et al. (2016). Microcavity-Free Broadband Light Outcoupling Enhancement in Flexible Organic Light-Emitting Diodes with Nanostructured Transparent Metal-Dielectric Composite Electrodes. *ACS Nano* 10 (1), 1625–1632. doi:10.1021/acsnano.5b07302

Yu, H., Tian, Y., Dirican, M., Fang, D., Yan, C., Xie, J., et al. (2021). Flexible, Transparent and Tough Silver Nanowire/nanocellulose Electrodes for Flexible Touch Screen Panels. *Carbohydr. Polym.* 273, 118539. doi:10.1016/j.carbpol.2021.118539

Yuvaraja, S., Nawaz, A., Liu, Q., Dubal, D., Surya, S. G., Salama, K. N., et al. (2020). Organic Field-Effect Transistor-Based Flexible Sensors. *Chem. Soc. Rev.* 49 (11), 3423–3460. doi:10.1039/c9cs00811j

Zhang, L., Song, T., Shi, L., Wen, N., Wu, Z., Sun, C., et al. (2021). Recent Progress for Silver Nanowires Conducting Film for Flexible Electronics. *J. Nanostruct Chem.* 11 (3), 323–341. doi:10.1007/s40097-021-00436-3

Zhang, R., and Engholm, M. (2018). Recent Progress on the Fabrication and Properties of Silver Nanowire-Based Transparent Electrodes. *Nanomaterials* 8 (8), 628. doi:10.3390/nano8080628

Zhou, G., Su, B., Huang, J., Zhang, Q., and Xia, Z. (2020). Broad-band Emission in Metal Halide Perovskites: Mechanism, Materials, and Applications. *Mater. Sci. Eng. R: Rep.* 141, 100548. doi:10.1016/j.mser.2020.100548

Zhu, Y., Deng, Y., Yi, P., Peng, L., Lai, X., and Lin, Z. (2019). Flexible Transparent Electrodes Based on Silver Nanowires: Material Synthesis, Fabrication, Performance, and Applications. *Adv. Mater. Technol.* 4 (10), 1900413. doi:10.1002/admt.201900413

Zou, S.-J., Shen, Y., Xie, F.-M., Chen, J.-D., Li, Y.-Q., and Tang, J.-X. (2020). Recent Advances in Organic Light-Emitting Diodes: toward Smart Lighting and Displays. *Mater. Chem. Front.* 4 (3), 788–820. doi:10.1039/c9qm00716d

Conflict of Interest: The authors declare that the research was conducted in the absence of any commercial or financial relationships that could be construed as a potential conflict of interest.

Publisher's Note: All claims expressed in this article are solely those of the authors and do not necessarily represent those of their affiliated organizations, or those of the publisher, the editors, and the reviewers. Any product that may be evaluated in this article, or claim that may be made by its manufacturer, is not guaranteed or endorsed by the publisher.

Advantages of publishing in Frontiers

OPEN ACCESS
Articles are free to read for greatest visibility and readership

FAST PUBLICATION
Around 90 days from submission to decision

HIGH QUALITY PEER-REVIEW
Rigorous, collaborative, and constructive peer-review

TRANSPARENT PEER-REVIEW
Editors and reviewers acknowledged by name on published articles

Frontiers
Avenue du Tribunal-Fédéral 34
1005 Lausanne | Switzerland

Visit us: www.frontiersin.org
Contact us: frontiersin.org/about/contact

REPRODUCIBILITY OF RESEARCH
Support open data and methods to enhance research reproducibility

DIGITAL PUBLISHING
Articles designed for optimal readership across devices

FOLLOW US
@frontiersin

IMPACT METRICS
Advanced article metrics track visibility across digital media

EXTENSIVE PROMOTION
Marketing and promotion of impactful research

LOOP RESEARCH NETWORK
Our network increases your article's readership